Aalto University
School of Chemical
Engineering

Tyko Viertiö

ATOMIC LAYER DEPOSITION COATINGS FOR CATALYTIC HIGH-TEMPERATURE FILTRATION OF GASIFICATION GAS

Master´s Programme in Chemical, Biochemical and Materials Engineering
Major in Chemical Engineering

Master's thesis for the degree of Master of Science in Technology submitted for inspection, Espoo, 2nd June, 2019.

Supervisor	Professor Riikka Puurunen
Instructor	M.Sc. (Tech) Viivi Kivelä

Author Tyko Viertiö

Title of thesis Atomic layer deposition coatings in catalytic high-temperature filtration of gasification gas

Degree Programme Master´s Programme in Chemical, Biochemical and Materials Engineering

Major Chemical Engineering

Thesis supervisor Professor Riikka Puurunen

Thesis advisor(s) / Thesis examiner(s) M.Sc. (Tech) Viivi Kivelä

Date 02.06.2019 **Number of pages** 79 + 8 **Language** English

Abstract

The aim of the thesis was to develop a method for preparation of catalytic filters for gasification gas cleaning by atomic layer deposition (ALD). In the literature part, catalysts for tar decomposition, the factors in filter and membrane coatings affecting the reactivity in catalytic filtration and atomic layer deposition prepared nickel and rhodium catalysts were reviewed. Main challenge of the gasification gas cleaning catalysts is maintaining high activity despite the deactivation due to sulphur poisoning and coke formation. Nickel and rhodium catalysts supported on Al_2O_3 were found to be the most promising catalyst options for further development. Challenge of the preparation of catalytic filters is the low surface area, which limits the amount and consequently the active surface area of the catalyst deposited on the filter. ALD is an interesting option for catalyst preparation, since it provides method for preparation of stabile and high active metal surface area catalysts.

In the experimental part, set of catalytic filters was prepared by atomic layer deposition of Al_2O_3 support layer and nickel or rhodium layers as active metals on steel filter discs. Catalytic filters were characterized with SEM-EDS and tested for catalytic filtration of model gasification gas in lab scale reactor at temperatures ranging from 650 to 920 °C and at pressure of 5 bar. Nickel catalysts were prepared with top surface nickel loading ranging from 1 to 14 w-% but no deposition on inner surfaces of the filter was achieved. Due to low overall amount of nickel, no significant catalytic activity was observed in reaction tests. The highest catalytic activity was achieved with nickel-containing steel alloy 316L filter at 920 °C. No sufficient deposition of rhodium on filters was achieved and major process development of parameters of ALD in current reactor setup is needed for reliable rhodium catalyst preparation.

Keywords Gasification gas cleaning, catalytic filtration, tar decomposition, atomic layer deposition, nickel catalyst, rhodium catalyst

Tekijä Tyko Viertiö

Työn nimi Atomikerroskasvatus-pinnoitus kaasutuskaasun katalyyttiseen suodatukseen korkeassa lämpötilassa

Koulutusohjelma Master´s Programme in Chemical, Biochemical and Materials Engineering

Pääaine Chemical Engineering

Työn valvoja Professori Riikka Puurunen

Työn ohjaaja(t)/Työn tarkastaja(t) DI Viivi Kivelä

Päivämäärä 02.06.2019 **Sivumäärä** 79+8 **Kieli** englanti

Tiivistelmä

Työn tarkoituksena oli katalyyttisten suodattimien ja niiden valmistusmenetelmän kehittäminen kaasutuskaasujen puhdistukseen atomikerroskasvatusta (ALD) hyödyntäen. Kirjallisuusosa käsittelee kaasutuskaasun tervojen reformointikatalyytteja, katalyyttisen suodattimen toimintaan vaikuttavia tekijöitä sekä atomikerroskasvatuksella valmistettuja nikkeli- ja rodiumkatalyytteja. Kaasutuskaasun tervakomponenttien reformointikatalyyttien suurimpana haasteena on välttää rikkimyrkyttymisestä tai koksinmuodostumisesta johtuva deaktivoituminen. Al_2O_3-kantajalle valmistetut nikkeli- ja rodiumkatalyytit todettiin parhaiksi vaihtoehdoiksi jatkokehitystä varten. Katalyyttisten suodattimien osalta suurin haaste on aikaansaada riittävän suuri aktiivisen metallin pinta-ala itse kantajan pinta-alan ollessa tyypillisesti pieni perinteiseen katalyyttiin verrattuna. ALD-menetelmä mahdollistaa aktiivisen metallin pinta-alalta suurien katalyyttien valmistamisen.

Työn kokeellisessa osassa valmistettiin sarja katalyyttisiä suodattimia pinnoittamalla teräksisiä suodattimia ensin Al_2O_3-kantajakerroksella ja tämän jälkeen katalyyttisesti aktiivisella nikkeli- tai rodiumkerroksella. Valmistetut suodattimet karakterisoitiin SEM-EDS -menetelmällä ja niitä kokeiltiin mallikaasutuskaasun katalyyttisessä suodatuksessa laboratoriomittakaavan reaktorissa 650-920 °C lämpötilassa ja 5 bar paineessa. Nikkelipinnoitettujen suodattimien osalta sarja katalyyttejä, yläpinnan nikkelimäärältään 1-14 m-% valmistettiin, mutta suodattimien sisäpuolen nikkelipinnoitus ei onnistunut. Tästä johtuen suodattimien nikkelin kokonaismäärä jäi pieneksi, eikä merkittävää katalyyttista aktiivisuutta havaittu reaktiokokeissa. Suurin katalyyttinen aktiivisuus mitattiin nikkelipitoisesta 316L-teräksestä valmistetulla pinnoittamattomalla suodattimella 920 °C lämpötilassa. Rodiumin atomikerroskasvatuksessa riittävää pinnoitusta suodattimille ei saatu aikaan, ja itse pinnoitusprosessi kyseisellä ALD-reaktorilaitteistolla vaatiikin laajempaa tutkimusta luotettavan pinnoitustuloksen mahdollistamiseksi.

Avainsanat Kaasutuskaasun puhdistus, katalyyttinen suodatus, tervakomponenttien reformointi, atomikerroskasvatus, nikkelikatalyytti, rodiumkatalyytti

Foreword

The background and funding of this master's thesis originates from COMSYN project (Compact Gasification and Synthesis process for Transport Fuels), which has received funding from the European Union's Horizon 2020 research and innovation programme under grant agreement No 727476. The thesis was carried out at laboratories of VTT Technical Research Centre of Finland in Otaniemi, Espoo, Finland, between October 2018 and May 2019.

First, I would like to thank Johanna Kihlman and Janne Hulkko for an oppourtunity to do my thesis for VTT in this kind of interesting project. Most importantly, I want to thank the advisor of the thesis Viivi Kivelä for sharing her expertise on the topic of the thesis, as well as positive and supportive attitude and guidance through the whole project, and supervising professor Riikka Puurunen for challenging questions and supportive comments. I would also like to thank Matti Putkonen and Johanna Kihlman for interesting discussions and comments of the final version of the thesis, and Matti Putkonen for guidance with the ALD part of the thesis. Additionally, I would like to thank Patrik Eskelinen for operation of the SEM tool and inspiring discussions, Mirja Muhola for conducting the physisorption experiments, Johannes Roine for preparing the plate tool for ALD experiments, and Katja Heiskanen, Päivi Jokimies, Petri Hietula and Mari-Leena Koskinen-Soivi for help and support with equipment and daily practical issues of the laboratory work. Finally I would like to thank all the others who have had a part in the project.

This thesis also crowns my studies at Aalto University. My thanks for Chemistry Guild, The Association for Process Engineering Students, engineering student community and Aalto University Student Union for helping me to live the best student's life in the World. I want to thank all friends that have been supporting me through this thesis project and my studies generally. Especially my lazy, stupid and idle flatmates, FTMK14 and the grumpy seals have been standing by me during the worst and the best moments of this journey, thank you. My final and the most important thank goes to my family for their endless and unconditional support on whatever I am doing.

Otaniemi, 2nd June 2019
Tyko Viertiö

Table of contents

List of abbreviations

AAO	anodized aluminum oxide
acac	acetyl acetonate, ligand common in ALD precursors
ALD	atomic layer deposition
BET area	Brunauer-Emmett-Teller surface area
cp	cyclopentadienyl, ligand common in ALD precursors
DFT	density functional theory
DRM	dry reforming of methane
EDS	Energy-dispersive X-ray spectroscopy
FT	Fischer-Tropsch
IWI	incipient wetness impregnation
PAH	polyaromatic hydrocarbons
ppm	parts per million
SCCM	standard cubic centimetre
SEM	scanning electron microscopy
TEM	transmission electron microscopy
TPR	temperature-programmed reduction
VOC	volatile organic compound
XPS	X-ray photoelectron spectroscopy

List of symbols

F	permeation flux of a membrane (mol/(m^2 bar s))
F_i	molar flow of component i (mol/s)
F_{tot}	total molar flowrate (mol/s)
F_{dry}	total molar inlet flow rate of dry gas (mol/s)
F_{water}	total molar inlet flowrate of water (mol/s)
L	membrane thickness (m)
P_{av}	average pressure across the membrane (bar)
r	pore radius (m)
R	gas constant (bar m^3/(mol K))
V_v	volume of the void in filter (m^3)
V_T	total volume of the filter (m^3)
V_M	volume of the metal in the filter (m^3)
X_i	conversion of the component i
Y_i	yield of the component i
y_i	molar fraction of component i
ϵ	membrane porosity
μ	viscosity (bar s)
τ	membrane tortuosity
Φ	void fraction
ΔA	absolute error of the measured quantity A

1 Introduction

Gasification is a thermochemical process that is used to convert carbonaceous fossil or biomass materials into mixture of gaseous, liquid and solid state products in oxygen-deficient environment at high temperature of over 700 ºC (Sikarwar *et al.,* 2016). For example, wood, agricultural and aquatic biomass, animal and human biomass waste and contaminated biomass, such as municipal solid waste, have been studied as feedstock for gasification. Elemental composition of the feedstock depends strongly on biomass origin (Vassilev *et al.,* 2010).

Gasification product gas contains mainly carbon monoxide CO, hydrogen H_2, carbon dioxide CO_2, methane CH_4, water H_2O, hydrogen sulfide H_2S and other trace compound fractions (Sikarwar *et al.,* 2016). Gaseous hydrocarbons produced in gasification include for example methane CH_4, ethane C_2H_6 and ethene C_2H_4 (Kurkela *et al.,* 2016). Non-volatile fixed carbon of biomass and inorganic ash compounds such as SiO_2, CaO and K_2O form solid products during gasification (Kurkela *et al.,* 2016). Product distribution of gasification depends on reactor set-up (Basu, 2013), composition of biomass feedstock (Van de Velden *et al.,* 2010, Sikarwar *et al.,* 2016), moisture content (Sikarwar *et al.,* 2016; Basu, 2013), gasifying agent (Gil *et al.,* 1999), process conditions (Basu, 2013), and catalysts (De Lasa *et al.,* 2011).

The product gas of gasification can be upgraded to synthesis gas, usually referred as syngas, that is a mixture of carbon monoxide and hydrogen. Syngas can be further upgraded to chemicals and biofuels, for example via methanol, ammonia or Fischer-Tropsch (FT) synthesis (Spath and Dayton, 2003). COMSYN project, which is the background of this thesis, is aiming to find feasible process for biofuel production from biomass by gasification and FT synthesis (Anon, 2018).

Due to the heterogeneous nature of the gasification feedstock and gasification process variables, the amount of impurities greatly varies in generated gasification gas (Woolcock and Brown, 2013). Major impurities include condensable hydrocarbons collectively called tars, sulphur compounds, ammonia, solid particulate

matter of ash and char, alkali compounds and chlorine (Woolcock and Brown, 2013). Potential hazards caused by impurities for downstream processes include for example corrosion and clogging of the pipelines, as well as catalyst deactivation due to coking or poisoning (Woolcock and Brown, 2013). Due to catalysts prone for deactivation, Fischer-Tropsch synthesis sets the most important requirements for gas cleaning (Tijmensen *et al.,* 2002).

Tars are a complex mixture of hydrocarbons formed in thermal reactions during gasification (Kiel *et al.*, 2004). Tars can be reduced by selection and optimization of reactants and process conditions of gasification (Sikarwar *et al.*, 2016), as well as by catalysts for tar oxidation and decomposition (Miyazawa *et al.*, 2006). Tar reduction methods include primary methods employed in the gasifier, for example tar decomposition catalyst added directly to gasifier, and secondary methods, for example separate reformer unit for tar removal (Sikarwar *et al.*, 2016). For FT synthesis, all tar components and particulate matter have to be removed from gasification gas to prevent catalyst deactivation (Tijmensen *et al.,* 2002).

Filtration is utilized for particulate matter removal (Woolcock and Brown, 2013). Also solid alkali chlorides formed in reactor can be separated by high temperature filtration (Simell *et al.,* 2014). By operating the filter at high temperature between 800 – 900 °C instead of traditional 500 °C for hot-gas filtration (Woolcock and Brown, 2013), energy efficiency of fuel production process is increased and cost savings of 5 % can be achieved (Simell *et al.,* 2014). In addition, high temperature filtration provides suitable conditions for tar decomposition reactions, as well as thermal tar formation reactions (Tuomi *et al.,* 2015). Catalytic activity for tar decomposition in filter can be promoted by catalytically active coating to employ the filter as pre-reformer for tar reformer (Kivelä, 2018).

This thesis aims to further develop catalytic filters prepared by atomic layer deposition (ALD) studied earlier by Kivelä (2018). The options for catalytic filtration are extended in terms of lower nickel loading, more efficient filter coating and ALD coating with rhodium instead of nickel to improve the catalytic filtration conversion. In the literature part, the factors affecting the reactivity of tar compounds in catalytic filters are reviewed, including tar reforming catalysts, catalytic filter modification, and ALD prepared catalysts. In the experimental part, set of catalytic filters is prepared,

characterized and tested for catalytic tar decomposition of model biomass gasification gas.

2 Tar decomposition and catalysts

Tars in biomass gasification gas are a complex mix of different chemical compounds. In this chapter, the definition, formation and decomposition of tars are presented. Different catalyst options and catalyst supports for secondary catalytic tar decomposition and similar high temperature reactions are reviewed. Due to scope of the thesis project in ALD-coated metallic filters, only oxide-supported metal catalysts with nickel or precious metals as active metal are discussed. For example, different catalyst promoters (Zhang *et al.*, 2002; Nacken *et al.*, 2010) effects of multiple active metals or natural catalysts (Devi *et al.,* 2005) are not discussed.

2.1 Tars

High molecular weight hydrocarbons in gasification gas are collectively called tars (Li and Suzuki, 2009; Torres *et al.*, 2007). Tars cause problems due to condensation or polymerization into pipes or process units, resulting for example increase of pressure drop and catalyst deactivation (Li and Suzuki, 2009; Torres *et al.*, 2007). In addition, decrease of the efficiency of the process is caused as part of the carbon is in useless form in tars instead of syngas components. (Li and Suzuki, 2009).

Typically, tars are further classified in five groups, being I) very heavy tars undetectable by gas chromatography with 7 or more aromatic rings, II) heterocyclic aromatics such as phenol and pyridine, III) light aromatics with one aromatic ring, IV) light polyaromatic compounds with 2-3 aromatic rings and V) heavy polyaromatic compounds with 4-7 aromatic rings (Li and Suzuki, 2009). Structural formulas of example tar compounds are presented in Figure 1, and an example of composition of biomass gasification gas tar is presented in Figure 2.

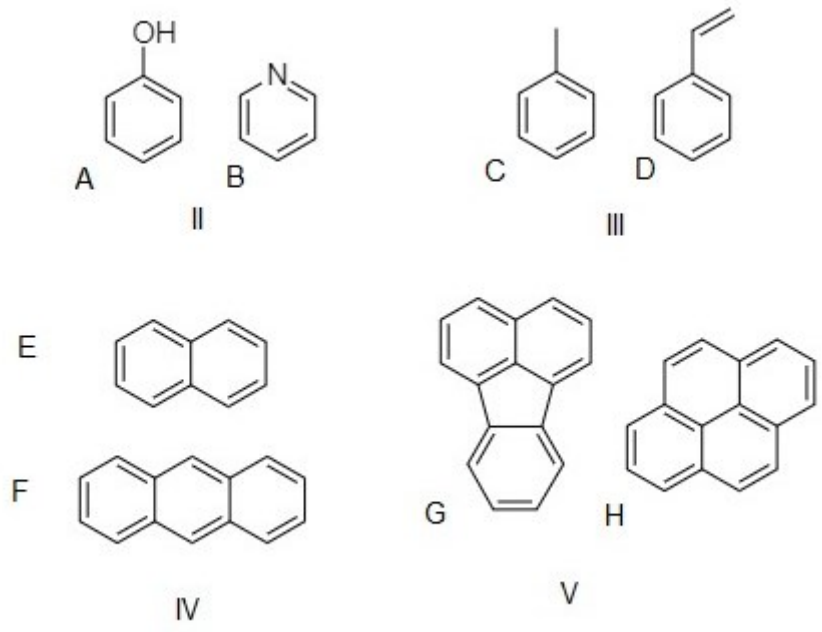

Figure 1. Structural formulas of tar compounds, roman numbers refer to tar classes presented above. Class II) heterocyclic aromatics phenol (A) and pyridine (B), III) light aromatics toluene (C) and styrene (D), IV) light polyaromatic compounds naphthalene (E) and anthracene (F) and V) heavy polyaromatic compounds fluoranthene (G) and pyrene (H).

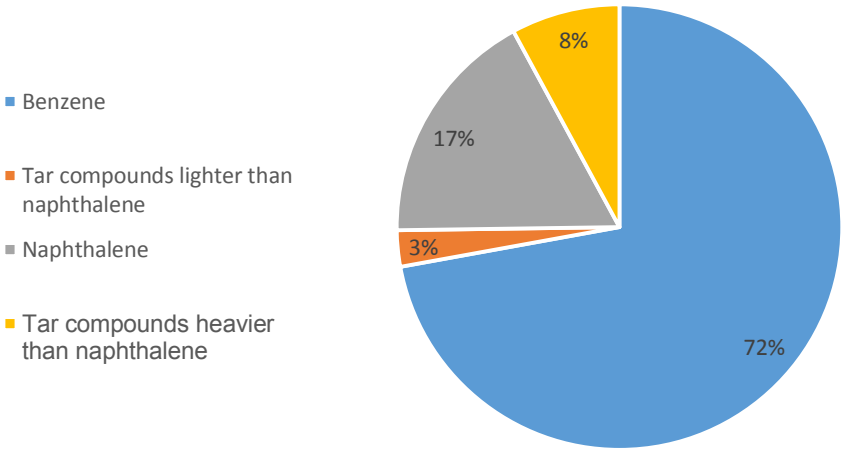

Figure 2. Measured tar composition of steam-oxygen gasification of bark, w-% (Kurkela *et al.,* 2016).

2.1.1 Tar formation

As visualized in Figure 3, composition of tars depends on the reagents and conditions of the gasifier, most important being the temperature (Guan *et al.,* 2016). Increase of temperature in gasifier and in downstream process units can cause formation of heavier tars, while oxygenated tar compounds are formed at lower reaction temperatures (Elliot, 1988). Tar classification according to tar formation instead of structure was proposed by Milne *et al.* (1998), by classifying tars to primary tars, including oxygenated compounds from decomposition of biomass, secondary tars, that include alkylated aromatic one- and two-ring compounds and heteroaromatics, and tertiary tars including aromatic hydrocarbons. This classification is shown in Figure 3, where primary tars are formed at lower temperature, and increase in temperature results to formation of secondary and tertiary tars.

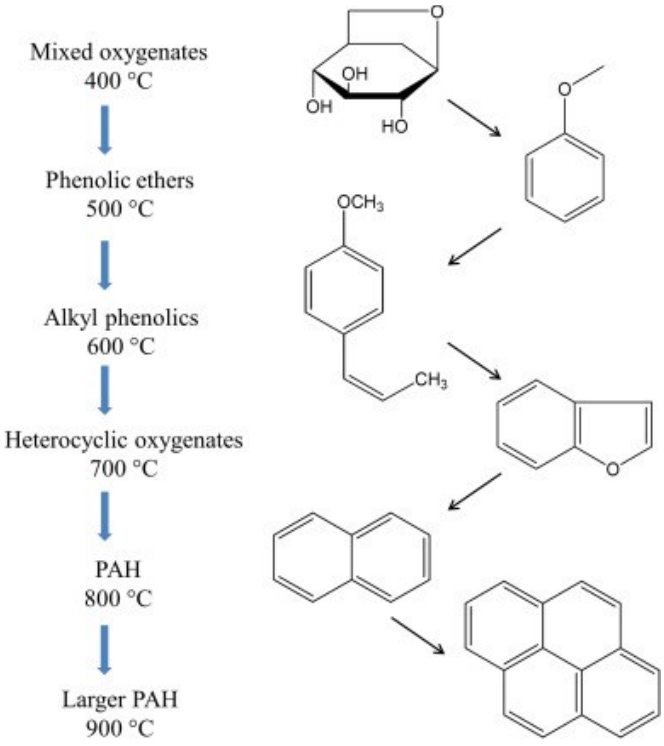

Figure 3. Tar formation scheme in biomass gasification and pyrolysis (Guan *et al.,* 2016).

Kiel *et al.* (2004) studied the effect of residence time on tar formation in gasification in fluidized bed reactor. Increase in gas phase residence time in gasifier from 1.2 s to 5.4 s increased the amount of 2-3 ring and 4-7 ring tars 25% and 286%, respectively.

Increase of residence time decreased the formation of lighter tars, while the fraction of heavy tars of all tars increased from 23 % to 39 % (Kiel *et al.,* 2004). On the other hand, Tuomi *et al.* (2005) obtained no increase in heavy tar formation in studies with residence time in tar filtration of 30-40 s. However, they proposed polymerization of lighter tars to heavy tar compounds undetectable to analysis methods used and coke deposition in filter might explain the difference to previous results by Kiel *et al.* (2004) (Tuomi *et al.,* 2015).

Tars are also formed due to thermal reactions of ethylene, and tar formation is promoted by increase in reaction temperature, reaction pressure and residence time (Kaisalo *et al.*, 2015a). Elevated pressure and high temperature increase especially the formation of heavier tars (Kaisalo *et al.*, 2015a). Ethylene present in gasification product gas can lead to tar formation in high temperature downstream process units (Kaisalo *et al.*, 2015a).

2.1.2 Tar decomposition

Multiple reactions are included in tar decomposition, forming a complex reaction system. The reaction pathway is dependent on for example the component distribution in the feed gas (Devi *et al.*, 2005; Simell *et al.*, 1997), temperature (Rönkkönen *et al.*, 2011b; Simell *et al.*, 1997) and catalyst (Devi *et al.*, 2005; Rönkkönen *et al.*, 2011b). The most important tar decomposition reactions include steam reforming, thermal cracking and hydrocracking, dry reforming and hydrocarbon decomposition (Devi *et al.* 2005; Simell *et al.* 1997), which are presented in Table 1.

Table 1. Tar decomposition reactions (Devi *et al.* 2005; Simell *et al.* 1997).

Reaction	Reaction equation	Equation no.
Steam reforming	$C_nH_m + n\,H_2O \rightarrow n\,CO + \left(n + \frac{x}{2}\right) H_2$	1
Cracking	$C_nH_m \rightarrow C_mH_y + r\,H_2$	2
Hydrocracking	$C_nH_m + \frac{4n - m}{2}\,H_2 \rightarrow n\,CH_4$	3
Dry reforming	$C_nH_m + n\,CO_2 \rightarrow 2n\,CO + \frac{m}{2}\,H_2$	4
Hydrocarbon decomposition	$C_nH_m \rightarrow n\,C + \frac{m}{2}\,H_2$	5

In addition to tar decomposition reactions, equilibrium reactions of the compounds in gasification gas affect the product distribution and chemistry of tar decomposition reactions (Simell *et al.* 1997). These reactions include water-gas shift (Equation 6) and methanation (7) reactions, affecting the product distribution in gasification gas, as well as methane decomposition (8), carbon gasification (9 and 10) and Bouduard reaction (11), interacting with carbon formed on the surfaces of the reactor and catalyst. Ammonia synthesis (12) and its reverse reaction convert the ammonia formed in gasification to nitrogen.

Table 2. Equilibrium reactions of gasification gas components (Simell *et al.* 1997).

Reaction	Reaction equation	Equation no.
Water-gas shift	$\mathrm{CO} + \mathrm{H_2O} \leftrightarrow \mathrm{CO_2} + \mathrm{H_2}$	6
Methanation	$\mathrm{CO} + 3\,\mathrm{H_2} \leftrightarrow \mathrm{CH_4} + \mathrm{H_2O}$	7
Methane decomposition	$\mathrm{CH_4} \leftrightarrow \mathrm{C} + 2\,\mathrm{H_2}$	8
Carbon gasification	$\mathrm{C} + \mathrm{H_2O} \leftrightarrow \mathrm{H_2} + \mathrm{CO}$	9
	$\mathrm{C} + 2\,\mathrm{H_2O} \leftrightarrow \mathrm{CO_2} + 2\,\mathrm{H_2}$	10
Bouduard reaction	$\mathrm{CO_2} + \mathrm{C} \leftrightarrow 2\,\mathrm{CO}$	11
Ammonia synthesis	$\mathrm{N_2} + 3\,\mathrm{H_2} \leftrightarrow 2\,\mathrm{NH_3}$	12

The reactivity of tar compounds in decomposition varies according to compound. Coll *et al.* (2001) and Artetxe *et al.* (2017) studied the reactivity of biomass tar model compounds in steam reforming reactions on nickel catalysts. Generally, naphthalene (Coll *et al.,* 2001) and methyl naphthalene (Artetxe *et al.,* 2017) are the least reactive tar compounds, followed by multiple-ring aromatic compounds. Benzene, non-aromatic compounds such as indene and oxygen-containing tar compounds are the most reactive tar components (Coll *et al.,* 2001; Artetxe *et al.,* 2017).

2.2 Deactivation of tar decomposition catalysts

Economic feasibility of catalyst is highly dependent on two factors, activity and lifetime of the catalyst (Yung *et al.,* 2009). Major mechanisms for deactivation of syngas conditioning catalysts are coking and sulphur poisoning (Rostrup-Nielsen and Christiansen, 2011; Yung *et al.,* 2009). High temperature decreases both,

deactivation due to poisoning (Hepola *et al.,* 2000) and carbon deposition (Kaisalo *et al.,* 2015b). However, high temperature increases irreversible catalyst deactivation due to metal particle sintering (Sehested, 2006).

2.2.1 Catalyst deactivation through coking

Carbon formation on the surface of the catalyst can cover the metal particles and prevent the adsorption of reactants on active sites thereby deactivating the catalyst (Forzatti and Lietti, 1999; Yung *et al.,* 2009). At high temperatures of over 600 °C, formation of pyrolytic coke via thermal cracking and polymerization is the main route for deactivation due to carbon deposition (Rostrup-Nielsen and Christiansen, 2011). The reaction occurs mainly through the decomposition of hydrocarbons directly to carbon (Equation 5) or through olefin formation (Equation 13) (Kaisalo *et al.,* 2015b). Coke formation is affected also by methane decomposition (Equation 8), carbon gasification (Equations 9 and 10) and Bouduard (Equation 11) reactions introduced before (Kaisalo *et al.,* 2015b; Rostrup-Nielsen and Christiansen, 2011). Whisker coking, in which carbon accumulation on active metal particle causes growth of a carbon fibre "whiskers" (Rostrup-Nielsen and Christiansen, 2011), is inhibited at temperature of over 700 °C due to presence of H_2S (Kihlman *et al.,* 2018).

$$C_nH_m \rightarrow \text{olefins} \rightarrow \text{coke} \tag{13}$$

Coking reactions follow pathway of carbon activation on catalyst surface for reaction and nucleation with other activated carbon to C-C bond to form coke on the catalyst surface (Yung *et al.*, 2009). Reaction pathways for activated carbon are presented in Figure 4. The step sites of catalyst particles are the most active for the steam reforming reactions, as well as for the nucleation causing carbon formation and coking deactivation of the catalyst (Rostrup-Nielsen and Christiansen, 2011, Bengaard *et al.,* 2002). Different surface structures of catalyst particles, including corner, step and terrace sites are presented in Figure 5.

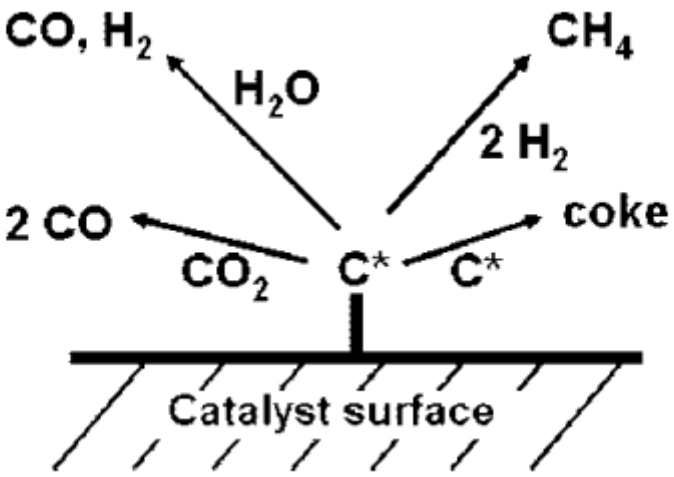

Figure 4. Reaction pathways for activated carbon on catalyst surface (adapted from Yung *et al.,* 2009).

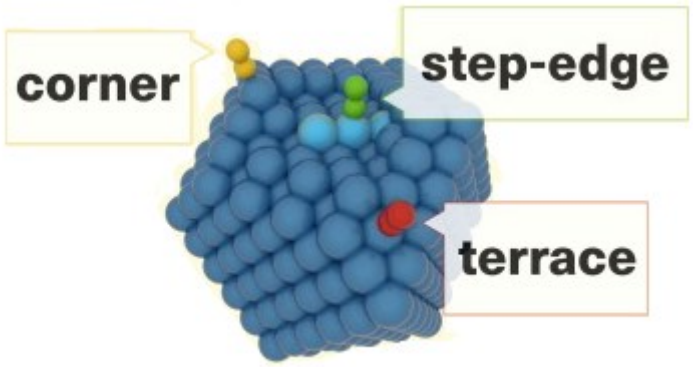

Figure 5. Surface structure of a catalytic metal particle (adapted from Ligthart *et al.*, 2016).

Coking tendency is also affected by the reactants. According to model component studies, increasing number of aromatic rings in tar component increases the tendency for coke formation (Coll *et al.*, 2001). Artetxe *et al.* (2017) and Koike *et al.* (2015) reported more coke formation in steam reforming of oxygenates, such as phenol, furfural and anisole, than tars without heteroatoms.

Coking tendency of catalyst can be decreased by promoting other reaction pathways presented in Figure 4. For example, CeO_2 support, with ability for high H_2O storage, promotes formation of CO and H_2 (Miyazawa *et al.*, 2006). On the other hand, the number of sites suitable for carbon nucleation can be decreased for example by

addition of Au promoter (Besenbacher, 1998). Also sulphur poisoning of active step sites ceases carbon deposition by blocking the sites active in coke formation (Yung *et al.,* 2009; Bengaard *et al.,* 2002). In addition, carbon accumulation can be avoided with high temperature, which is thermodynamically more favorable for gasification of carbon (Equations 9 and 10) (Kaisalo *et al.,* 2015b).

2.2.2 Poisoning by sulphur

Strong selective adsorption of sulphur components on catalytically active sites prevents reactants from reacting on those sites (Forzatti and Lietti, 1999; Yung *et al.*, 2009). In gasification gas, sulphur components, mainly H_2S and COS are present in the range of 50-500 ppm (Kurkela *et al.*, 2016; Kuramochi *et al.,* 2005). Sulphur compounds adsorb mainly on catalytically active step sites of metal catalyst particles (Bengaard 2002), therefore decreasing the overall reaction rate. As previously mentioned, step sites are as well the reactive sites for carbon formation reactions, and presence of H_2S has a decreasing effect on deactivation of the catalyst by coking (Bengaard *et al.,* 2002; Rostrup-Nielsen and Christiansen, 2011).

Effect of sulphur on the activity of the catalyst is more significant for the decomposition rate of tar model compounds toluene and benzene at high pressure of 20 bar, compared to tests at 5 bar (Hepola, 2000). Increase of temperature decreases the possibility for sulphur compound adsorption on catalyst due to shift in reaction thermodynamic equilibrium and promotes desorption of sulphur by hydrogenation, occurring mainly at temperature over 850 °C (Hepola, 2000). Space velocity does not significantly affect the effect of sulphur poisoning on conversion of tar compounds (Hepola, 2000).

2.3 Nickel catalysts

Due to relatively low price (Kaisalo *et al.*, 2015b), high activity in reforming reactions (Rönkkönen *et al.,* 2010), and ammonia conversion efficiency (Rönkkönen *et al.,* 2011b), nickel is widely researched catalyst for tar decomposition. Poisoning due to sulphur components (Hepola, 2000), as well as high activity towards coke formation (Kaisalo *et al.,* 2015b), are the downsides of nickel catalysts.

Main reactions for tar decomposition on Ni particles supported on Al_2O_3 are dry reforming (Equation 4) and steam reforming (1) reactions (Simell *et al.*, 1997). At high temperature of 900 °C, dry reforming is favored (Simell *et al.*, 1997). To avoid sulphur poisoning of nickel catalyst in tar decomposition, operation of reactor at temperature of at least 900 °C is proposed by Hepola (2000).

Coking tendency of nickel is promoted due to carbon dissolving and diffusion in the metal (Trimm, 1997). Bengaard *et al.* (2002) proposed that step site with length of 2.5 nm is needed for stable carbon island nucleation according to density functional theory (DFT) calculations.

High metal loading for nickel catalysts has been studied by Chen *et al.* (2013) and Garbarino *et al.* (2013). Chen *et al.* (2013) found that increasing metal loading from 2 w-% to 8 w-% increased the H_2 yield of toluene CO_2 reforming on Ni catalyst supported on palygorskite mineral at temperatures of 650 - 800 °C. Similarly, Garbarino *et al.* (2013) found the increasing effect on activity of increased nickel loading, while Ni catalyst with loading of 39 w-% and particle size of 25 nm showed the highest activity when compared to catalyst with metal loading of 16 w-% and particle size of 10 nm in steam reforming of mixture of ethanol and phenol at temperatures of 600 - 750 °C. High metal loading is required for successful nickel catalysts. However, also other parameters, such as active metal surface area, are essential for catalyst optimization (Ross, 2012).

2.4 Precious metal catalysts

Precious metals catalysts have gained attention as potential catalysts for tar decomposition reactions due to their high resistance towards sulphur poisoning and activity in decomposition of tar components (Rönkkönen *et al.,* 2010). Problem with precious metals is the high cost compared to nickel (Rönkkönen *et al.,* 2010). In addition to Ni, the highest reforming activities have been achieved with rhodium catalysts (Yung *et al.,* 2009).

Results of Xie *et al.* (2012), shown in Figure 6, highlighted the sulphur tolerance of Rh catalysts in steam reforming of paraffinic hydrocarbons at high temperature when compared to other noble metal catalysts. While other catalysts were deactivated due

to coke formation in presence of sulphur compounds, Rh catalyst supported on Al_2O_3 stood out with high activity for steam reforming of paraffins at 800 °C (Xie *et al.*, 2012).

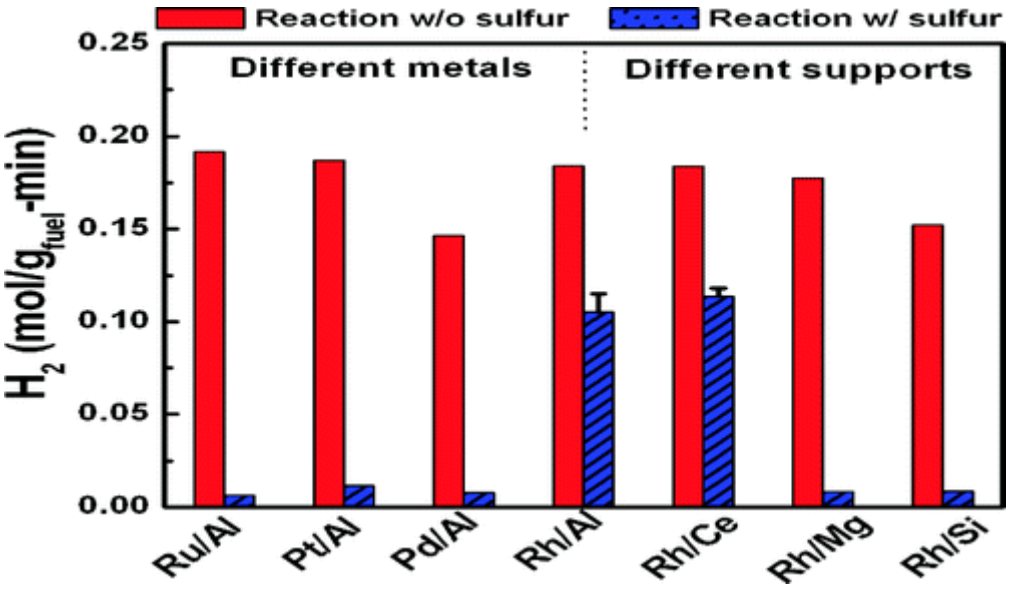

Figure 6. Hydrogen production performance of noble metal catalyst with loading of 2 w-% supported on Al_2O_3 and Rh catalysts supported on metal oxide in steam reforming of normal paraffins at 800 °C. Reaction with sulphur: 350 ppm by weight 3-methylbenzothiophene (adapted from Xie *et al.*, 2012).

In addition to rhodium, also other precious metals have been studied for reforming reactions. Iridium as an active metal for steam reforming of methane was studied by Mei *et al.* (2014). Ir with metal loading of 5 w-% formed well-dispersed particles and high metal surface area on $MgAl_2O_4$ spinel support, and out-performed Rh catalyst in steam reforming of methane, partly due to smaller particle size of Ir (Mei *et al.,* 2014). Activity of iridium has been recognized also by Wei and Iglesia (2004).

At high temperature of over 800 °C, tar decomposition on Rh catalyst mainly occurs via steam reforming (Equation 1) and steam dealkylation of toluene to benzene, hydrogen and carbon monoxide (Rönkkönen *et al.,* 2011b). Ru is only precious metal active towards decomposition of ammonia, while Pt and Pd are active in oxidation reactions of tars (Rönkkönen *et al.,* 2011b).

For steam reforming reaction, the edge and corner sites of Rh define the rate of reaction (Ligthart *et al.,* 2011). Increase of Rh content from 0.5 w-% to 5.0 w-% does

not significantly increase total catalytic activity if H_2S is present (Rönkkönen *et al.,* 2011a). Especially at temperature above 655 °C, Rh catalyst with 0.5 w-% loading presented superior performance per gram of Rh in production of H_2 compared to catalyst with Rh loading of 1.5 w-% (Polychronopoulou *et al.,* 2004).

The negative effect of sulphur poisoning on Rh catalyst decreases at temperature above 800 °C (Rönkkönen *et al.,* 2011a). Similarly, Xie *et al.* (2010) observed a significant increase in stability of Rh catalyst in steam reforming of paraffinic hydrocarbons with presence of sulphur compounds at temperatures of 550 °C and 800 °C. Xie *et al.* (2012) proposed the superior sulphur tolerance of rhodium catalysts to result from resistance for electron withdrawing effect of sulphur, as well as promotion of sulphur oxidation, decomposition of oxidized species and sulphur migration to suitable catalyst support (Xie *et al.,* 2010).

Additionally, Rh does not dissolve carbon which decreases coking tendency (Trimm, 1997). Net formation rate of coke on noble metal catalysts is also decreased due to faster kinetics of carbon gasification (Equations 9 and 10) (Kaisalo *et al.,* 2015b, Xie *et al.,* 2012). However, poisoning due to deposition of potassium species to Rh catalysts increases the activity in small concentrations (< 30 mg K / g Rh) but causes severe deactivation in high concentrations (> 150 mg K / g Rh). (Wangen *et al.,* 2011)

2.5 Effect of support on Rh and Ni catalysts

The direct effect of Al_2O_3, ZrO_2, TiO_2, CeO_2 and MgO supports on activity of Ni catalyst in steam reforming of pyrolysis tar in temperature range of 550-650 °C on nickel catalyst is minor, unless support affects the dispersion and surface area of Ni metal. (Miyazawa *et al.,* 2006). Al_2O_3 or ZrO_2 supports have no effect on reforming performance of Rh catalysts neither in steam reforming or dry reforming reactions at 600 °C (Wei and Iglesia, 2004) nor CeO_2, $CeZrO_2$, ZrO_2 or SiO_2 supports in steam reforming of methane at 500 °C (Ligthart *et al.,* 2011).

High active metal surface area has been recognized as cause for high activity of nickel supported on Al_2O_3 (Park *et al.,* 2010). Also, Shang *et al.* (2017) reported high stability against sintering for Ni steam reforming catalyst supported on porous Al_2O_3 due to the formation of $NiAl_2O_4$ spinel.

Intimate interaction of rhodium and Al_2O_3 support promotes high dispersion and small particle size for Al_2O_3-supported Rh-catalysts (Xie *et al.,* 2012). Rh particles of 1-3 nm (Xie *et al.,* 2012) and 1.2-1.3 nm (Italiano *et al.,* 2018) in catalysts with Rh loadings of 2 w-% and 0.5 w-%, respectively, have been reported for Rh catalysts. No significant sintering of Rh was detected on porous Al_2O_3 support in steam reforming of methane in experiment of Italiano *et al.* (2018). Also, Wang and Ruckenstein (2000) recognized the effect of support on Rh catalyst, while the highest activities for catalysts with 0.5 w-% Rh were reported on γ-Al_2O_3 and MgO supports in methane dry reforming on Rh catalysts with various supports. The highest Rh surface area per gram catalyst was measured for γ-Al_2O_3, SiO_2, Y_2O_3 and MgO among tested catalysts but significant deactivation of catalysts supported on Y_2O_3 and SiO_2 was reported (Wang and Ruckenstein, 2000).

In addition to role of Al_2O_3 support for the surface area of Rh, Xie *et al.* (2012) proposed also role of Al_2O_3 support as sulphur trap. The ability of Rh catalyst to oxidize sulphur compounds is utilized as oxidized sulphur species migrate from metal surface to surface of Al_2O_3 support (Xie *et al.*, 2012).

Al_2O_3 or ZrO_2 supports for steam reforming of naphthalene as tar model compound were tested by Ferella *et al.* (2013) in pilot-scale reactor. Both supports alone showed similar activity in steam reforming in temperature range of 500 - 900 °C, but H_2 selectivity of zirconia was significantly higher, 117% versus 63% of Al_2O_3 support at 900 °C (Ferella *et al.,* 2013). Viinikainen *et al.* (2009) studied role of zirconia support in decomposition of naphthalene and toluene. Zirconia showed activity in decomposition of model tar compounds at temperature under 800 °C, but when temperature exceeded 800 °C, similar activities were observed for ZrO_2 -washcoated and blank cordierite monoliths (Viinikainen *et al.*, 2009).

Mei *et al.* (2014) prepared 5 w-% Rh on Al_2O_3 and $MgAl_2O_4$ spinel supports for methane steam reforming reaction in gas mixture representing gasification gas at 850 °C. Negligible deactivation for $MgAl_2O_4$ spinel supported catalyst in 80 h experiment was reported, while γ-Al_2O_3 supported catalyst suffered an activity loss of 15 % (Mei *et al.,* 2014). Coking due to acidic nature of the Al_2O_3-support was proposed as cause for deactivation (Mei *et al.,* 2014).

High oxygen storage capacity and dissociation of water on surface of CeO_2 has been recognized in reaction tests for both rhodium (Xie *et al.,* 2012) and nickel (Miyazawa *et al.,* 2006). Coke formation on CeO_2 supported Ni catalyst was decreased due to CeO_2 promoted reaction of active carbon and steam in steam reforming of pyrolysis tar (Miyazawa *et al.,* 2006). Similar results have been presented also by Xie *et al.* (2012) in steam reforming of paraffins at 800 °C on Pt/CeO_2 and Rh/CeO_2 catalysts and Park *et al.* (2010) in steam reforming of benzene on Ni/CeO_2(75 w-%)–ZrO_2(25 w-%) at 700 °C. On the other hand, Italiano *et al.* (2018) studied Rh supported on 25% CeO_2-Al_2O_3 in steam reforming of methane at 700 - 800 °C, and similar activity was measured for CeO_2- Al_2O_3 as Al_2O_3 alone as support.

To conclude, rhodium and nickel have been studied as catalysts for tar decomposition and other similar reactions, for example steam reforming and dry reforming of various hydrocarbons, at high temperature. Deactivation due to coking and sulphur poisoning are main issues to be solved in design of optimal catalyst for tar reforming. Al_2O_3 support has been widely studied for both active metals, and formation of stable catalysts with high active metal surface area on alumina has been reported.

3 Rh and Ni catalyst by atomic layer deposition

Atomic layer deposition (ALD) is a technique for vapor-phase deposition of films and nanoparticles on various supports (O'Neill, 2015; Puurunen, 2005). In this chapter, possibilities of ALD for design of nickel and rhodium metal catalysts are reviewed.

3.1 Atomic layer deposition technology

ALD process consists of cycles of reactions, in which one of the reactants is alternatively introduced (O'Neill, 2015; Puurunen, 2005). Principle of ALD cycle is presented in Figure 7. First, one of the reactants, typically the metal precursor, is introduced (Pulse A in Figure 7). After the reaction ((b) in Figure 7) of the first reactant and active surface sites reaches completion, excess reactants and reaction byproducts are removed from reactor by inert gas or high vacuum ((c) in Figure 7).

After purge, other reactant, typically oxygen-containing compound or hydrogen, is introduced ((Pulse B in Figure 7) and it reacts with the ligands left in chemisorbed metal precursor ((d) in Figure 7). Then, reactor is purged again and it is ready for introduction of metal precursor for deposition of next layer ((e) in Figure 7) (O'Neill *et al.,* 2015; Puurunen, 2005).

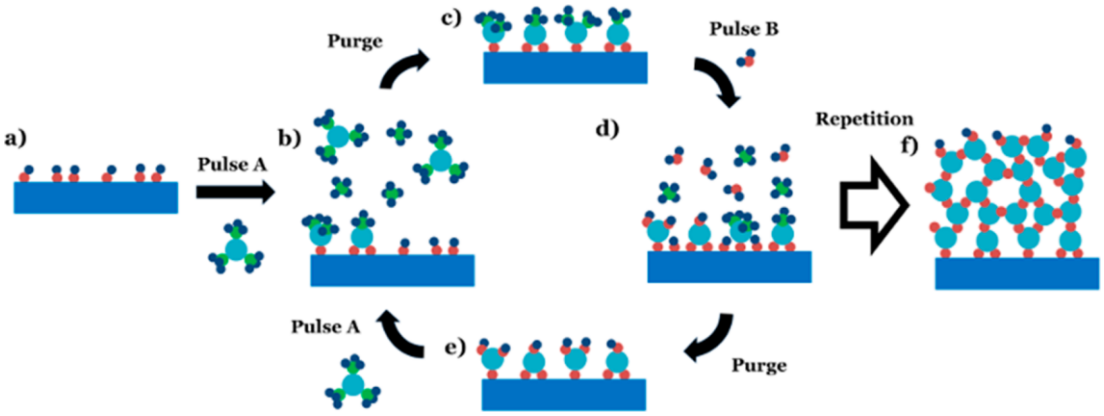

Figure 7. Principle of ALD: a) surface with reactive sites; Pulse A) precursor pulse; b) reaction with precursor; c) purged surface after reaction with precursor; Pulse B) Reactant pulse for other reactant; d) reaction with other reactant; e) surface after both reactions; f) surface after 5 ALD cycles (adopted from O'Neill *et al.,* 2015).

Sufficient exposure time is required to reach the surface saturation of reactants for high surface area catalyst support within pulse time (Lakomaa, 1994). Growth of ALD is limited by the saturation of active sites in surface of substrate, for example OH-groups on Al_2O_3 surface (Lindblad *et al.,* 1994), or the steric hindrance of the precursor ligands (Puurunen, 2005).

In addition to surface and ligands, the nature of ALD-grown layer is dependent on arrangement of the material on the surface, defined as growth mode (Puurunen, 2005). Growth mode affects if either film or nanoparticles is formed on the surface of substrate (Singh *et al.*, 2017).

3.2 Atomic layer deposition for catalysis

Due to adsorption-controlled self-limited nature of the technique, atomic scale control of deposited layer and reproducibility, ALD has been widely studied for preparation of novel catalysts (Haukka *et al.*, 1999; O'Neill *et al.*, 2015; Singh *et al.*, 2017). ALD provides possibility to control the amount of metal deposited and thus the metal loading via amount of deposition cycles (Lindfors, 1994), as well as surface density of reactive sites (Lindblad *et al.,* 1994; Puurunen, 2005) and size of particles deposited (Mackus *et al.*, 2015).

As described earlier, step sites are often the most important sites for catalytic reactions. Deng *et al.* (2011) proposed that formation of ALD film instead of nanoparticles led to activity of several magnitudes lower compared to similar catalyst with nanoparticles in the oxidation of the O-C-O bonds in 1-methoxy-2-methyl-2-propanol on cobalt catalyst. Formation of nanoparticles instead of film is desired in preparation of catalysts by ALD, according to results of Deng *et al.* (2011).

In addition to deposition of catalytically active material deposition, ALD provides opportunity for catalyst modification. For example, ALD layer selectively deposited on catalytic material has been reported to decrease deactivation of catalyst by coking and sintering (Lu *et al.*, 2012) and to modify the product distribution (Yi *et al.*, 2015).

3.3 Ni catalysts prepared by atomic layer deposition

Nickel catalysts have been prepared by ALD method and tested at least for toluene hydrogenation (Lindblad *et al.,* 1994; Lindfors, 1994) and oxidation (Jeong *et al.,* 2014), propylene hydrogenation and propylene hydrogenolysis (Gould *et al.,* 2013) and methane dry reforming (DRM) (Kim *et al.,* 2013; Gould *et al.,* 2015; Shang *et al.,* 2017, Shang *et al.,* 2018). Especially dry reforming experiments represented similar high temperature of over 800 °C comparable to the harsh conditions of hot gas filtration of biomass gasification gas. Most of the experiments have used Al_2O_3 as catalyst support, however, also SiO_2 (Kim *et al.,* 2013, Jeong *et al.,* 2014) has been studied.

Particle sizes of 2 - 4 nm, that are extraordinary for Al_2O_3-supported Ni catalysts with metal loadings of 5 - 20 w-% prepared by traditional methods (Gould *et al.,* 2013), have been synthesized by ALD method (Gould *et al* 2013; Shang *et al* 2017; Lindblad *et al.,* 1994). These catalysts with small particle size and high loading, leading to high Ni surface area and dispersion, have been reached by using ALD process of either nickel *bis*-cyclopentadienyl ($NiCp_2$) and H_2 (Gould *et al* 2013; Shang *et al* 2017), or nickel *bis*-acetyl acetonate ($Ni(acac)_2$) and air (Lindblad *et al.,* 1994). In SiO_2 supported catalysts, particle size of around 10 nm and dispersion of 56 % have been reached with ALD process of $NiCp_2$ and water (Kim *et al.,* 2013; Jeong *et al.,* 2014).

In addition to exceptional dispersion and particle size, ALD catalysts deposited on porous Al_2O_3 by synthesis of $NiCp_2$ and H_2 stand out due to strong particle-support interaction (Shang *et al*, 2017). ALD-prepared nickel and porous Al_2O_3 support form highly stable $NiAl_2O_4$ spinel, which results in high dispersion and thermal stability of nickel clusters on surface (Shang *et al.*, 2017). As metallic nickel is the most reactive form of Ni (Chen and Ren, 1994), $NiAl_2O_4$ spinel reduction is needed for catalyst activation. Shang *et al.* (2017) observed that the gas mixture of CO and H_2 produced in dry reforming can activate the highly stable $NiAl_2O_4$ spinel at 850 °C, while reduction of NiO is easier. For hydrogen alone, temperature-programmed reduction (TPR) results of Barroso-Quiroga and Castro-Luna (2010) showed reduction temperatures of 430 °C for NiO and 960 °C for $NiAl_2O_4$ on porous Al_2O_3 support.

Porous γ-Al_2O_3 (Shang *et al.*, 2017) and α-Al_2O_3 (Shang *et al.*, 2018) supported Ni-ALD -catalysts have shown high activity in methane dry reforming (DRM) reaction at high temperature of 850 °C when compared to catalysts prepared by incipient wetness impregnation (IWI). The effect is mainly due to exceptionally high Ni dispersion and thereby, high Ni surface area, as well as previously described reducibility of $NiAl_2O_4$ spinel on porous support (Shang *et al.*, 2017). In addition, coking might be decreased due to small size of nickel nanoparticles leading to decrease of suitable sites for stable carbon nucleation and carbon cluster formation, as described earlier (Shang *et al.*, 2017, Bengaard *et al.*, 2002).

However, sintering is a serious deactivation problem for DRM catalyst prepared by ALD. Heavy sintering was detected for example by Gould *et al.* (2015), when the average particle diameter of Ni catalyst supported on nonporous γ-Al_2O_3 with surface

area of 40 m^2/g increased from 3.5 nm to 9.4 nm during 200 h DRM reaction at 600 °C. Catalyst lost total 64 % of its activity, 60 % during first 25 h on stream. Deactivation followed well the sintering kinetics model presented by Bartholomew (1993) (Gould *et al.,* 2015). In addition to catalyst deactivation due to sintering, increasing size of Ni particles can also cause coking problems, since larger particles are more active in coke formation (Bengaard *et al.*, 2002), as presented by Gould *et al.* (2015) by testing pre-sintered particles for DRM. Sintering can be prevented for example by porous support (Shang *et al.,* 2017) or additional ALD-Al_2O_3 coating (Shang *et al.,* 2018) to improve the interaction of support and metal.

3.4 Rh catalysts prepared by atomic layer deposition

Rhodium is one of the least studied noble metals in terms of ALD processes (Hämäläinen *et al.*, 2014). In addition to small amount of ALD studies, not much research has been conducted about catalysts with Rh as active metal deposited by ALD. In addition to patent of Elam *et al.* (2010), only Li *et al.* (2018) have published their results of rhodium catalysts by ALD. ALD process for Rh deposition has been presented by Aaltonen *et al.* (2005), Hämäläinen *et al.* (2009) and Hämäläinen *et al.* (2013).

In studies of Li *et al* (2018), 2.4 w-% Rh particles on γ-Al_2O_3 by ALD process of $Rh(acac)_3$, ozone and hydrogen showed higher activity and stability in methane dry reforming compared to similar catalysts (2.7 w-% Rh) prepared by IWI method. While reaction ignited at the same temperature of 250 °C on both catalysts, ALD catalyst showed higher activity in CH_4 conversion of about 20 percentage points until reaching full conversion at 800 °C.

At reaction temperature of 500 °C, neither catalyst showed signs of deactivation during 15 h with CH_4 conversions of 23 % for ALD catalyst and 10 % for IWI catalyst (Li *et al.*, 2018). However, in 15 h experiment at 800 °C, decrease of conversion from 95 % to 90 % and from 90 % to 78 % with ALD and IWI catalysts, respectively, was detected. As no signs of coke formation were detected, the decrease is supposed to occur due to sintering. Increases of Rh particle sizes from 1.8 nm to 2.8 nm and from 4.2 nm to 7.3 nm were detected for ALD and IWI catalysts, respectively, in transmission electron microscopy (TEM) images (Li *et al.*, 2018).

Higher activity of ALD catalysts is proposed to be due to higher Rh surface area as a consequence of smaller Rh particle size of 1.8 nm compared to 4.2 nm of IWI catalyst, (Li *et al.*, 2018). In addition to particle size, higher proportion of Rh present in catalyst is in metallic form Rh^0, is proposed to explain higher activity by Li *et al.* (2018). Proportion of metallic Rh, which is the active form of rhodium for methane activation in DRM reaction (Pakhare *et al*, 2014), was higher compared to Rh^{3+} in catalyst prepared by ALD, according to X-ray photoelectron spectroscopy (XPS) analysis (Li *et al.*, 2018). Higher proportion of Rh^0 is proposed to occur due to thermodynamic limitations of reduction reaction following the Rh deposition by IWI method, while Rh is deposited directly in metallic form in ALD method (Li *et al.*, 2018; Aaltonen *et al.*, 2005; Hämäläinen *et al.*, 2014).

4 Catalytic filters and membranes for gas phase applications

Catalytic filters are utilized for simultaneous separation and reaction in filter medium. In addition to syngas cleaning (Nacken *et al.,* 2010; Kivelä, 2018), catalytic filtration is studied for example for soot oxidation (Russo *et al.,* 2003), as well as for removal of particulate matter, volatile organic compounds (VOCs) (Pina *et al.*, 1996) and nitrogen oxides (NOx) (Schaub *et al.*, 2003; Heidenreich *et al.,* 2008) from gas flow. In this chapter, multiple factors affecting reactivity in catalytic membranes and filters are reviewed. However, the effect of process conditions, such as pressure and superficial velocity, was earlier extensively reviewed and studied by Kivelä (2018), and is not reviewed in this work.

4.1 Pore diameter and mass transfer

In catalytic flow-through membrane applications, membrane is operated in dead-end mode, and while reactants are flowing through the membrane, intensive contact is provided for reactants with the catalyst (Westermann and Melin, 2009). Pina *et al.* (1996) and Zalamea *et al.* (1999) studied catalytic membranes for VOC oxidation as an example of mass-transfer hindered reaction. Pt-catalyst deposited on γ-Al_2O_3 coated membrane with 200 nm diameter pores was effective in toluene oxidation

(Zalamea *et al.*, 1999). Increase of pore size to 2-10 µm pores transformed the flow in pores from diffusive dominated flow to mixed regime of diffusive and laminar convective flow. Increase in pore size increased the required combustion temperature for n-hexane and methyl ethyl ketone with 15 - 50 °C in range of 120 °C to 300 °C, but decreased the pressure drop of the membrane (Zalamea *et al.,* 1999). Lower combustion temperature is due to improved mass transfer in smaller pores (Zalamea *et al.,* 1999). The molecules advancing through the membrane with smaller pores collide with membrane walls including the catalytically active sites more often (Zalamea *et al.,* 1999). Small pores force a diffusion-driven flow with only diffusing species. However, smaller pores increase the pressure difference over the membrane needed to keep the volumetric flow through the membrane on same level compared to membrane with higher pore diameter (Zalamea *et al.,* 1999).

The contribution of diffusive (α) and convective flow (β) as function of pressure across the membrane is presented in Equation (14) by Lin and Burggraaf (1991). The activity of the catalytic membrane is higher with diffusion-dominated flow and shift of the flow regime to mixed or convective flow allows higher flow rate with lower pressure drop. On diffusive flow regime, molar flux through the membrane is controlled by the diameter and increase of average pressure over the membrane P_{av} increases the contribution of convective flow.

$$F = 1.06\frac{\epsilon\, r}{L\tau\sqrt{MRT}} + 0.125\frac{\epsilon\, r^2}{L\tau\mu RT}P_{av} = \alpha + \beta P_{av} \quad (14)$$

F is the permeation flux (mol/(m^2 bar s)),
P_{av} is the average pressure across the membrane (bar),
L is the membrane thickness (m),
ϵ is membrane porosity,
M is the molecular weight of the permeating gas (g/mol),
μ is the viscosity of the permeating gas (bar s)
τ is tortuosity,
r is pore radius (m),
T is temperature (K) and
R is gas constant ((bar m^3)/(mol K)).

The effect of pore size was noticed also by Pellin *et al.* (2005) in test runs of AAO membrane with catalytic uniform vanadate-coating applied by ALD technique. Cyclohexane partial oxidation conversions of 3.0% and 4.2% were measured in membranes with pore diameter of 10 nm and 40 nm, respectively (Pellin *et al.*, 2005), which is controversial to results presented by for example Zalamea *et al.* (1999). However, when the conversion was calculated per catalytically active area, significantly higher conversion was achieved with small pore size membrane, as higher activity of membrane with higher pore size was probably due to higher amount of catalyst (Pellin *et al.*, 2005).

4.2 Selective permeability of membrane

Catalytic membranes can also increase the selectivity and conversion in reaction due to selective removal of reaction products by permeability. Kurungot *et al.* (2003) prepared a α-Al_2O_3 membrane with pore diameter of 4.3 nm and Rh/γ-Al_2O_3 catalytic layer for catalytic steam reforming of methane. To improve the separation, catalytic membrane was coated with microporous silica. Due to lower kinetic diameter of hydrogen (2.8 Å) compared to methane (3.7 Å), separation factor of 31 was achieved in permeability test at 525 °C. For reaction test, silica-coated membrane showed conversions exceeding the equilibrium concentration with 36% in atmospheric pressure, temperature of 525 °C and contact time of 0.015 (s g)/cm^3.

Similarly, Amanipour *et al.* (2016) observed methane conversion exceeding the equilibrium in nickel and γ-Al_2O_3 coated membrane with average pore diameter of 285 nm in dry reforming of methane at temperature of 750 °C and pressure of 3 bar. Selectivity of membrane at 650 °C for membrane with 285 nm pore diameter was 3.3 for H_2/CO_2 and 18.1 for H_2/CH_4 (Amanipour *et al.,* 2016).

Catalytic membranes provide intensive contact for reactants with each other and catalyst coated walls (Westermann and Melin, 2009), but they also enhance separation due to different permeability of membranes for example for hydrogen production (Kurungot *et al.,* 2003). However, due to scale difference, for example pore diameter, catalytic membranes and filters are not comparable in every situation.

4.3 Effect of filtrated particles and filter structure

The filtrated particles can have an effect on the reaction taking place in the catalytic filter, as the particles can for example catalyze the reaction or cause deactivation of the catalyst. Tuomi *et al.* (2015) considered the catalytic activity of solid char particles in fly ash of the filter cake to influence tar decomposition and coke formation in filtration of gasification gas. Tar decomposition catalyzed by charcoal proceeds via carbon formation on charcoal and coke gasification (Tuomi *et al.*, 2015; Hosokai *et al.,* 2008). Micropores of char serve as active sites for coke deposition (Hosokai *et al.,* 2008). Especially heavy tars of 2 or more rings are decomposed over charcoal, as for example Hosokai *et al.* (2008) measured conversion of 100 % for naphthalene, phenanthrene and pyrene. Net effect of charcoal on tar conversion in filter depends on the rates of coke formation and carbon gasification (Hosokai *et al.*, 2008; Tuomi *et al.,* 2015).

Russo *et al.* (2003) compared two different Cu-V-K-Cl -activated filter materials, ceramic foam and sintered aluminosilicate monolith for soot removal and oxidation of gas-oil burner exhaust gas. Foam was found to be more efficient in removal, possibly due to deep-bed filtration, which allows the entrance and oxidation of soot particles inside the filter medium, causing better utilization of the catalyst material when more catalyst surface is used, as well as lower pressure drop (Russo *et al.,* 2003). However, also a layer blocking the entrance of particulate matter to the material can be advantageous, since the particles entering the catalytic part of the filter could cause deactivation of active sites due to particle deposition (Heidenreich *et al.,* 2008).

For catalytic filtration, catalyst can either be located for example as catalytic coating of filter medium, as presented in Figure 8 A, or as fixed catalyst bed between two porous filter layers, as presented in Figure 8 B (Nacken *et al.,* 2010). These catalytic filter types were compared by Nacken *et al.* (2010), and higher activity was proven for fixed bed catalyst than for catalytic layer filter candles. This was probably partly due to higher amount and better accessibility of nickel catalyst. While preparation of filters with fixed bed inside can be costly, also method of candle preparation from catalytic foam has been proposed (Nacken *et al.,* 2015).

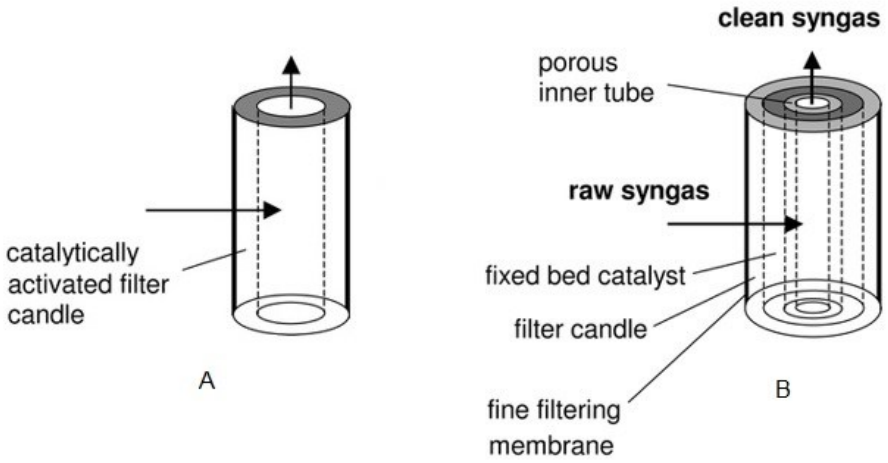

Figure 8. A) Catalytic layer on filter candle; B) fixed bed catalyst bed between two porous tubes (adapted from Nacken *et al.*, 2010).

4.4 Catalyst loading and form

Zhang et al. (2002) deposited Ni and CaO on α-Al_2O_3 filter discs for biomass gasification gas cleaning. No significant increase in activity was found when increasing the nickel loading from 1 w-% to 3 w-% (Zhang *et al.*, 2002). The lack of activity increase was assigned to low surface area of 0.3 m^2/g of the filter disc by Zhang *et al.* (2002), since no adequate active metal surface area is formed on low surface area support. Addition of porous Al_2O_3-coating on discs to increase the surface area was proposed by Zhang *et al.* (2002).

Sulphur deactivation was proposed to cause the lower activity of low surface area catalytic filter discs by Zhang *et al.* (2003). Higher nickel loading catalysts were less prone in terms of activity decrease to increase of H_2S in feed gas. Zhang *et al.* (2003) restated the need for higher nickel loading and dispersion, which however could not be achieved with precipitation-deposition method with urea. Filter disc of higher surface area was proposed to achieve increased nickel surface area by Zhang *et al.* (2003) as well.

Deng *et al.* (2011) studied ALD-coated anodized aluminum oxide membrane (AAO-membrane) for oxidation breaking the O-C-O bonds in 1-methoxy-2-methyl-2-

propanol, cellulose model surrogate. Membrane with thickness of 70 µm and pore diameter of 40 nm was coated with Al_2O_3, and with catalytic cobalt oxide by ALD. However, the deposited cobalt oxide nanoparticles achieved conversion of 4-5 orders of magnitude higher than cobalt oxide ALD-coated membrane. This was probably due to low number of low-coordinated catalytically active cobalt surface atoms, compared to subnanometer particle catalyst. According to results of Deng *et al.* (2011), a film-coated catalyst by ALD can have significantly lower activity than catalyst that is in form of particles.

With their particle-deposited catalyst, Deng *et al.* (2011) observed also the effect of gas flow direction through the membrane on the selectivity of the reaction. When catalyst was deposited on the entrance of the membrane, longer contact time with catalyst promoted the decomposition of C_5 components to C_3 and C_1 components, while catalyst particles on the exit of the membrane promoted formation of C_4 components (Deng *et al.*, 2011). According to these results, the location of the catalyst in the catalytic membrane can significantly affect the product distribution of the catalytic reaction.

Methods for optimization of catalytic layer surface deposition depth in porous membrane have been presented for example by Elam *et al.* (2007), who deposited layers of ZnO, TiO_2, V_2O_5 and Nb_2O_5 in different depths as “stripes” on 70 µm thick AAO membrane with pore size of 56 nm. Elam *et al.* (2007) combined the effect of selectivity of ALD depending on the previous exposures of the surface, as well as Knudsen diffusion, as depth of the precursor exposure is a function of exposure time, for preparation of “stripe coating” of catalytic membrane. Stripe coating could be applied for preparation of catalytic membrane systems with multiple catalytically active zones, intensifying complex reactor system to one membrane (Elam *et al.*, 2007).

5 Experimental

In the experimental part of the thesis project, set of catalytic filters was prepared by ALD, characterized and tested for tar decomposition in reaction experiments. Since most of the process parameters, such as pressure and volumetric flow rate of feed gas, were previously studied in experiments of Kivelä (2018), the experiments of this thesis concentrated on studying the effect of different catalyst properties. The experiments were conducted in laboratories of VTT Technical Research Centre of Finland in Otaniemi, Espoo, Finland.

5.1 Filter materials

Metallic filter discs were provided by GKN Sinter Metals. Different filter materials are presented in Table 3, filters prepared and their properties are presented in Appendix 1, and filter discs are presented in Figure 9. Diameter for all filters was close to 2.50 cm and thickness was 0.30 cm. Void fraction was calculated according to Equation 15 to evaluate the porosity of the filters.

$$\Phi = \frac{V_V}{V_T} = \frac{1-V_M}{V_T} \quad (15)$$

Where

Φ is the void fraction,

V_V is the volume of the void in filter (m^3),

V_T is the total volume of the filter (m^3), and

V_M is the volume of the metal in the filter (m^3).

Table 3. Catalytic filter materials (Data was received from a) GKN Sinter Metals, 2019; b) Baboian, 2016; c) BGH Edelstahl, 2019; d) Resistant Alloy, 2019)

Steel material	Cr, w-% [a]	Ni, w-% [a]	In addition [a]	Density of steel material (g/cm^3) [b, c, d]	Void fraction
1.4767 mod.2	19-22	-	<0.1 w-% of C, 5-6 w% of Al with rare earths	7.2	0.4
AISI 316L	16-18	10-14	<0.03 w-% of C, 2-3 w-% of Mo	7.9	0.5

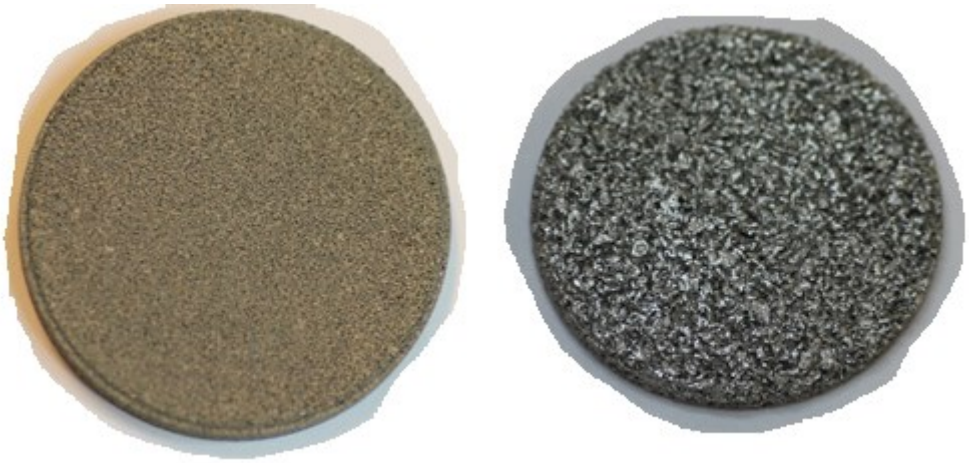

Figure 9. Uncoated filters, M3000416 filter manufactured of 1.4767 mod.2 steel alloy with pores of 160-300 µm on left and SIKA R 100AX filter manufactured of AISI 316L steel alloy on right.

5.2 ALD coatings

ALD coatings for filters were conducted in Picosun SUNALE R-200 ALD reactor. Uniformity and distribution of the deposition in different parts of the reactor chamber was monitored with chips of silicon wafer. Nitrogen (99.9999%) was used as inert purge and carrier gas. Thickness of layer formed on silicon wafer chips was measured by ellipsometry at Sentech SE400adv tool. List of performed ALD runs is presented in Appendix 2.

5.2.1 Alumina coatings

Al_2O_3 coating was deposited on all filters to act as catalyst support. Similar deposition conditions and same ALD recipe were used for all filters to focus on studying the effect of active metal on catalytic properties. Trimethylaluminum (TMA) (SAFC, purity 99%) and H_2O (Milli-Q) were used as precursors. For alumina coatings, filter discs were positioned on metal stand with height of 6 mm providing contact and diffusion of precursor to pores of the filters on both sides of the discs. The stand was set on silicon wafer on the single silicon wafer sample holder of the reactor. The setting of alumina coating of filter discs is presented in Figure 9. 90 cycles of TMA and H_2O were introduced to filter discs at the reactor temperature of 225 °C. Stop-flow setting of the

Picosun tool was used to increase the diffusion of precursors inside the filter, and this coating method is referred as stop-flow coating method in this work.

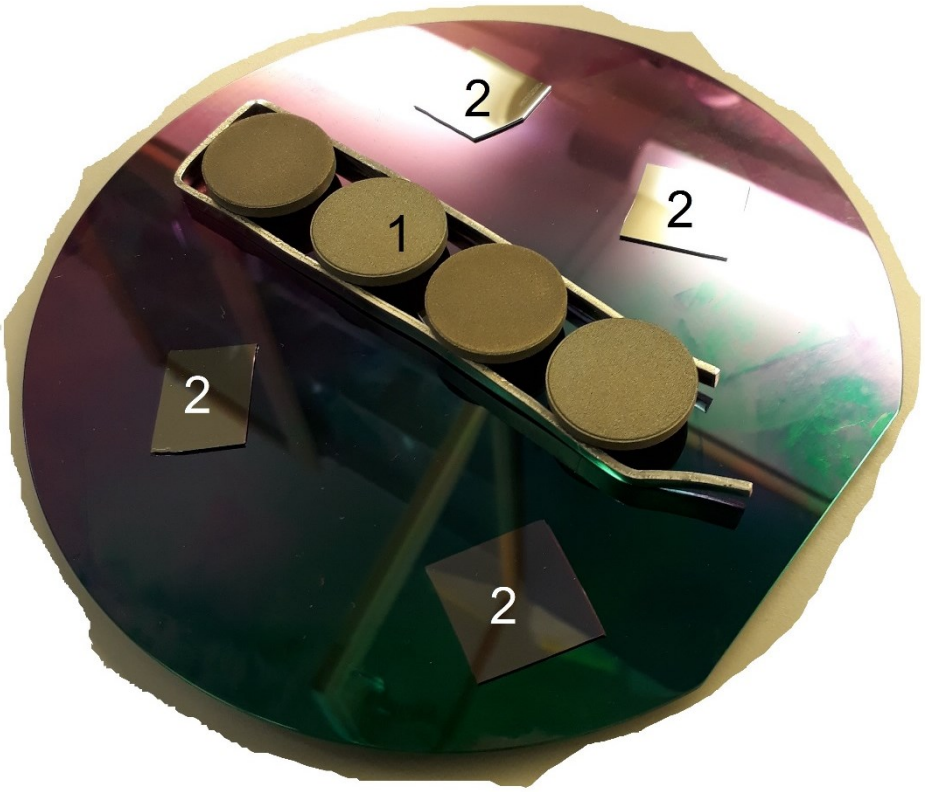

Figure 9: Metallic filters on stand on top of the silicon wafer for alumina deposition (1) and silicon wafer chips to monitor the uniformity of the coating (2).

5.2.2 Nickel oxide coatings

Nickel oxide coatings were deposited using bis(2,2,6,6-tetramethylheptane-3,5-dionato)nickel(II) ($Ni(thd)_2$) and ozone as precursors. $Ni(thd)_2$ (98%) was provided by Strem Chemicals and sublimated at 175 °C. Ozone was generated from oxygen (99.999%) provided by AGA in IN USA, Inc. ozone generator.

Unlike alumina coatings, nickel oxide coatings were performed by precursor flow forced through the filter, referred as flow-through coating. For this purpose, special additional plate prepared in the VTT workshop was installed in the reactor chamber. Setting for NiO coatings is presented in Figure 10. Nickel coatings of 5-300 cycles were performed at 225 °C. As an attempt to confirm the uniform distribution of

precursor on filter surfaces, each reaction step consisted of five consecutive pulses of nickel precursor or ozone, respectively.

In addition, Ni-coating of 1600 ALD-cycles was performed in similar stop-flow deposition set-up as alumina-coatings, presented in Figure 11. Schematic pictures of the deposition methods utilised are presented in Figures 12 and 13.

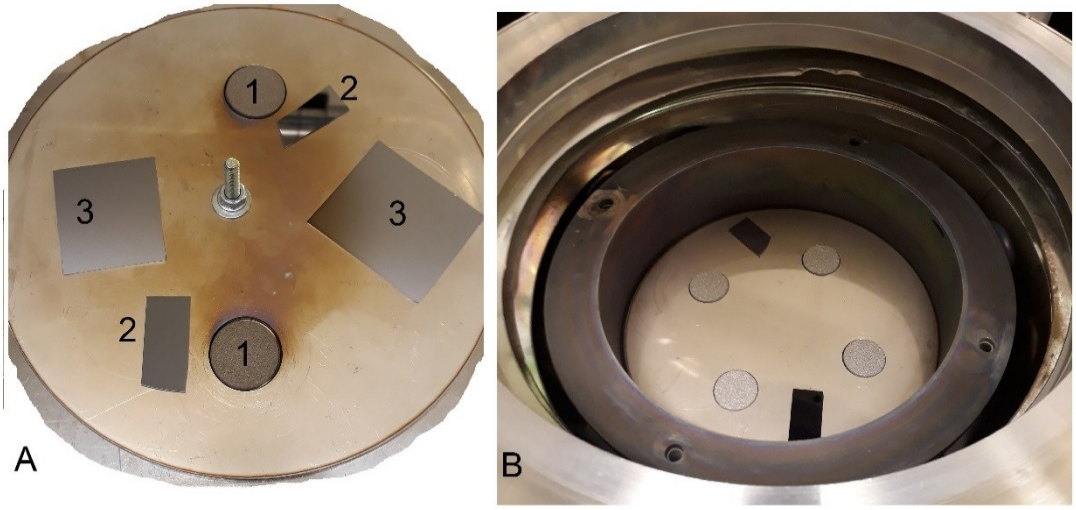

Figure 10. A) Plate to force the flow through the filter; 1) filter; 2) silicon wafer chip to monitor the deposition distribution and film thickness; 3) silicon wafer chips to prevent gas flow through two other filter stands; B) plate located in Picosun R-200 ALD reactor.

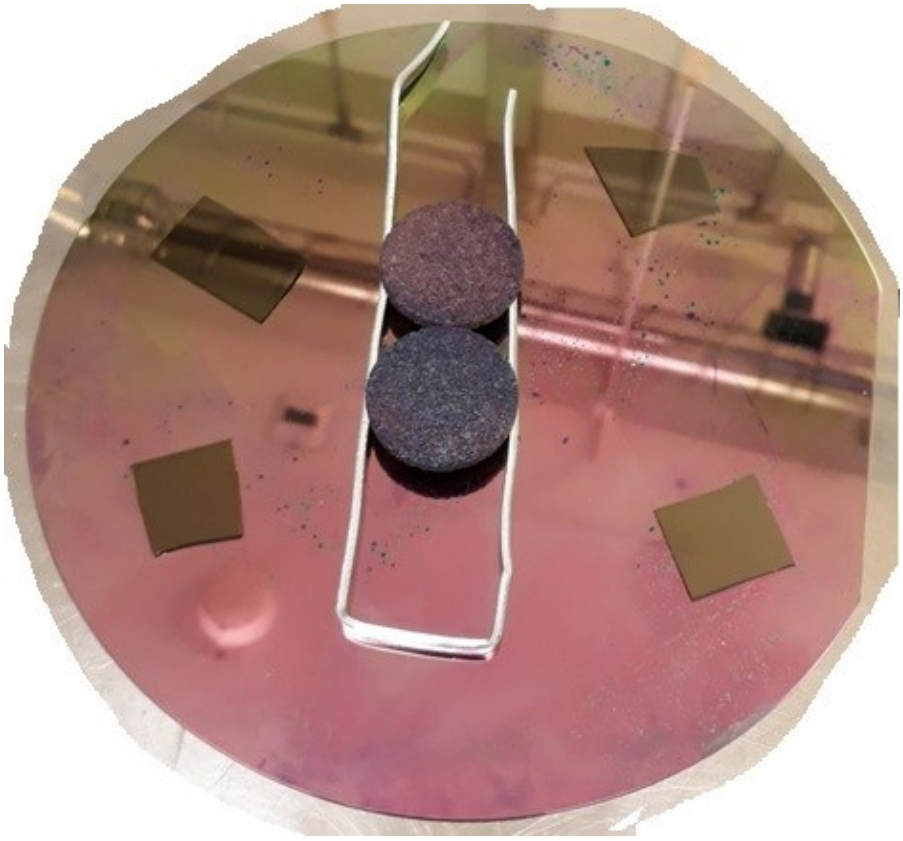

Figure 11. 1600 cycles of NiO deposited on filters located on stand on silicon wafer.

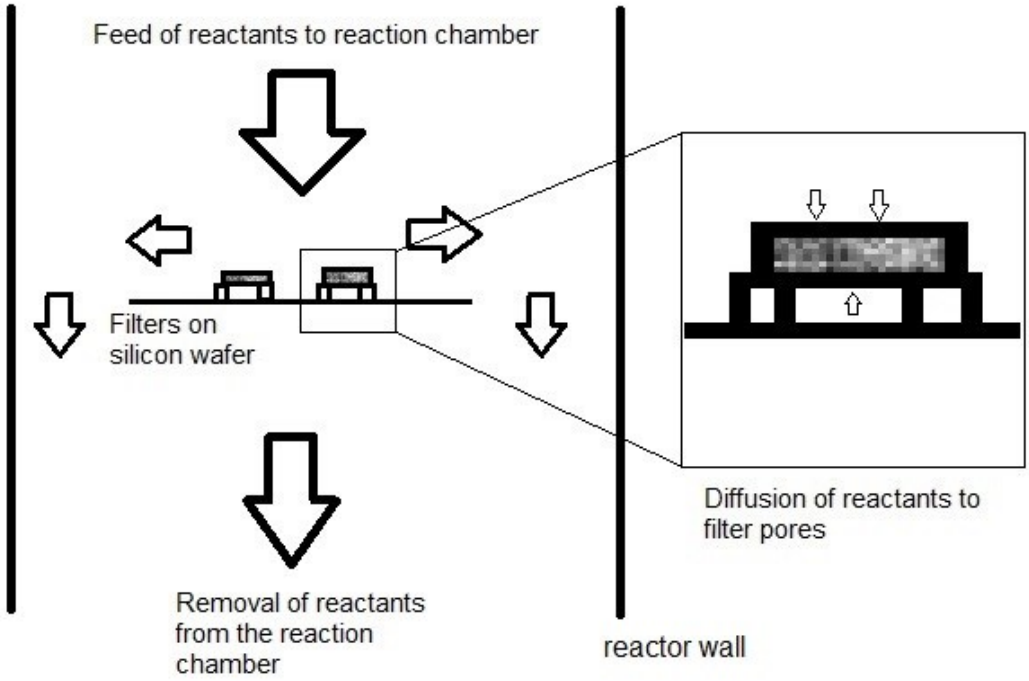

Figure 12. Schematic figure of the diffusion-driven stop-flow deposition method utilised in deposition of Al_2O_3 and filter with 1600 cycles of NiO.

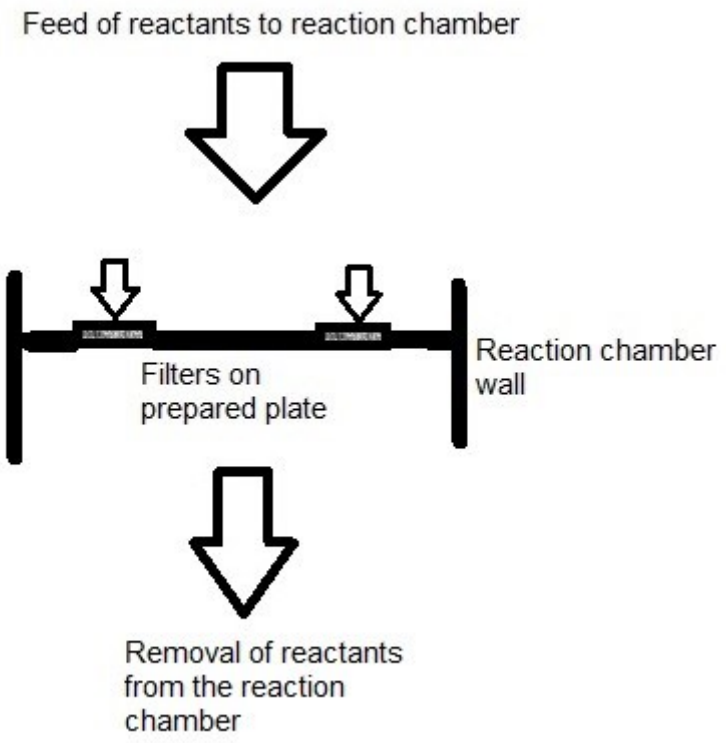

Figure 13. Schematic figure of flow-through deposition method, where the flow attempted to be forced through the filter with prepared sample holder plate.

5.2.3 Rhodium coatings

Rhodium coatings were performed using rhodium(III) acetylacetonate ($Rh(acac)_3$) and oxygen as precursors. $Rh(acac)_3$ (97 %) was provided by Strem Chemicals, and oxygen (99.999%) by AGA. For finding suitable temperature for $Rh(acac)_3$ sublimation, temperatures ranging from 170 °C to 200 °C were tested. In filter preparation runs, $Rh(acac)_3$ was sublimated at 180 °C. Deposition temperature for Rh was 250 °C. ALD runs with 100 cycles were used in Rh deposition test runs and filter coating attempts. Both methods, flow-through the filter used for NiO coatings and stop-flow setting used for alumina coatings were used in attempts of preparing Rh coatings on filters.

5.3 Characterization

Physisorption analysis was performed for uncoated filters to find the Brunauer-Emmett-Teller (BET) surface area of the discs before ALD coatings. BET surface area

measurement is based on the adsorption of nitrogen on the surface of the sample at different pressures at isothermal conditions. Analysis was performed in 3Flex version 3.4 tool at measurement temperature of -196 °C. Small pieces of about 1 g filter material for analysis were cleaved using chisel and hammer.

Scanning electron microscopy (SEM) combined with energy-dispersive X-ray spectrometry (EDS) was used in elemental distribution analysis of prepared catalytic filters. Analysis was conducted by Merlin scanning electron microscope equipped with ThermoFisher UltraDry spectrometer (Silicon drift detector). SEM-EDS results were analysed using ThermoFisher NSS 3.2.298 software. The analysis was conducted on various parts of the filters, including the top and bottom sides of the filters, as well as cleaved filters to observe the depth of the coating.

In EDS analysis, detecting the quality and quantity of elements present is based on the characteristic X-rays emitted by atoms excited by high-energy beam (Leng, 2013). The principle is similar to for example X-ray fluorescence (XRF) analysis, but instead of X-rays which are used for exciting the atoms in XRF, electron beam used for SEM imaging is used in EDS coupled with SEM device (Leng, 2013). While XRF can be used for measuring the whole sample, specific microscopic areas are analysed with SEM-EDS (Leng, 2013). The analysis can be conducted by for example as linescan, where the intensity of the specific characteristic X-rays can be measured from line in the sample surface, to detect the possible concentration gradients of specific elements in the sample surface (Leng, 2013). This ability was applied for analysis of ALD deposition depth through the filter in this work.

In addition to filters prepared as described earlier, one of the filters tested by Kivelä (2018) was characterized by SEM-EDS for comparison. After cleavage, which removed most of the coke and carbon formed on top of the filter tested for reaction, filter was dipped in isopropanol and dried overnight in oven at 67 °C.

5.4 Reaction testing

Prepared catalytic filters were tested for the decomposition of tars at temperatures between 650-920 °C, absolute pressure of 5 bar and gas flow rate of 1.0 l/min. Process conditions, as well as simulated gasification gas composition used, were

selected according to earlier studies by Kivelä (2018), and gas composition was also based on earlier pilot-tests. Toluene, benzene and naphthalene were used as tar model compounds. The gas composition used, as well as the composition of model tar solution are presented in Table 4. The providers and purities of gases and chemicals used are presented in Appendix 3.

Table 4. Composition of the wet inlet gas.

Gas component	vol-%
CO	10.7
CO_2	15.5
CH_4	2.8
H_2	22.7
C_2H_4	1.7
H_2O	44.3
N_2	1.9
=	99.6
	vol-ppm
benzene	1715
toluene	1670
naphthalene	223
H_2S	60
=	3668

5.4.1 Experimental set-up

Reaction testing equipment consisted of gas, water and tar feeding parts, reactor part and product analysis part. In gas feeding part, gas components of model gasification gas were fed from separate gas bottles, while water and tar solution were fed to the reactor system in liquid phase and thus through the vaporizer. Tar solution for all the experiments was prepared according to weight, first dissolving 7 w-% of naphthalene to 50 w-% of toluene and after that adding of 43 w-% benzene.

In the reactor part, the gas flow, including gas feed and vaporised water and tars was fed to either the reactor, positioned in Carbolite 3-zone furnace, or to reactor bypass line. In product analysis part, product gas composition was analysed by gas chromatography for wet gas, including all the components of product gas, and in gas

analyser, for dry gas after removal of tar compounds and water. Water and tar compounds were removed from gas mixture in condenser and gas washing bottles of isopropanol and water in ice bath. Simplified flowchart of experimental set-up for reaction experiments is presented in Figure 14.

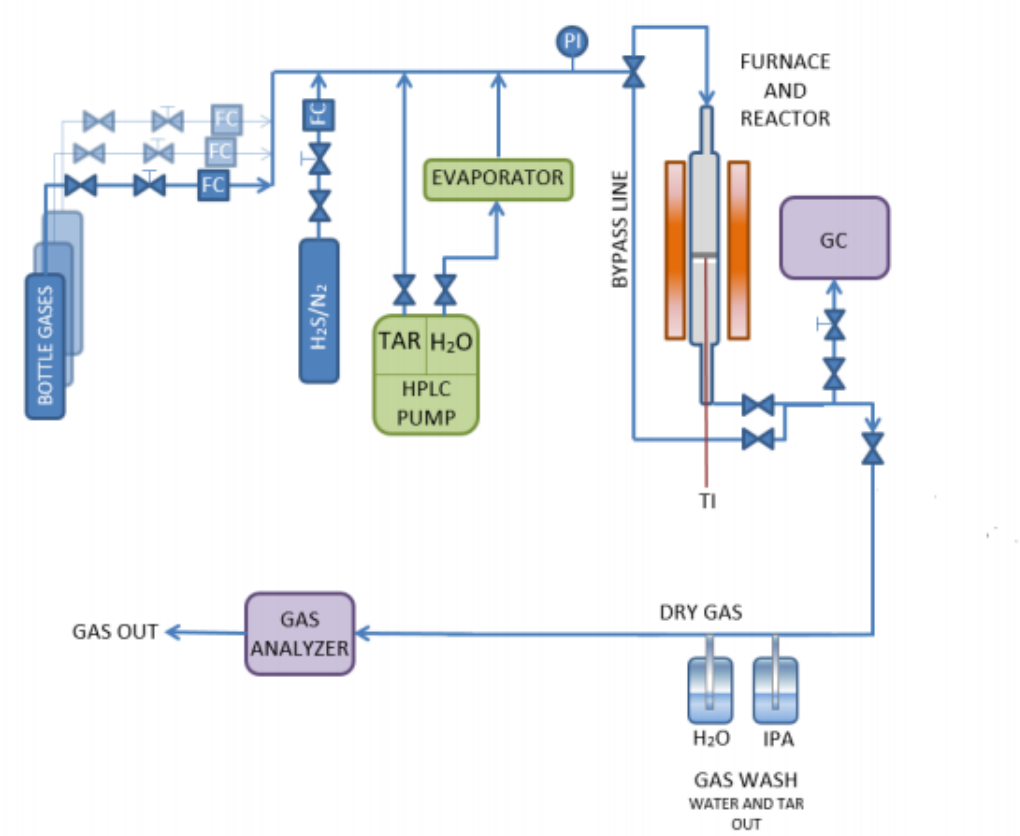

Figure 14. Simplified flowchart of the experimental set-up (VTT Technical Research Centre of Finland).

The amounts of component gases in the feed were controlled by mass flow controllers (Bronkhorst). Tar solution and water were fed to system in liquid phase, and controlled by Shimadzu isocratic pumps. The pumps were calibrated for the needed liquid feed before starting the experiments. Similarly, the calibration data of mass flow controllers was reviewed and recalibration was performed, if needed. Total flow rate of dry gas was measured from dry inlet gas before several test runs with Kimmon SK25 gas meter.

The reactor consisted of two quartz reactor parts and is presented in Figure 15. The filter was packed on top of the sinter located in the lower part of the reactor and quartz wool was added to direct the flow through the filter, as shown in Figure 16.

Figure 15. The quartz reactor

Figure 16. Filter packed in reactor part and sealed with quartz wool.

Test runs were performed at temperatures of 650-920 °C with constant pressure of 5 bar and gas flow rate of 1.0 l/min. Temperature setting was changed in periods of 4 h from lower temperature to higher. Before each run, the catalyst was reduced under 1:1 H_2:N_2 flow of 1.0 l/min at 1 bar and at 750 or 800 °C for 1 h. After each run, the catalytic filter disc was removed from the glass reactor and reactor was oxidized under 1 l/min flow of 15:61:24 of O_2:N_2:H_2O at 850-950 °C to remove the carbon formed on the glass reactor, furnace walls and reactor sinter. To confirm the proper operation of the reaction test equipment, test run with bed of IWI deposited nickel catalyst prepared on α-alumina particles was performed.

5.4.2 Product gas analysis

The composition of product gas was analysed by online gas chromatography and online gas analyser. Gas chromatography was applied to all product gases and used for analysis of hydrocarbons, such as tar compounds, methane (CH_4) and ethane (C_2H_4), while only dry product gas was fed to the gas analyser for detection of CO, CO_2, CH_4, H_2 and O_2.

The product gas composition was analysed by Agilent 7890 gas chromatograph, including HP-5 and HP-PLOT-Q columns and two flame ionization detectors (FID). Helium was used as carrier gas to elute the compounds in the gas to be measured separately at the detectors. The sample was first fed from sample loop to HP-5 column. Light hydrocarbons (C_1-C_5), for example methane, ethene and propane, were advancing through the column faster than heavier hydrocarbons and were directed from HP-5 column to HP-PLOT-Q column, and after that to FID B. Dean switch was automatically closed before the elution of benzene to direct the heavier hydrocarbons directly from the HP-5 column to the FID A. Calibration for gas chromatograph was performed before each test run by feeding the inlet gas through the bypass line before changing the flow to reactor.

Dry gas was analysed in ABB AO2020 device with Magnos 206, Uras 26 and Caldos 25 analysers. Recalibration of gas analyser was performed regularly, at least once in every two weeks. The analyser was calibrated by nitrogen as zero gas and separate calibration gas (AGA) as span gas.

5.4.3 Result calculation for reaction experiments

The results of reaction testing part were calculated from results gained from gas chromatograph and gas analyser. Average values of results measured during a temperature setting were used for calculation. Reactor inlet values were recorded as average of the gas flow in bypass line before the flow was turned to reactor.

Conversion of component *i* X_i was calculated as presented in Equation 16.

$$X_i = \frac{F_{i,IN} - F_{i,OUT}}{F_{i,IN}} \quad (16)$$

Where

$F_{i,IN/OUT}$ is the molar flow of component i to reactor and from the reactor (mol/s).

Similarly, yield of component *i* Y_i was calculated for gas compounds to compare the results to results presented by Kivelä (2018), and is presented in Equation 17.

$$Y_i = \frac{F_{i,OUT} - F_{i,IN}}{F_{i,OUT}} \quad (17)$$

The volumetric flow rate of product gas was assumed according to elemental balances of carbon, hydrogen and oxygen using total product gas flow rate and water composition of product gas as variables. Nitrogen and H_2S were assumed to be inert and molar flows of these components to be constants. All components were assumed to be ideal gases, thus molar percentages were assumed to be equal to volumetric percentages in constant pressure and temperature.

Amount of carbon formed on reactor walls and sinter was monitored by measuring the amount of carbon dioxide produced during the oxidation of reactor. Similarly, coke formation in filter was measured as weight increase of the filter. However, these carbon deposits were assumed to be negligible in terms of the carbon balance of the reaction experiment.

6 Results and discussion

In this chapter, first, the analysis of ALD coatings and characterization are reported, and then the performance of the filters in reaction tests is presented. Additionally, the results of experiment repeated in this work from work presented earlier by Kivelä (2018) are presented, including catalytic filter preparation with 1600 cycles of NiO by stop-flow method, characterization and reaction test run.

6.1 ALD coatings and characterization

6.1.1 Different nickel-loadings

Nickel oxide coatings were applied on filters to improve the catalytic activity. As presented in Figure 17, it can be seen that the amount of nickel measured by SEM-EDS from the top surface of the filter is dependent on the number of cycles deposited, as expected.

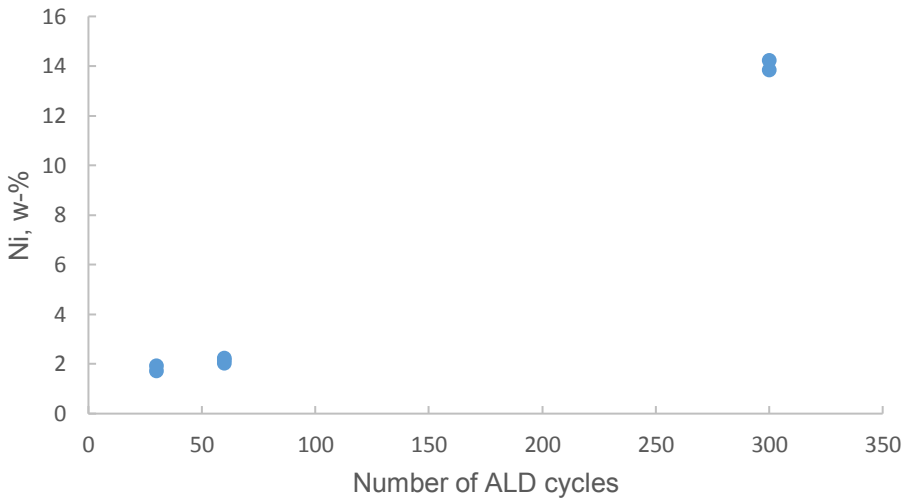

Figure 17. The nickel loading on top surface of coated filter as function of ALD cycles of NiO.

On the silicon wafer chips, the thickness of nickel layer increased as well, but was affected also by other factors, possibly the reactor geometry, location of chips on the

plate in the reactor and fast removal of reactants from the reactor. The thicknesses of layer formed on the silicon wafer chips is presented in Table 5.

Table 5. Measured thickness of NiO layer on silicon wafer chips measured by ellipsometry. Two chips were used in one ALD run.

Number of cycles	Thickness of NiO layer (nm)	
30	3.9-4.1	3.6-4.3
60	6.3-11.1	5.9-18.1
300	10.6-13.0	11.4-13.2

The variation of layer thickness between chips in one run, as well as inside a single piece has been probably caused due to flow patterns of precursors in the reactor during flow-through depositions. As seen earlier in Figure 10 A, brown NiO pattern has been clearly formed on the center of the plate. If the chip has been partly located on area with high amount of precursors and partly with less precursors, gradient of NiO layer thickness on the chip is probably formed.

6.1.2 Effect of deposition method on nickel loading and distribution

Two deposition methods were tested for nickel deposition. Most of the filters were coated by flow-through method, as described in Figure 13, and one filter with the stop-flow method, which is shown in Figure 12. Flow-through deposition was applied to increase the deposition through the filter in inner surfaces.

On top side of the filters coated by flow-through method, the amount of nickel was proportional to the number of cycles deposited, as described earlier in Figure 17. However, bottom side of the filters were completely free of nickel in all filters prepared by flow-through method. To find the nickel gradient through the filter, linescan analysis for Ni, Fe, Cr and Al by SEM-EDS was analysed to measure the depth of deposition in filter with 300 cycles of NiO. Results of the linescan performed are presented in Figures 18, 19 and 20.

In Figure 18, the SEM image of the scanned area and line is presented. In Figure 19, the results of the linescan as counts of different elements are shown as unrefined data of the linescan analysis. It is seen that the amount of nickel is low compared to other elements present, and the program used for analysis was not able to detect nickel in most of the measured positions. In Figure 20, the amount of nickel is compared to amounts of other elements measured. To find the possible trends of nickel compared to other elements, all numbers are normalized to the value of Ni/X when the distance was 0 µm.

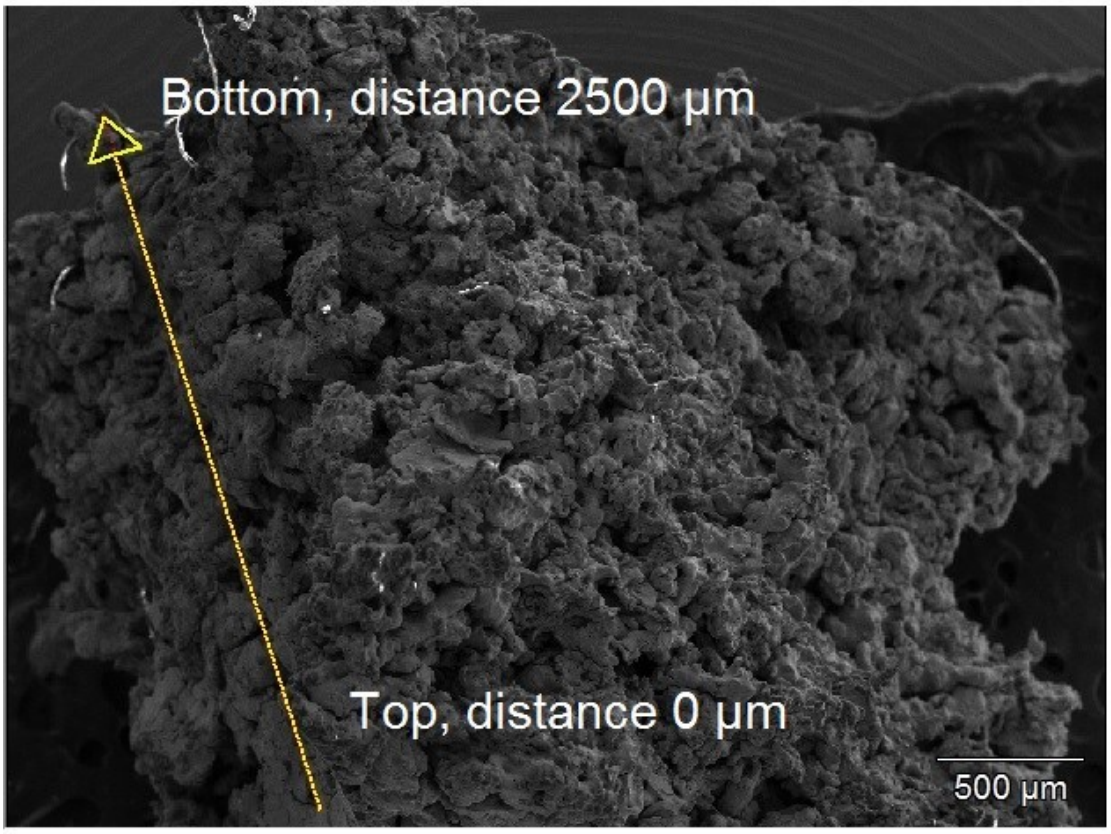

Figure 18. Position of the linescan line, and top and bottom sides of the filter presented. Filter with 300 cycles of NiO deposited with flow-through method.

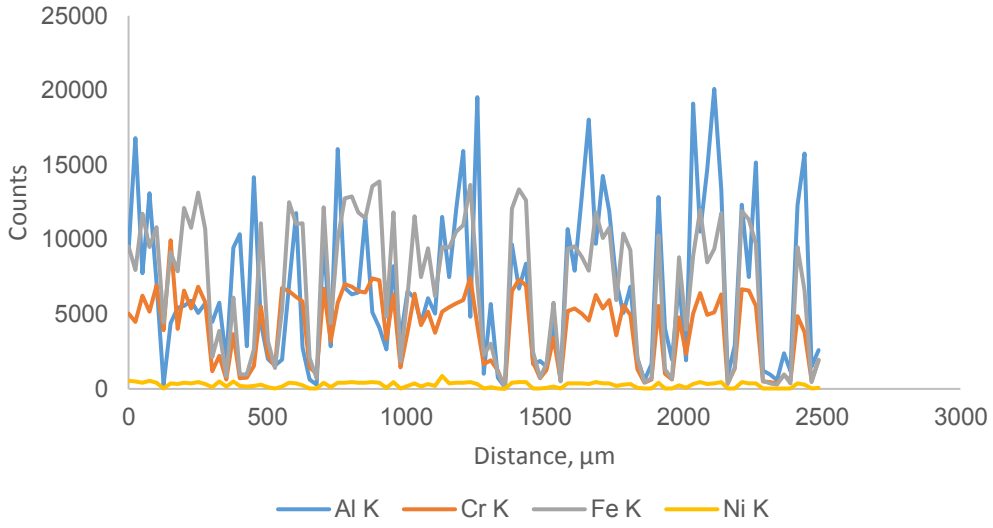

Figure 19. X-ray linescan result counts for Al, Cr, Fe and Ni of filter with 300 cycles of NiO deposited with flow-through method.

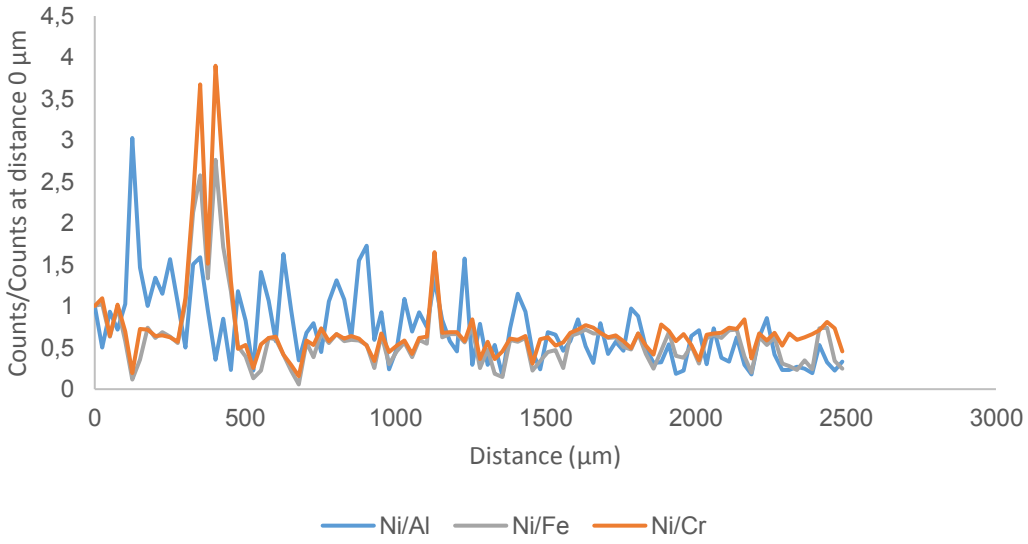

Figure 20. X-ray linescan results for nickel at compared to other measured elements and normalized. Filter with 300 cycles of NiO deposited with flow-through method.

It can be seen in Figure 20 that excluding the peak at the spot of about 400 µm, the nickel content is close to constant. The relative increase of amount of Ni at 400 µm can be explained with low amount of Al, Cr and Fe present at particular spot, as seen in Figure 19. Nickel content is low, close to 0 w-%, and in most parts of the linescan, no nickel can be detected in the EDS spectrum by the software. According to linescan, it can be stated that negligible amount of nickel has been deposited on inside part of

the filter. Similarly, as stated earlier, no nickel is found from the bottom surface of the filter.

Lack of nickel inside the filter is surprising, since high amount of 14 w-% of nickel can be still found from the top surface by measuring the surface directly. This can be due to nickel flowing by the filter, either between the filter and the holder wall, or between the holder and reactor chamber wall. The top side of the filter is the easiest to access, which could explain the high amount of nickel.

To evaluate the difference of deposition methods, SEM-EDS analysis was conducted to filter with 1600 cycles of NiO deposited with stop-flow setting. The resulting image is presented in Figure 21. It can be seen that with stop-flow setting, there is clear deposited nickel layer of 200-300 µm compared to aluminium in top part of the filter, seen as blue line in the figure. Unfortunately no similar linescan analysis was carried out for this particular filter. The layer is clearly seen, even if the steel material of the filter contains nickel.

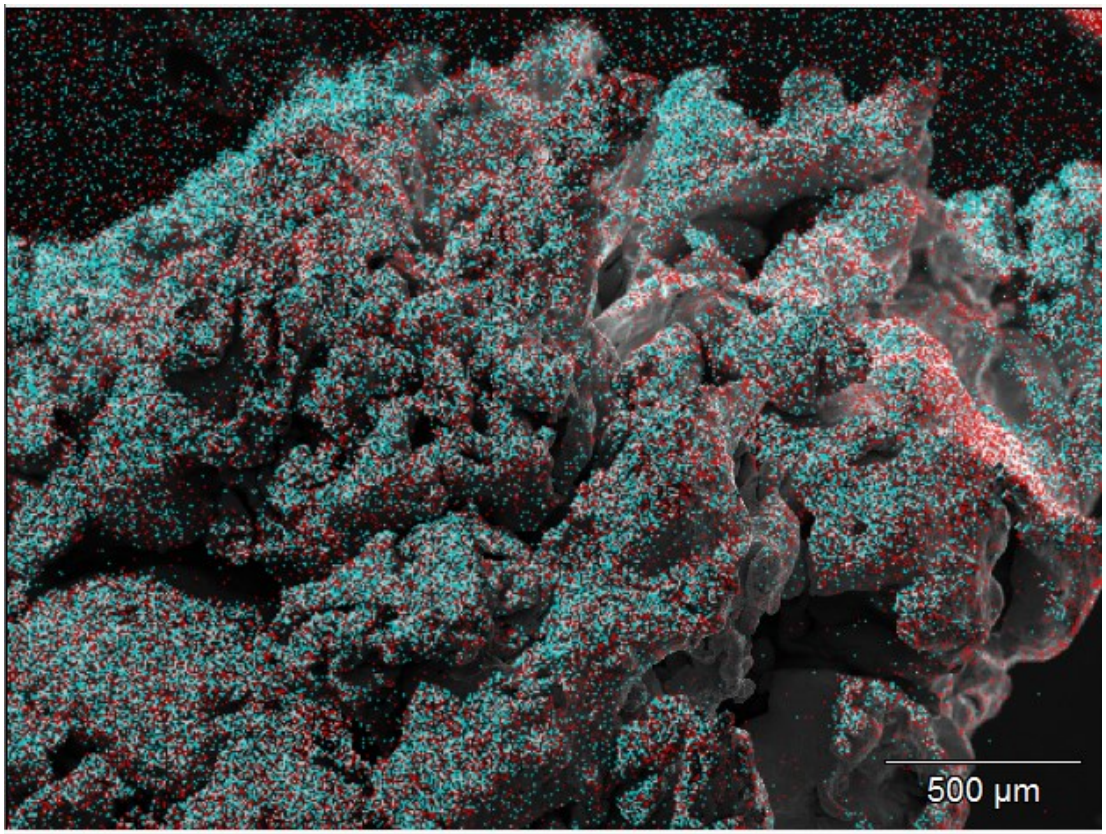

Figure 21. Filter with 1600 cycles of NiO made with stop-flow setting. Nickel gradient can be seen in top part of the filter, in right top corner of the image. Nickel counts are highlighted with blue and aluminium counts with red.

Similar trend of formation of Ni layer of 200-300 µm was observed on filter prepared by similar method with same amount of cycles and used for reactor test by Kivelä (2018) on steel filter containing no nickel, presented in Figure 22. However, no nickel gradient was detected in linescan analysis of filter prepared, presented in Figures 23, 24 and 25. Similarly as in results of linescan analysis of filter with 300 cycles of nickel prepared in this work and presented above, no significant amount of nickel is detected inside the filter.

The low amount of nickel detected raises doubt of the reliability of the results of linescan analysis performed for another filter in this work as well, since catalytic activity of filter reported by Kivelä (2018) referred to successful deposition of nickel. To confirm the results, multiple similar analyses should be conducted for multiple pieces of filter from same filter. The results presented here are based on one measurement. In addition, the results are not directly comparable, since filter of Kivelä

(2018) has been tested for reaction and coke formation on the surface is detected in SEM-EDS analysis.

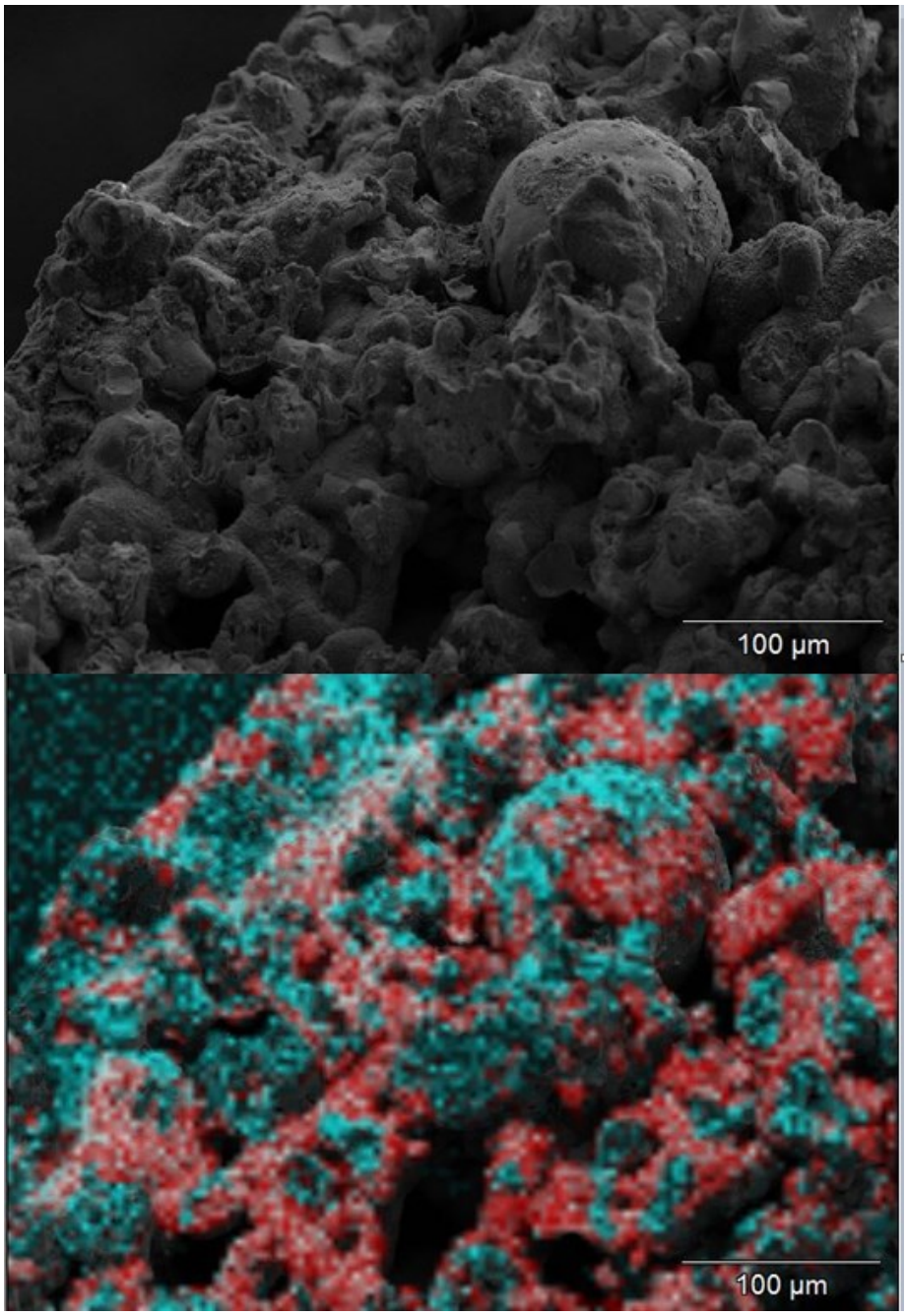

Figure 22. Grey image (above) and nickel and alumina counts highlighted image (below) of filter of Kivelä (2018). Nickel is highlighted with blue and aluminium with red. More nickel compared to aluminium is detected on left according to image.

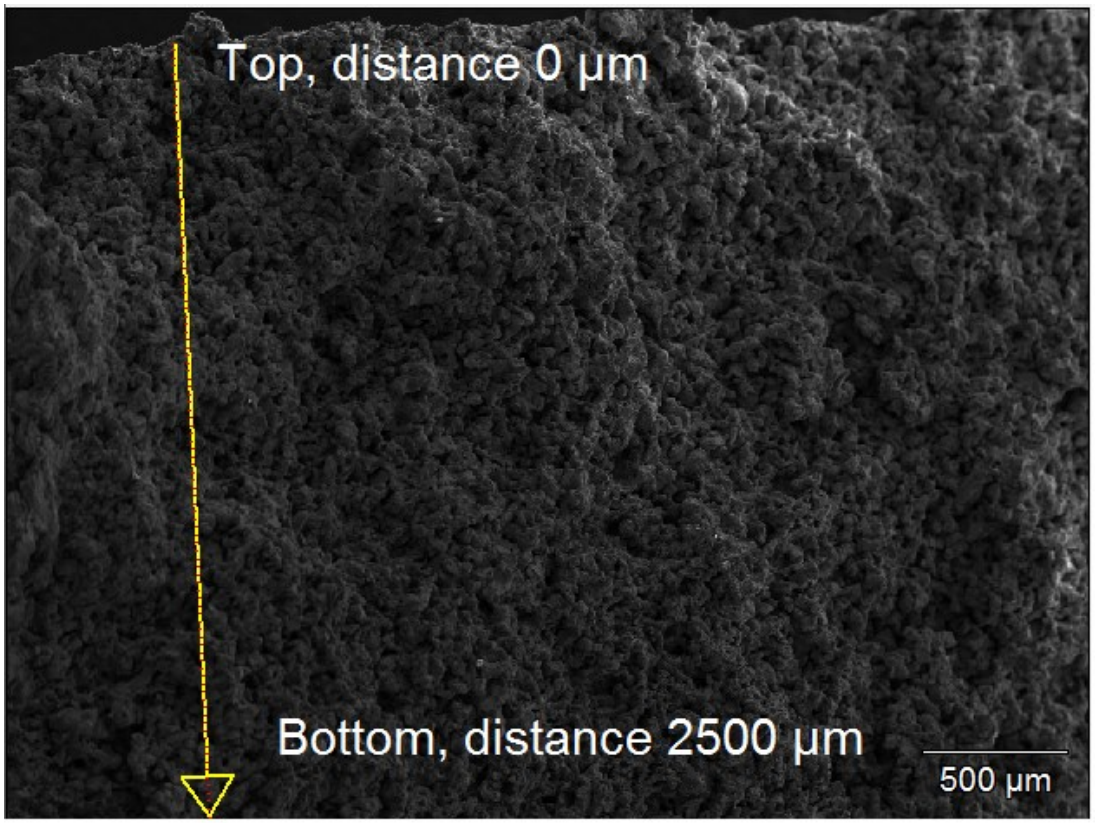

Figure 23. Position of the linescan line, and top and bottom sides of the filter presented. Filter of Kivelä (2018).

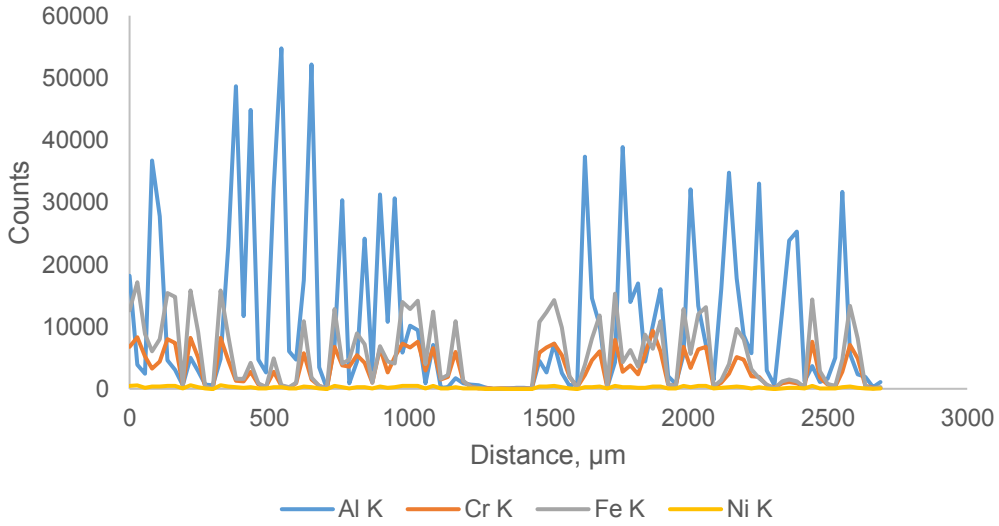

Figure 24. X-ray linescan result counts for Al, Cr, Fe and Ni of filter of Kivelä (2018).

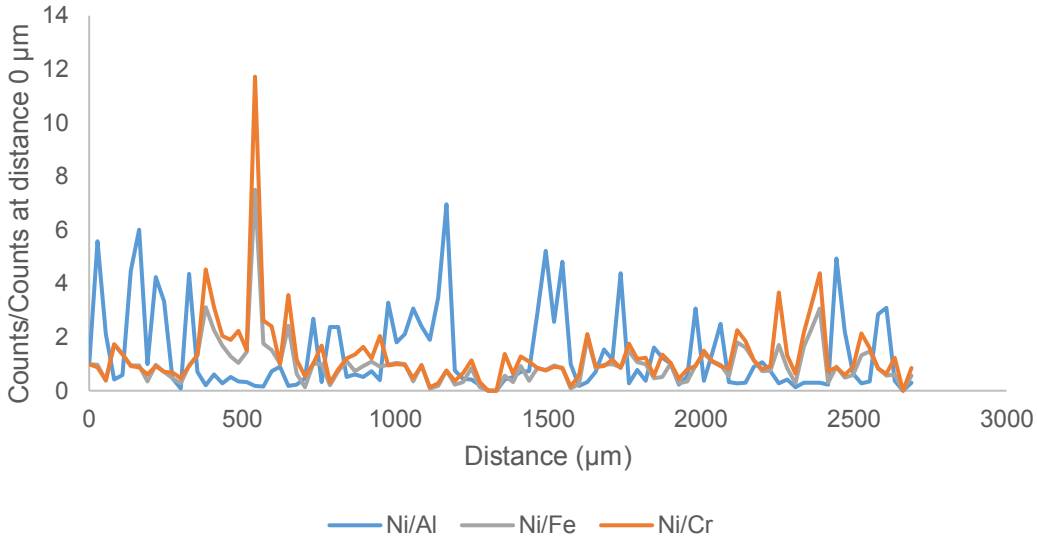

Figure 25. X-ray linescan results for nickel at compared to other measured elements and normalized. Filter of Kivelä (2018).

To conclude, the targeted nickel deposition all over the filter was not achieved. ALD process chosen for flow-through experiments was not successful, and flow either did not go through the filter or deposition inside the filter was not achieved. The plate set inside the reactor was possibly untighten, and the flow was able to pass the filter either between the reactor wall and the plate, or between the filter and the plate, without going through the pores of the filter. In these experiments, better deposition with respect to SEM-EDS analysis was achieved with diffusion-driven process with stop-flow setting. No similar characterization of ALD coated filters has been previously reported. However, Zhao *et al.* (2000) reported successful deposition with nickel all over the Al_2O_3-filter with nickel deposition on urea-coprecipitation method, while IWI deposition of nickel left inside parts of the ceramic filters without nickel.

6.1.3 Rhodium depositions

ALD process for preparation of rhodium-coated filters was tested and developed. However, no rhodium was detected in SEM-EDS analysis on catalytic filters after multiple deposition runs. Since no rhodium was detected after 100 deposition cycles, these filters were not tested for tar decomposition.

In ALD of $Rh(acac)_3$ and oxygen, metallic rhodium was formed on specific silicon

wafer chips, as well as on plate placed in reactor. Rhodium layers of 0-11 nm were detected on silicon wafer chips, depending on their location in the reactor: higher amount of Rh was formed on silicon wafer chips closer to the rhodium precursor inlet. Tested deposition temperature of 250 °C was same as used by Aaltonen *et al.* (2005) in F-120 ALD reactor. Even close to similar deposition of rhodium was not detected, when the growth of Rh layer was dependent on the location of the substrate in the reactor, as presented in Figure 26. Metallic rhodium could be seen as metallic layer on silicon wafer chips marked with A, B and C, located close to each other. Similar results were gained in other ALD runs of Rh as well.

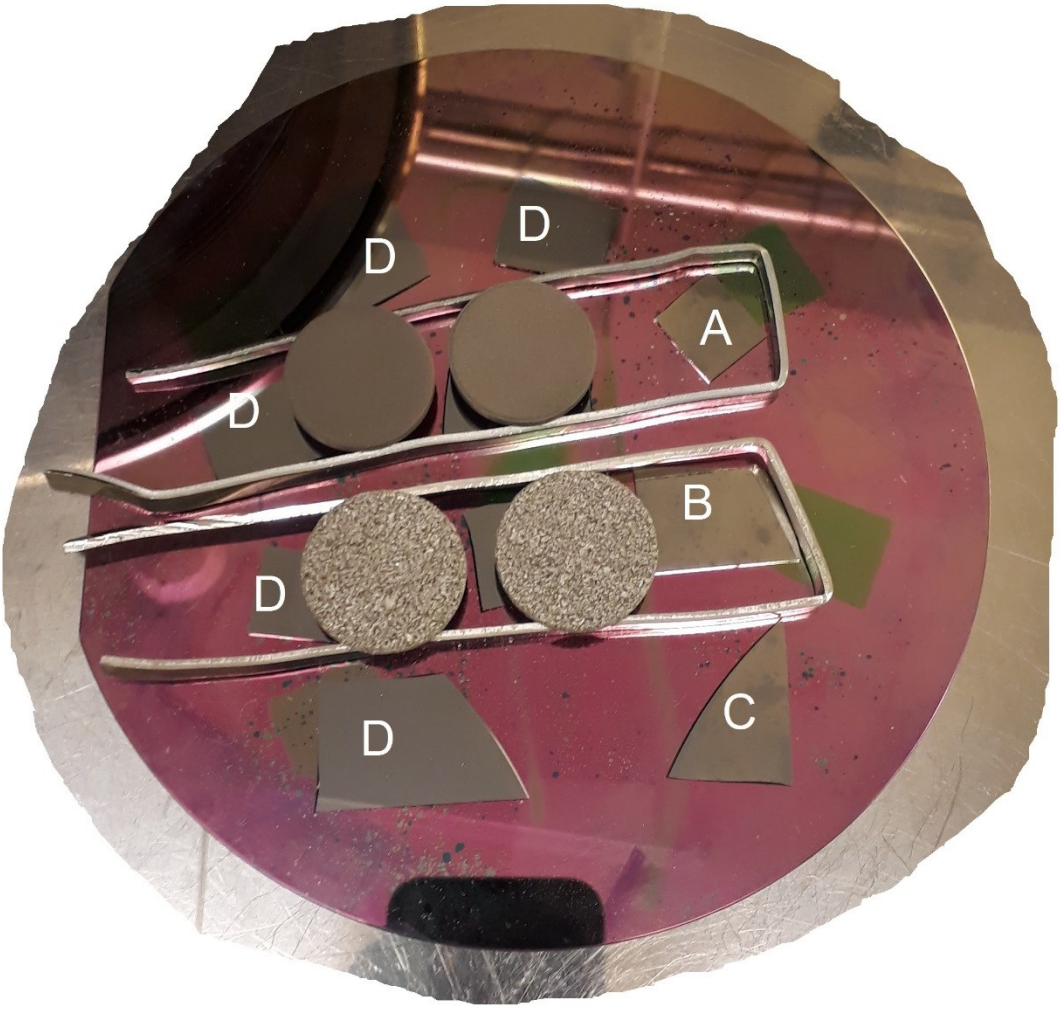

Figure 26. Filter discs after ALD-coating of rhodium. No Rh detected in filters in SEM-EDS analysis, silicon wafer chips A) 2.7-7.7 nm Rh, B) 9.5 nm Rh, C) 1.6-3.8 nm Rh, D) 0.0 nm Rh.

During ALD run of 100 cycles of $Rh(acac)_3$, total amount of rhodium sublimated from the source was typically about 20 mg, which is small compared to for example nickel depositions, where about 25 mg was sublimated per deposition cycle. Since the sublimation temperature was found by testing the temperatures step by step between 170 °C and 200 °C, it was noticed that even higher temperature did not increase the amount of $Rh(acac)_3$ sublimated.

Major development and basic research is needed for the ALD process of Rh to be sufficient and reliable for catalyst preparation in the tested reactor set-up. Most importantly, optimal temperature and conditions for sublimation and for adsorption have to be found for ALD process to deposit stabile layers with adequate control of the deposition.

6.2 Reaction tests

The reaction test results presented and analysed in this chapter focus on decomposition of benzene, toluene and naphthalene. Full results, including the conversions of all tar compounds and ethene and yields of gas compounds H_2, CO, CO_2 and CH_4 are presented as table in Appendix 4. However, due to high inlet concentration of mentioned gases compared to tar compounds and inaccuracy of the gas analyser, no significant analysis of tar decomposition product distribution can be done based on gas concentration results. Negative conversions are reported in this work for tar compounds, when the amount of reactant increases in the reaction. For example formation of naphthalene from lower molecular weight tars or decomposition of toluene to benzene can cause negative naphthalene or benzene conversions, respectively.

6.2.1 Thermal reactions in empty reactor

Empty reactor was tested for model gasification gas to identify the effect of thermal reactions that take place without a catalyst. Results of reaction test in reactor without filter for toluene, benzene and naphthalene are presented in Figures 27, 28 and 29, respectively.

Thermal reactions of gasification gas at pressure of 5 bar and temperature of 700-920 °C include the decomposition of toluene to methane and benzene. Toluene decomposition conversion can be seen in Figure 27, and increase in benzene as negative conversion in Figure 28.

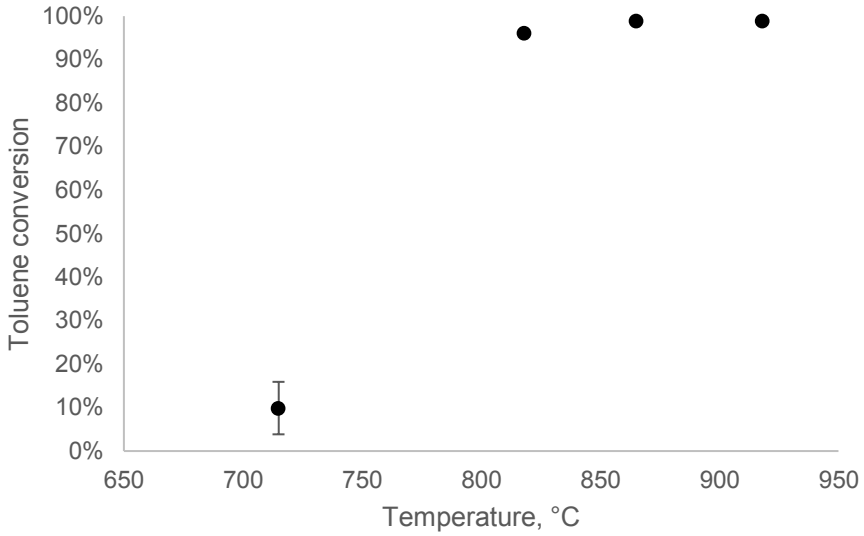

Figure 27. Conversion of toluene in empty reactor.

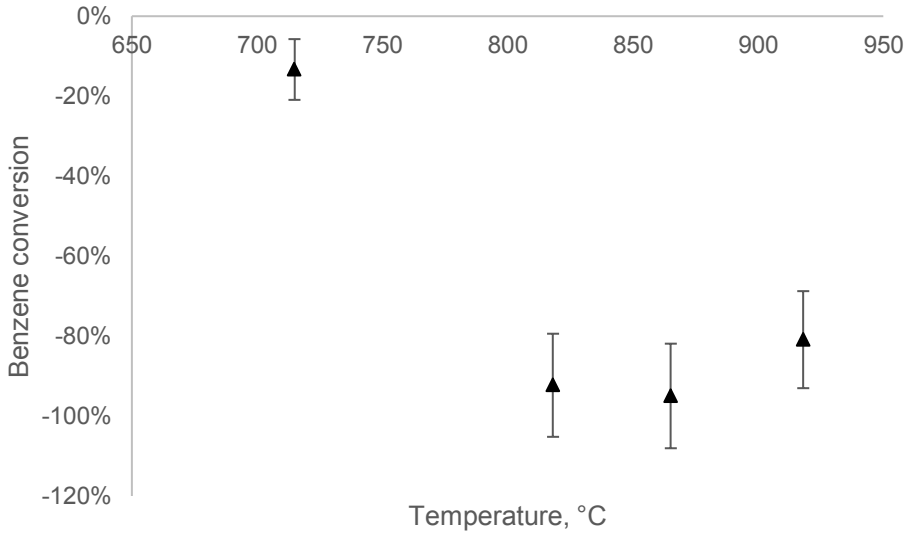

Figure 28. Conversion of benzene in empty reactor.

Naphthalene formation at temperature of over 850 °C is detected as amount of naphthalene increases 15%, which can be caused due to thermal reactions of ethene promoted by high pressure of 5 bar, as presented by Kaisalo *et al.* (2015a). At high temperature of over 900 °C, no increase in amount of naphthalene is detected.

Formation of heavier tars, which are not analysed, can potentially explain the decrease of naphthalene, similarly as in experiments of Tuomi *et al.* (2015). Thermal decomposition of naphthalene is not probable, since the thermal decomposition without a catalyst starts only above 1100 °C (Jess, 1996). Naphthalene conversion is presented in Figure 29.

Formation of heavier, undetected tars likely explains as well the decrease of benzene at 920 °C compared to 865 °C, seen in Figure 28. However, the decrease is inside the error limit, and also thermal decomposition of benzene is possible with low conversion even at temperature of 920 °C (Jess, 1996).

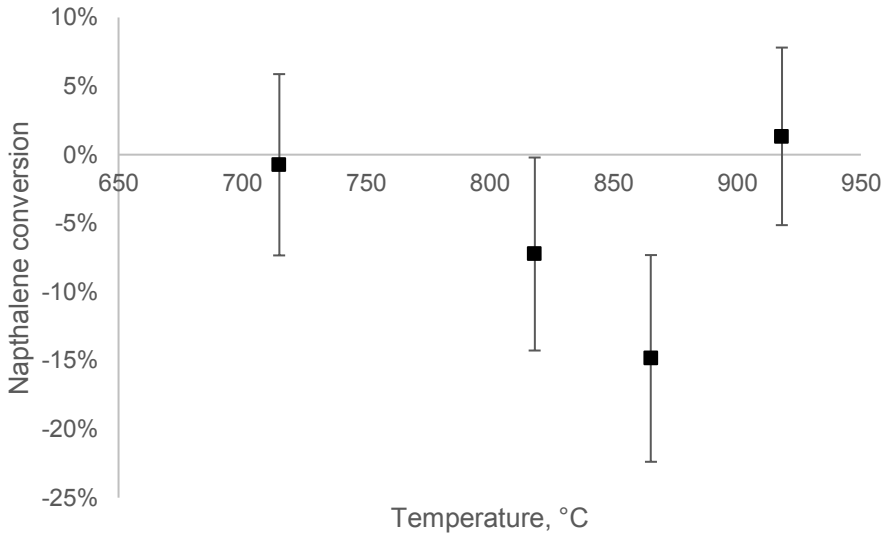

Figure 29. Conversion of naphthalene in empty reactor.

Toluene thermal decomposition conversion of over 90% is achieved at temperatures exceeding 800 °C and maintained at higher temperature in every experiment. Similarly, the amount of benzene increased as a results of toluene decomposition, and is similar in every experiment. Thus, the benzene and toluene conversions are not reported here when presenting the other results, but are presented with all results in Appendix 4.

6.2.2 Uncoated filters

Two different steel alloys were tested as uncoated, blank filters. The most important difference between alloys is the amount of nickel, 0 and 10-14 w-% of Ni for steel alloys 1.4767 mod.2 and 316L, respectively. The properties of the filters are presented earlier in Table 3. The results of naphthalene reforming with blank filters are presented in Figure 30.

When there was a filter inside the reactor instead of empty reactor, the amount of naphthalene detected is decreased especially at higher temperature of over 860 °C, either by increasing the formation of heavier tars and soot or by improving the decomposition of naphthalene to smaller hydrocarbon components. No major increase of lower molecular weight hydrocarbons is detected in experiments, which would refer to formation of heavier tars.

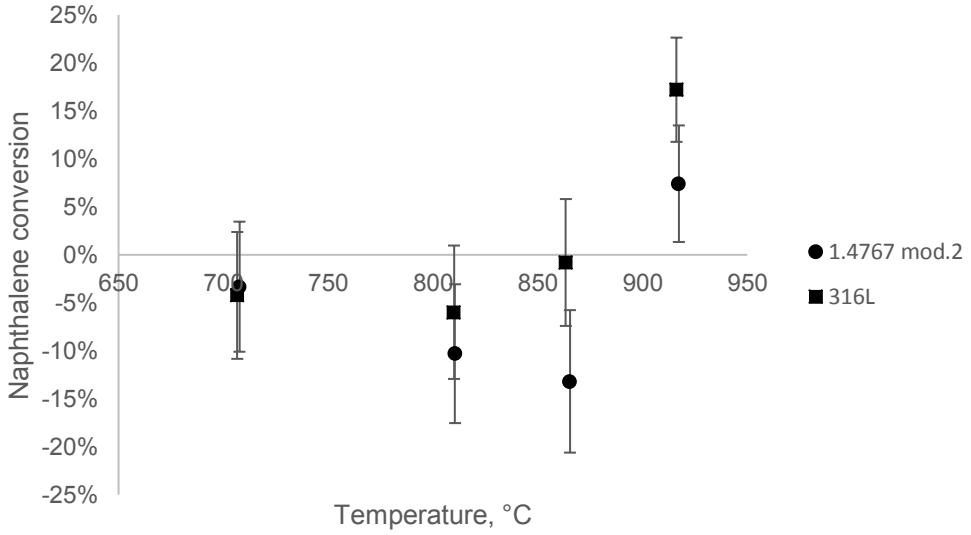

Figure 30. Conversion of naphthalene on blank filters made of different steel alloys.

In test runs of blank filters made of 1.4767 mod.2 steel, results similar to results of Kivelä (2018) were achieved in terms of tar conversion, as minor naphthalene conversion was detected. No difference in conversion was detected on blank test runs with different pore sizes of 75-100 µm and 160-300 µm of 1.4767 mod.2 steel.

Nickel-containing steel alloy 316L was detected to be more active in naphthalene conversion at high temperature, since conversion of 17% was achieved at 920 °C, as seen in Figure 30. Results of the activity of nickel-containing alloys on hydrocarbon reforming have been previously reported as well (Tomishige *et al.*, 2017). Abbas and Wan Daud (2010) recognized the activation of steel reactor walls (SS310S steel) at temperature of higher than 850 °C in methane thermocatalytic decomposition. Di Mondo *et al.* (2011) stated the chromium oxide layer formed on the surface of the steel 316 material to cause the catalytic inactivity, and were able to activate the steel material by etching the protective layer in aqueous acidic conditions. Activation of catalytic properties of nickel-chromium steel alloy at temperature of over 850 °C could explain why no catalytic activity of steel is detected at lower temperature.

It would be interesting to study if steel grades with even higher nickel content than studied 316L steel (10-14% Ni) could improve the tar reforming activity, for example Li *et al.* (2014) found iron-nickel nanoparticle catalyst with Fe/Ni ratio of 0.25 to be the most efficient in tar reforming. For example the SS310S steel used in experiments of Abbas and Wan Daud (2010) contains 19-22 w-% of nickel. Still, in application to real gasification gas filtration at temperature of over 800 °C the selection of the material is highly limited due to challenging conditions, including alkali, sulphur and chloride impurities, as well as high temperature and mechanical stress (Heidenreich, 2013).

6.2.3 Coated filters

No significant difference in naphthalene conversion was noticed on reaction experiments of coatings prepared on 1.4767 mod.2 steel with 30, 60 or 300 cycles of nickel oxide. Unfortunately no results were gained from the highest temperature of over 900 °C with any of the coated filters. The results of experiments with these filters in conversion of naphthalene are presented in Figure 31.

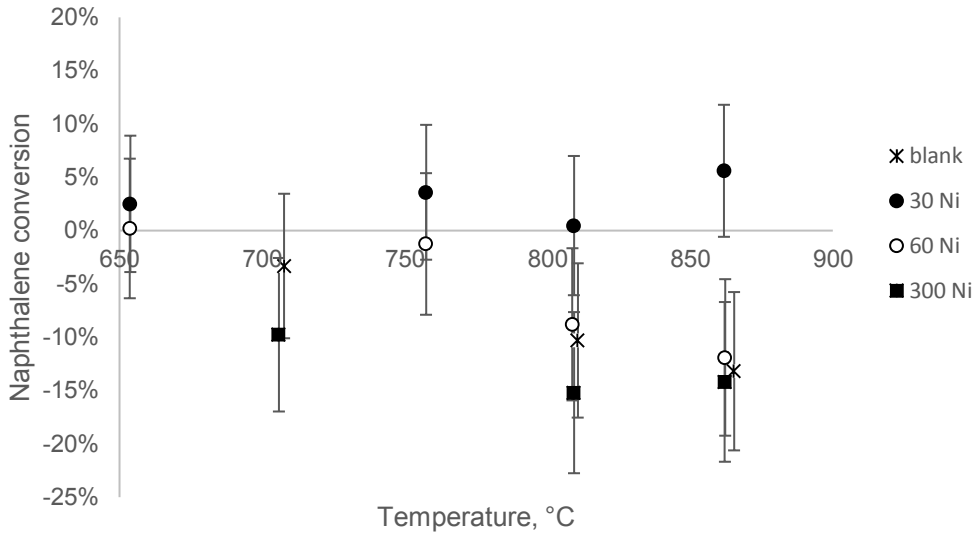

Figure 31. Conversion of naphthalene on 1.4767 mod.2 filters with Ni coating.

On 316L steel alloy filter, that showed reasonable activity as blank filter at high temperature, no activity was detected after Al_2O_3 coating or nickel coating of 30 cycles. This supports the theory of steel alloy surface activation at temperature of over 850 °C. The results for filters and coatings deposited on 316L steel are presented in Figure 32.

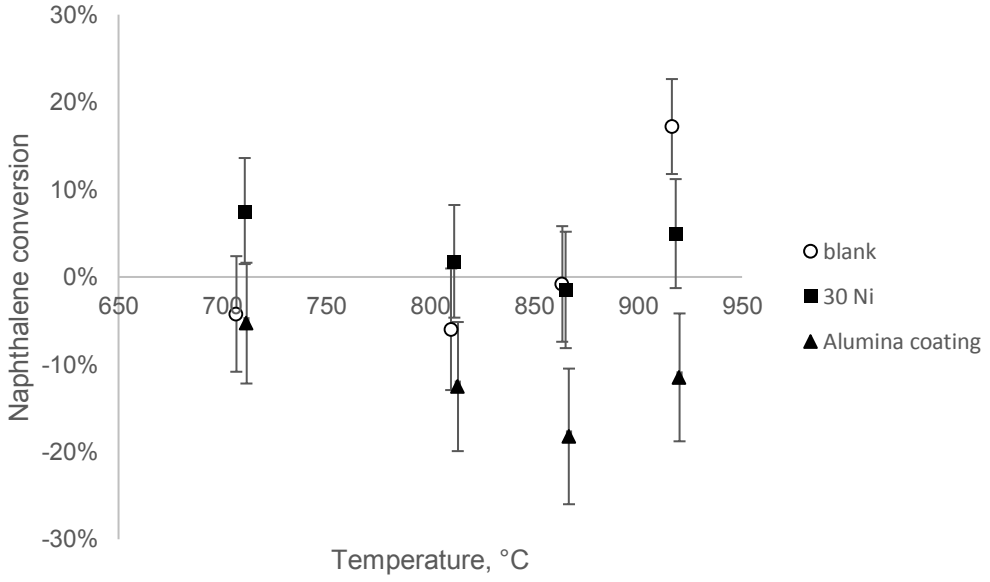

Figure 32. Conversion of naphthalene on 316L filters.

In reaction tests of filters with nickel coating, no major difference was found on filters compared to blank filters, with respect to tar conversion. Compared to results of Kivelä (2018), low activity can be caused due to low amount of nickel, since samples used by Kivelä contained from 400 to 1600 ALD cycles of nickel, compared to from 30 to 300 ALD cycles used in these experiments. Low overall amount of nickel causes low nickel surface area, and as a consequence, low number of active sites. The presence of sulphur compounds in feed gas even increases the number of active sites needed, since activity is lost due to sulphur adsorption. Additionally, the sintering of metallic nickel due to high temperature might decrease the surface area even more.

Estimation of low active metal surface area was done in this work only according to SEM-EDS analysis and low nickel content inside the filter. In the future, the result could be confirmed with chemisorption analysis. In addition, chemisorption could give more information about the nickel surface area of catalytically active filters prepared earlier by Kivelä (2018) for comparison.

6.2.4 Coke formation and pressure drop increase

Surprisingly, no significant pressure drop over the filter was observed in the test runs, while Kivelä (2018) observed major increase of pressure drop of 245 - 1123 mbar, and even causing the clogging of the filter at higher temperature settings. In this work, the highest measured pressure drop in similar conditions was 148 mbar with filter with 300 cycles of NiO. This can be explained by the coke formation caused by decomposition of naphthalene, where coke and soot are formed especially at high temperature of over 800 °C (Gai *et al.*, 2016). While Kivelä (2018) achieved high naphthalene conversion, also coke formation was significant.

Increase of coke formation can be detected also in the mass of carbon deposited on filters after the test run. The highest amount of 0.65 g of carbon was formed on uncoated filter made of nickel-containing 316L steel, where also naphthalene conversion of 17% was achieved. On 316L steel filters, mass of coke formed on the filter in reaction run increased as proportional to naphthalene conversion.

Interestingly, generally more weight addition due to coking regardless of naphthalene conversion was detected on 316L filters than on 1.4767 mod.2 steel filters. This could be assigned to higher void volume and surface area of the filters.

6.3 Filter with 1600 cycles of nickel oxide

One of the tests of catalytically active filters of Kivelä (2018) was repeated with newly made filter of 15 nm of Al_2O_3 and 28-35 nm of NiO, deposited using same process, temperatures and set-up in ALD reactor. However, no increased catalytic activity was detected with this filter either, as seen in Figure 33. SEM-EDS analysis highlights that high amount of nickel is present on top surface of the filter, as well as inside and bottom surface of the filter, when the other filter disc from same ALD run was characterized.

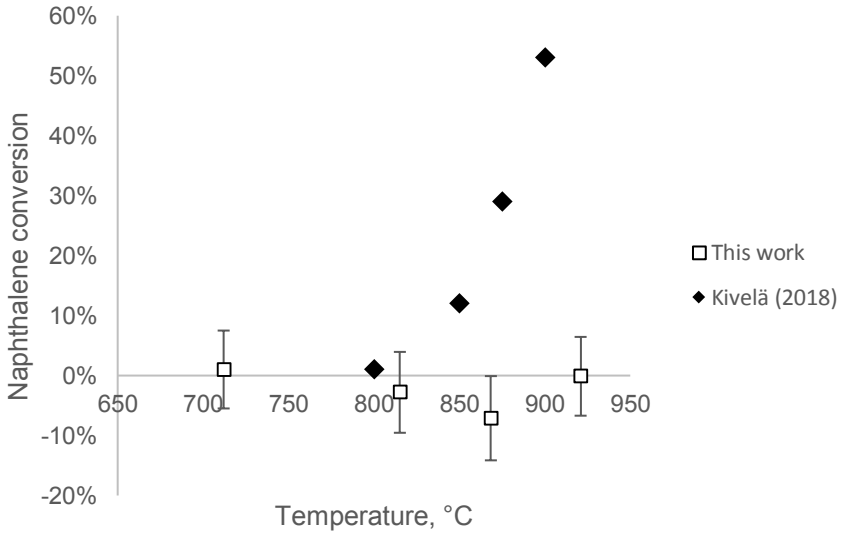

Figure 33. Conversion of naphthalene gained in this work compared to conversion measured for filter with similar coating by Kivelä (2018).

Possible explanations for inactivity of the filter include the contamination of the ALD nickel precursor, unexpected form of the catalyst in terms of nickel oxide or metallic nickel, poisoning of the catalyst during the experiment or during handling of the catalyst, failure of analytical devices or analysis or inadequate contact of feed and catalyst due to flow past the filter through the quartz wool sealant instead of flowing

through the filter. Also high sulphur-containing pulse at the start of the experiment could poison the catalyst.

However, no sign of sulphur pulse was found, and according to earlier studies the activity loss due to sulphur can be neglected at temperature of over 900 °C (Kivelä, 2018). High temperature and reductive feed gas containing H_2 and CO should reduce the nickel layer to catalytically active metallic form (Shang *et al.*, 2017). No sign of failure of analytical devices was detected since the results were realistic and steady in gas analyser and gas chromatograph. In addition, no sign of flow by the filter was shown after the reaction experiment. According to these observations, the most probable reasons for inactivity was the contamination or other failure in the catalytic layer preparation. However, the flow passing by the filter could not be ruled out.

Interestingly, filters coated with nickel oxide had purple coating on top of the filters, as shown earlier in Figure 11. The colour of the film formed on the silicon wafer chips was brown, as well as the colour formed on the surfaces and filters in previous runs. Purple colour was formed on top and sides of the filter, while the inside and bottom were metallic and brown. No purple colour was reported by Kivelä (2018) nor Seim *et al.* (1997) in deposition of nickel oxide with $Ni(thd)_2$ and ozone as precursors. Seim *et al.* (1997) list possible causes for colour change in $LaNiO_3$ ALD film to be I) film thickness, II) impurities in deposited film, III) crystallinity of the film, IV) multiple phases in the film and V) oxygen non-stoichiometry.

Film thickness can explain the difference in colour, when the thickest film has been formed on top and sides of the filters, where the colour has been formed. Diffusion limitations during the deposition process limit the thickness of the film inside and under the discs. However, if the film thickness is assumed to be the cause for different colour, it does not explain the inactivity.

It is noteworthy that high amount of carbon is characterized both, top and bottom side of the filter disc. While the blank sample or the sample with only alumina layer contains only 2 w-% carbon, 4 w-% of carbon is found from the bottom and 6 w-% from the top of the disc in SEM-EDS analysis. Additionally, amount of carbon added is proportional to amount of nickel added in the deposition process, as shown in Figure 34. The proportionality might be caused due to impurity during ALD deposition, caused either

by impurity in reactor, contaminated reagent or error in pulsing leading to inadequate removal of carbon-containing ligands during deposition. Similar trend is noticed in silicon wafer chips used for monitoring the deposition, while a silicon wafer chip with 28-35 nm of nickel oxide contains 4.5 w-% of carbon, compared to 3.1 w-% detected on silicon wafer chip with 11-13 nm of NiO.

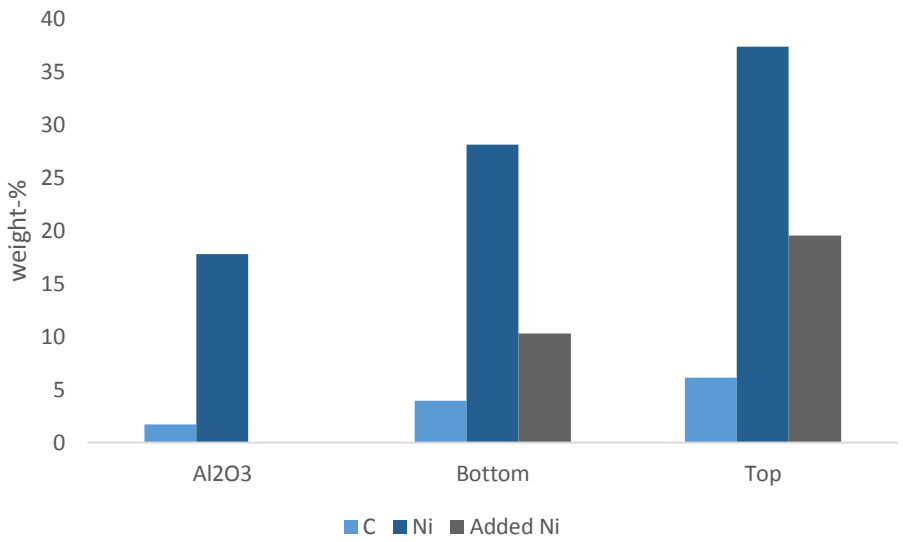

Figure 34. Carbon and nickel on unused catalytic filter with only alumina coating, and coating of 1600 cycles of NiO on top and bottom surfaces of the filter. Nickel coating added the difference of nickel compared to filter with only Al_2O_3.

However, EDS mapping of the surface of the sample from the top of the filter shows most of the carbon to be present in specific areas, as shown in Figure 35. High amount of carbon on specific areas could be caused due to contamination from for example the graphene tape that is used for preparation of the SEM-EDS samples.

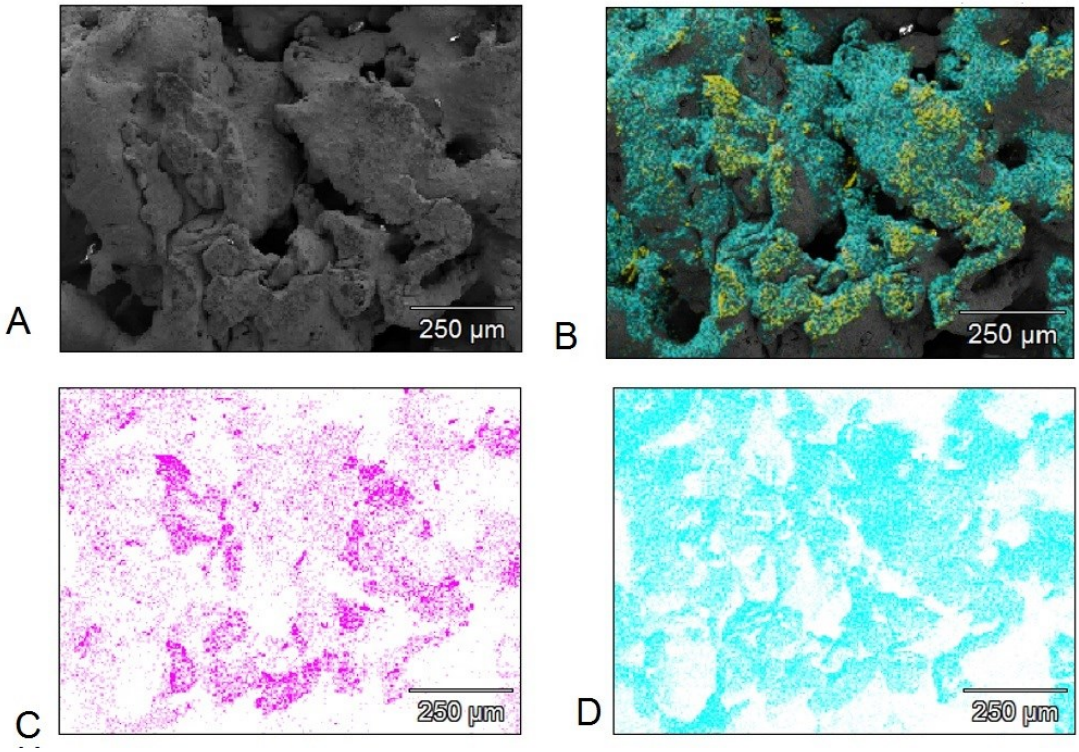

Figure 35. SEM-EDS image of top side of 1600 cycles of NiO containing filter disc. A) Grey colour of background, B) Nickel and carbon highlighted with blue and yellow, respectively, C) Carbon counts highlighted with red, D) Nickel counts highlighted with blue.

Carbon contamination in nickel oxide film during the deposition could possibly explain also the change in colour, as well as the lack of catalytic activity, if it prevents the formation of catalytically active metallic nickel, or blocks or poisons the catalytically active sites. Possible effect of carbon could be further studied by additional SEM-EDS analysis of the filter from different spots to confirm or repeal the high amount of carbon. In addition, repetition of the deposition and re-testing filter could confirm the inactivity, if similar layer is formed.

6.4 Error estimation

6.4.1 Sources of error in ALD

During the ALD coating, process conditions are assumed to be constant, and the variation of temperature and pressure is assumed not to have effect on coating

results. Results for alumina coatings are consistent. For nickel coatings, error in deposition monitoring and filter deposition distribution is caused due to precursor probably not flowing directly through the filter, but bypassing it from between the filter and the holder or between the holder and reactor wall. In addition, contamination of samples during the ALD process is possible due to impurities in the reactor, as well as incomplete removal of precursor ligands.

6.4.2 Sources of error in SEM-EDS analysis

During SEM-EDS analysis, error is caused especially in samples with low amount of nickel from other peaks close to the low energy nickel L lines used for detection, especially iron. Use of high acceleration voltage for electron beams and therefore detection and analysis of nickel from K lines could be used for more accurate results.

SEM-EDS is not analysing the composition of the surface but the volume under it (Leng, 2013). The range of this spatial resolution depends on the acceleration voltage and the atom detected, which causes error to results (Leng, 2013). Typically, the range is between 0 and 5 µm (Leng, 2013). To detect concentrations lower than 1 w-% with SEM-EDS, long measurement times are needed (Leng, 2013).

To gain more reliable results, multiple analyses should be conducted for multiple samples of same disc from different spots and the measurements should be repeated. Especially the shadows caused by rough surface of the filters can cause variation to analysis results. In these results, the number of measurements per sample varies between 1 and 3.

Additionally, while the samples prepared by cleaving the filters were unequal in size and shape, the control of the take-off angle from specimen to the detector was not controlled, which may affect the results (Leng, 2013). For further studies, the proper sample preparation method for cleaved filters should be introduced, including cleavage of filters to equal pieces without risk for contamination from tools and preparation of the surface for measurement by polishing to avoid the shadows created by rough surface.

6.4.3 Sources of error in reaction tests

In reaction tests, errors were caused due to errors in control of the feed and analysis of the product, as well as temperature and pressure control of the reactor. Also the sample preparation, for example tightening the filter to the quartz reactor, might cause error to the results.

As previously mentioned, the decomposition of the tar reactants fed to the system cannot be verified with used analysis setup, where naphthalene is the highest molecular weight tar detected. The decrease of naphthalene or other tar compounds can be due to formation of even higher molecular weight tars that are not detected in analysis used, instead of tar decomposition. However, minimisation of the error due to the formation of higher molecular weight tars was performed by monitoring the amount and height of the gas chromatography peaks after the eluation of naphthalene.

To avoid the errors in the feed fatal to the activity of the catalyst, the concentration of H_2S in the feed gas was measured by Dräger tube analysis (Dräger, 2011). The analysis equipment was shown to operate properly by performing one test run with catalytic Ni/Al_2O_3 bed instead of prepared catalytic filters.

Results of reaction tests were calculated from the analysis results gained from the gas chromatograph and gas analyser and from known inlet flowrate of ideal gas. Inaccuracy for gas analyser and gas chromatograph was assumed to be ±5%. Calibration of mass flow controllers was checked before starting the reaction tests, and two independent flow controllers measured with gas flow rate meter showed an error of ±2% for inlet flow of dry gas. Error for isocratic pumps feeding water and tars was assumed to be ±1%. Ideal gas assumption is reasonable in relatively low pressure and high temperature, and error caused due to ideal gas assumption is negligible compared to other errors. Temperature control of the furnace is assumed to have an error of ±3 ºC, and more error in temperature is caused due to exothermic and endothermic reactions taking place in reactor. Temperature was measured from the bottom surface of the filters.

Error for measured tar and other conversions was calculated by partial derivation of the equation of conversion presented in Equation 18. The equation for calculation of error in conversion for component i is presented in Equation 19, and the derivation is presented in Appendix 5.

$$X_i = \frac{F_{i,in} - F_{i,out}}{F_{i,in}} = \frac{F_{tot,in} \cdot y_{i,in} - F_{tot,out} \cdot y_{i,out}}{F_{tot,in} \cdot y_{i,in}} = \frac{(F_{dry,in} + F_{water,in}) \cdot y_{i,in} - F_{tot,out} \cdot y_{i,out}}{(F_{dry,in} + F_{water,in}) \cdot y_{i,in}} \quad (18)$$

$$\Delta X_i = \left|\frac{\partial X_i}{\partial F_{water,in}}\right| \Delta F_{water,in} + \left|\frac{\partial X_i}{\partial F_{dry,in}}\right| \Delta F_{dry,in} + \left|\frac{\partial X_i}{\partial y_{i,in}}\right| \Delta y_{i,in} + \left|\frac{\partial X_i}{\partial y_{i,out}}\right| \Delta y_{i,out} =$$
$$\left|\frac{F_{tot,out} \cdot y_{i,out}}{(F_{dry,in} + F_{water,in})^2 \cdot y_{i,in}}\right| (\Delta F_{dry,in} + \Delta F_{water,in}) + \left|\frac{F_{tot,out} \cdot y_{i,out}}{F_{dry,in} + F_{water,in}}\right| \Delta y_{i,in} +$$
$$\left|-\frac{F_{tot,out}}{(F_{dry,in} + F_{water,in}) \cdot y_{i,in}}\right| \Delta y_{i,out} \quad (19)$$

Where

y_i is the molar fraction, and when ideal gas assumption is applied, the volume fraction of component i, available as result from analysis device (mol-%),

F_{tot} is the total molar flow that is directly proportional to total volumetric flow due to ideal gas assumption (mol/s),

$F_{dry,in}$ is the total molar inlet flow rate of dry gas (mol/s),

$F_{water,in}$ is the total molar inlet flow rate of water (mol/s),

$F_{tot,out}$ is the total molar flow rate out from the system, that is used as variable in calculations (mol/s) and

$\Delta F_{dry,in}, \Delta F_{water,in}, \Delta y_{i,in}, \Delta y_{i,out}$ are the absolute errors of the measured quantities in respective units.

7 Conclusions and proposals for future studies

The aim of this thesis was to develop methods for preparation of catalytic coatings by ALD for catalytic filtration of gasification gas. Catalytic filters were prepared with ALD method for tar reforming with flow-through deposition method aiming to form a uniform catalytic coating on all surfaces of the filter. Rhodium was studied as an alternative active metal for catalytic filter preparation. Filters were characterized by SEM-EDS method.

In the deposition of catalytic nickel coating by flow-through method, the coating was observed only on the top surface of the filter, probably due to suboptimal flow of precursor. Deposition method, where ALD coating of filter pores is based on the diffusion of the precursor is more effective in filter coating in terms of amount of nickel inside the filter. To improve the flow-through coating method, steady flow of precursor through the filter should be confirmed by improved tool. On the other hand, for example combination of stop-flow and flow-through method could be applied to improve the deposition on the filter inner surfaces. Also, other methods for filter coating could be studied, since successful results of nickel coating of filter elements have been presented with for example co-precipitation deposition.

Development of catalytic filter characterization methods is required for further studies. Coherent sample preparation and measurement method for steel filters should be developed to improve the reliability of the characterization results of the SEM-EDS analysis. The size and shape of the sample and roughness of the sample surface are issues to be solved to achieve comparable results between different samples, especially for inside parts of the filters. Additionally, chemisorption analysis could be conducted as a part of the research to study the surface area of the active metal deposited on filter.

Rhodium coating of catalytic filters was studied, but no rhodium was detected on filters in SEM-EDS analysis. No controlled ALD growth of Rh layer was detected during the experiments. Since no rhodium was detected on filters, the activity of rhodium coated filters was not tested in reaction tests. Major development is needed for rhodium ALD process, focusing on sublimation conditions and adsorption chemistry of the

precursor. However, literature review demonstrates the potential of Rh as catalyst, and resolving the issues regarding the ALD process could open vast possibilities in catalyst research and development.

The activities of the coated filters were tested in reaction experiments. Due to low amount of nickel deposited on filters, no significant activity in tar decomposition was observed. The best activity in the reaction tests was observed on nickel-containing steel alloy 316L as blank steel, where naphthalene conversion of 17% was reached at 920 ˚C. Activation of nickel-containing steel alloys at high temperature of 850 ˚C has been previously reported as well. Even more nickel containing material could be studied as filter material, if suitable material for challenging conditions is found. In addition, nickel-containing steel could be applied as construction material for high-temperature process equipment to improve the conversion of tar compounds. However, drastic increase of catalytic activity and naphthalene conversion from observed 17% is needed for steel to be an interesting catalyst in terms of catalytic filtration for gasification gas.

8 Bibliography

Aaltonen, T., Ritala, M. & Leskelä, M. 2005, ALD of rhodium thin films from Rh(acac)3 and oxygen, Electrochemical and Solid-State Letters, vol. 8, no. 8, pp. C101. DOI: 10.1149/1.1940507.

Abbas, H.F. & Daud, W. M. A. Wan 2010, Influence of Reactor Material and Activated Carbon on the Thermocatalytic Decomposition of Methane for Hydrogen Production, Applied Catalysis A: General, vol. 388, pp. 232-239, DOI: 10.1016/j.apcata.2010.08.057.

Amanipour, M., Towfighi, J., Zamaniyan, A., Babakhani, E.G. & Heidari, M. 2016, Performance of a nickel–alumina catalytic layer for simultaneous production and purification of hydrogen in a tubular membrane reactor, RSC Advances, vol. 6, no. 79, pp. 75686-75692. DOI: 10.1039/C6RA12870J.

Anon 2018, COMSYN - Technology. [Cited 2019, Mar 18th]. Available online: https://www.comsynproject.eu/technology/.

Artetxe, M., Alvarez, J., Nahil, M.A., Olazar, M. & Williams, P.T. 2017, Steam Reforming of Different Biomass Tar Model Compounds Over Ni/Al2O3 Catalysts, Energy Conversion and Management, vol. 136, pp. 119-126, DOI: 10.1016/j.enconman.2016.12.092.

Baboian, Robert. 2016. NACE Corrosion Engineer's Reference Book, 4th Edition. NACE International. ISBN 978-1-5231-0657-8 (electronic). Available online: https://app.knovel.com/hotlink/toc/id:kpNACECE01/nace-corrosion-engineers/nace-corrosion-engineers

Barroso-Quiroga, M.M. & Castro-Luna, A.E. 2010, Catalytic Activity and Effect of Modifiers on Ni-Based Catalysts for the Dry Reforming of Methane, International Journal of Hydrogen Energy, vol. 35, pp. 6052-6056, DOI: 10.1016/j.ijhydene.2009.12.073.

Bartholomew, C.H. 1993, Sintering Kinetics of Supported Metals: New Perspectives from a Unifying GPLE Treatment, Applied Catalysis A: General, vol. 107, pp. 1-57, DOI: 10.1016/0926-860X(93)85114-5.

Basu, P. 2013. Biomass Gasification, Pyrolysis and Torrefaction. 2nd ed. Academic Press. pp. 249-313, ISBN 9780-123964885.

Bengaard, H.S., Nørskov, J.K., Sehested, J., Clausen, B.S., Nielsen, L.P., Molenbroek, A.M. & Rostrup-Nielsen, J.R. 2002, Steam Reforming and Graphite Formation on Ni Catalysts, Journal of Catalysis, vol. 209, pp. 365-384, DOI: 10.1006/jcat.2002.3579.

Besenbacher, F., Chorkendorff, I., Clausen, B.S., Hammer, B., Molenbroek, A.M., Nørskov, J.K. & Stensgaard, I. 1998, Design of a surface alloy catalyst for steam reforming, Science, vol. 279, no. 5358, pp. 1913-1915. DOI: 10.1126/science.279.5358.1913

BGH Edelstahl, Material Data Sheet 1.4767. [Cited 2019, Mar 18th]. Available online: https://www.baykalrezistans.com/yuklenen/pdf/kategoriler/1521028908/1521546575 14767engl.pdf [2019, .

Chen, T., Liu, H., Shi, P., Chen, D., Song, L., He, H. & Frost, R.L. 2013, CO2 Reforming of Toluene as Model Compound of Biomass Tar on Ni/Palygorskite, Fuel, vol. 107, pp. 699-705, DOI: 10.1016/j.fuel.2012.12.036.

Chen, Y. & Ren, J. 1994, Conversion of methane and carbon dioxide into synthesis gas over alumina-supported nickel catalysts. Effect of Ni-Al2O3 interactions, Catalysis Letters, vol. 29, no. 1-2, pp. 39-48. DOI: 10.1007/BF00814250.

Coll, R., Salvadó, J., Farriol, X. & Montané, D. 2001, Steam Reforming Model Compounds of Biomass Gasification Tars: Conversion at Different Operating Conditions and Tendency Towards Coke Formation, Fuel Processing Technology, vol. 74, pp. 19-31, DOI: 10.1016/S0378-3820(01)00214-4.

de Lasa, H., Salaices, E., Mazumder, J. & Lucky, R. 2011, Catalytic Steam Gasification of Biomass: Catalysts, Thermodynamics and Kinetics, Chemical reviews, vol. 111, no. 9, pp. 5404-5433. DOI: 10.1021/cr200024w.

Deng, W., Lee, S., Libera, J.A., Elam, J.W., Vajda, S. & Marshall, C.L. 2011, Cleavage of the C–O–C Bond on Size-Selected Subnanometer Cobalt Catalysts and on ALD-Cobalt Coated Nanoporous Membranes, Applied Catalysis A: General, vol. 393, pp. 29-35, DOI: 10.1016/j.apcata.2010.11.022.

Devi, L., Ptasinski, K.J., Janssen, Frans J. J. G., van Paasen, Sander V. B., Bergman, P.C.A. & Kiel, J.H.A. 2005, Catalytic Decomposition of Biomass Tars: Use of Dolomite and Untreated Olivine, Renewable Energy, vol. 30, pp. 565-587, DOI: 10.1016/j.renene.2004.07.014.

Di Mondo, D., Ashok, D., Waldie, F., Schrier, N., Morrison, M. & Schlaf, M. 2011, Stainless Steel as a Catalyst for the Total Deoxygenation of Glycerol and Levulinic Acid in Aqueous Acidic Medium, ACS Catalysis, vol. 1, no. 4, pp. 355-364. DOI: 10.1021/cs200053h.

Dräger 2011, Dräger-Tubes. CMS-Handbook 16th edition. Available: https://www.draeger.com/library/content/tubeshandbook_br_9092086_en.pdf.

Elam, J.W., Libera, J.A., Pellin, M.J. & Stair, P.C. 2007, Spatially controlled atomic layer deposition in porous materials, Applied Physics Letters, vol. 91, no. 24. DOI: 10.1063/1.2822897.

Elam, J.W., Pellin, M.J. & Stair, P.C. 2010. US 7713907B2. Method of Preparing Size-Selected Metal Clusters.

Elliot, D.C., Soltes, E.J. (ed.) & Milne, T.A. (ed.) 1988, Relation of reaction time and temperature to chemical composition of pyrolysis oils. pp. 55-65. (Pyrolysis oils from biomass) ISBN: 9780841215368.

Engelen, K., Zhang, Y., Draelants, D.J. & Baron, G.V. 2003, A Novel Catalytic Filter for Tar Removal from Biomass Gasification Gas: Improvement of the Catalytic Activity

in Presence of H_2S, Chemical Engineering Science, vol. 58, pp. 665-670, DOI: 10.1016/S0009-2509(02)00593-6.

Ferella, F., Stoehr, J., Michelis, I.D. & Hornung, A. 2013, Zirconia and Alumina Based Catalysts for Steam Reforming of Naphthalene, Fuel, vol. 105, pp. 614-629, DOI: 10.1016/j.fuel.2012.09.052.

Forzatti, P. & Lietti, L. 1999, Catalyst Deactivation, Catalysis Today, vol. 52, pp. 165-181, DOI: 10.1016/S0920-5861(99)00074-7.

Gai, C., Dong, Y., Yang, S., Zhang, Z., Liang, J. & Li, J. 2016, Thermal decomposition kinetics of light polycyclic aromatic hydrocarbons as surrogate biomass tar, RSC Advances, vol. 6, no. 86, pp. 83154-83162. DOI: 10.1039/C6RA15513H

Garbarino, G., Lagazzo, A., Riani, P. & Busca, G. 2013, Steam Reforming of Ethanol–phenol Mixture on Ni/Al2O3: Effect of Ni Loading and Sulphur Deactivation, Applied Catalysis B: Environmental, vol. 129, pp. 460-472, DOI: 10.1016/j.apcatb.2012.09.036.

Gil, J., Corella, J., Aznar, M.P. & Caballero, M.A. 1999, Biomass Gasification in Atmospheric and Bubbling Fluidized Bed: Effect of the Type of Gasifying Agent on the Product Distribution, Biomass and Bioenergy, vol. 17, pp. 389-403, DOI: 10.1016/S0961-9534(99)00055-0.

GKN Sinter Metals, Standard Materials. [Cited 2019, Mar 18th]. Available online: https://www.gknpm.com/globalassets/downloads/powder-met-pdf/porous-metal-filter-materials-table.pdf/.

Gould, T.D., Lubers, A.M., Neltner, B.T., Carrier, J.V., Weimer, A.W., Falconer, J.L. & Will Medlin, J. 2013, Synthesis of Supported Ni Catalysts by Atomic Layer Deposition, Journal of Catalysis, vol. 303, pp. 9-15, DOI: 10.1016/j.jcat.2013.03.013.

Gould, T.D., Montemore, M.M., Lubers, A.M., Ellis, L.D., Weimer, A.W., Falconer, J.L. & Medlin, J.W. 2015, Enhanced Dry Reforming of Methane on Ni and Ni-Pt Catalysts

Synthesized by Atomic Layer Deposition, Applied Catalysis A: General, vol. 492, pp. 107-116, DOI: 10.1016/j.apcata.2014.11.037.

Hämäläinen, J., Ritala, M. & Leskelä, M. 2014, Atomic layer deposition of noble metals and their oxides, Chemistry of Materials, vol. 26, no. 1, pp. 786-801. DOI: 10.1021/cm402221y

Hämäläinen, J., Munnik, F., Ritala, M. & Leskelä, M. 2009, Study on Atomic Layer Deposition of Amorphous Rhodium Oxide Thin Films, Journal of the Electrochemical Society, vol. 156, no. 10, pp. D423. DOI: 10.1149/1.3190157

Hämäläinen, J., Puukilainen, E., Sajavaara, T., Ritala, M. & Leskelä, M. 2013, Low Temperature Atomic Layer Deposition of Noble Metals using Ozone and Molecular Hydrogen as Reactants, Thin Solid Films, vol. 531, pp. 243-250, DOI: 10.1016/j.tsf.2013.01.091.

Haukka, S., Lakomaa, E.-L. & Suntola, T. 1999, Adsorption Controlled Preparation of Heterogeneous Catalysts, Elsevier, Studies in Surface Science and Catalysis, vol. 120, pp. 715-750, DOI: 10.1016/S0167-2991(99)80570-9 ".

Heidenreich, S. 2013, Hot Gas Filtration – A Review, Fuel, vol. 104, pp. 83-94, DOI: 10.1016/j.fuel.2012.07.059.

Heidenreich, S., Nacken, M., Hackel, M. & Schaub, G. 2008, Catalytic Filter Elements for Combined Particle Separation and Nitrogen Oxides Removal from Gas Streams, Powder Technology, vol. 180, pp. 86-90, DOI: 10.1016/j.powtec.2007.02.033.

Hepola, J. 2000, Sulfur Transformations in Catalytic Hot-Gas Cleaning of Gasification Gas, doctoral dissertation. Department of Chemical Technology, Helsinki University of Technology. VTT Publ. 54 p.

Hosokai, S., Kumabe, K., Ohshita, M., Norinaga, K., Li, C. & Hayashi, J. 2008, Mechanism of Decomposition of Aromatics Over Charcoal and Necessary Condition for Maintaining its Activity, Fuel, vol. 87, pp. 2914-2922, DOI: 10.1016/j.fuel.2008.04.019.

Italiano, C., Luchters, N.T.J., Pino, L., Fletcher, J.V., Specchia, S., Fletcher, J.C.Q. & Vita, A. 2018, High Specific Surface Area Supports for Highly Active Rh Catalysts: Syngas Production from Methane at High Space Velocity, International Journal of Hydrogen Energy, vol. 43, pp. 11755-11765, DOI: 10.1016/j.ijhydene.2018.01.136.

Jeong, M., Park, E.J., Jeong, B., Kim, D.H. & Kim, Y.D. 2014, Toluene Combustion Over NiO Nanoparticles on Mesoporous SiO2 Prepared by Atomic Layer Deposition, Chemical Engineering Journal, vol. 237, pp. 62-69, DOI: 10.1016/j.cej.2013.09.100.

Jess, A. 1996, Mechanisms and Kinetics of Thermal Reactions of Aromatic Hydrocarbons from Pyrolysis of Solid Fuels, Fuel, vol. 75, pp. 1441-1448, DOI: 10.1016/0016-2361(96)00136-6.

Kaisalo, N.K., Koskinen-Soivi, M., Simell, P.A. & Lehtonen, J. 2015, Effect of Process Conditions on Tar Formation from Thermal Reactions of Ethylene, Fuel, vol. 153, pp. 118-127, DOI: 10.1016/j.fuel.2015.02.085.

Kaisalo, N., Kihlman, J., Hannula, I. & Simell, P. 2015, Reforming Solutions for Biomass-Derived Gasification Gas – Experimental Results and Concept Assessment, Fuel, vol. 147, pp. 208-220, DOI: 10.1016/j.fuel.2015.01.056.

Kiel, J.H.A., van Paasen, S. V. B., Neeft, J.P.A., Devi, L., Ptasinski, K.J., Janssen, F. J. J. G., Meijer, R., Berends, R.H., Temmink, H.M.G., Brem, G., Padban, N. & Bramer, E.A. 2004, Primary measures to reduce tar formation in fluidised-bed biomass gasifiers - Final report SDE project P1999-012. Available online: https://pure.tue.nl/ws/files/4367413/576697.pdf

Kihlman, J., Kaisalo, N., Koskinen-Soivi, M., Simell, P., Niemelä, M. & Lehtonen, J. 2018, Whisker Carbon Formation in Catalytic Steam Reforming of Biomass Gasification Gas, Applied Catalysis A: General, vol. 564, pp. 133-141, DOI: 10.1016/j.apcata.2018.07.011.

Kim, D.H., Sim, J.K., Lee, J., Seo, H.O., Jeong, M.-G, Kim, Y.D. & Kim, S.H. 2013, Carbon dioxide reforming of methane over mesoporous Ni/SiO2, Fuel, vol. 112, pp. 111-116. DOI: 10.1016/j.fuel.2013.04.089.

Kivelä, V. 2018, Filtration of biomass-based gasification gas at elevated temperatures. Master's thesis. Aalto University, School of Chemical Engineering.

Koike, M., Li, D., Watanabe, H., Nakagawa, Y. & Tomishige, K. 2015, Comparative Study on Steam Reforming of Model Aromatic Compounds of Biomass Tar Over Ni and Ni–Fe Alloy Nanoparticles, Applied Catalysis A: General, vol. 506, pp. 151-162, DOI: 10.1016/j.apcata.2015.09.007.

Kuramochi, H., Wu, W. & Kawamoto, K. 2005, Prediction of the Behaviors of H2S and HCl during Gasification of Selected Residual Biomass Fuels by Equilibrium Calculation, Fuel, vol. 84, pp. 377-387, DOI: 10.1016/j.fuel.2004.09.009.

Kurkela, E., Kurkela, M. & Hiltunen, I. 2016, Steam–oxygen Gasification of Forest Residues and Bark Followed by Hot Gas Filtration and Catalytic Reforming of Tars: Results of an Extended Time Test, Fuel Processing Technology, vol. 141, pp. 148-158, DOI: 10.1016/j.fuproc.2015.06.005.

Kurungot, S., Yamaguchi, T. & Nakao, S. 2003, Rh/γ-Al2O3 Catalytic Layer Integrated with Sol–Gel Synthesized Microporous Silica Membrane for Compact Membrane Reactor Applications, Catalysis Letters, vol. 86, no. 4, pp. 273-278. DOI: 10.1023/A:1022636606705

Lakomaa, E. 1994, Atomic Layer Epitaxy (ALE) on Porous Substrates, Applied Surface Science, vol. 75, pp. 185-196, DOI: 10.1016/0169-4332(94)90158-9.

Leng, Y. 2013, Materials Characterization: Introduction to Microscopic and Spectroscopic Methods, John Wiley & Sons, Weinheim. 337 p. ISBN 9780470822982.

Li, C. & Suzuki, K. 2009, Tar Property, Analysis, Reforming Mechanism and Model for Biomass gasification—An Overview, Renewable and Sustainable Energy Reviews, vol. 13, pp. 594-604, DOI: 10.1016/j.rser.2008.01.009.

Li, D., Koike, M., Wang, L., Nakagawa, Y., Xu, Y. & Tomishige, K. 2014, Regenerability of Hydrotalcite-Derived Nickel–Iron Alloy Nanoparticles for Syngas Production from Biomass Tar, ChemSusChem, vol. 7, no. 2, pp. 510-522. DOI: 10.1002/cssc.201300855.

Li, Y., Jiang, J., Zhu, C., Li, L., Li, Q., Ding, Y. & Yang, W. 2018, The Enhanced Catalytic Performance and Stability of Rh/γ-Al_2O_3 Catalyst Synthesized by Atomic Layer Deposition (ALD) for Methane Dry Reforming, Materials, vol. 11, no. 1, pp. 172. DOI: 10.3390/ma11010172.

Ligthart, D. A. J. M., van Santen, R.A. & Hensen, E.J.M. 2011, Influence of Particle Size on the Activity and Stability in Steam Methane Reforming of Supported Rh Nanoparticles, Journal of Catalysis, vol. 280, pp. 206-220, DOI: 10.1016/j.jcat.2011.03.015.

Ligthart, D. A. J. Michel, Filot, I.A.W., Almutairi, A.A.H. & Hensen, E.J.M. 2016, Identification of Step-Edge Sites on Rh Nanoparticles for Facile CO Dissociation, Catalysis Communications, vol. 77, pp. 5-8, DOI: 10.1016/j.catcom.2016.01.006.

Lin, Y.-S. & Burggraaf, A.J. 1991, Preparation and Characterization of High-Temperature Thermally Stable Alumina Composite Membrane, Journal of the American Ceramic Society, vol. 74, no. 1, pp. 219-224. DOI: 10.1111/j.1151-2916.1991.tb07320.x

Lindblad, M., Lindfors, L.P. & Suntola, T. 1994, Preparation of Ni/Al2O3 catalysts from vapor phase by atomic layer epitaxy, Catalysis Letters, vol. 27, no. 3-4, pp. 323-336. DOI: 10.1007/BF00813919.

Lindfors, L.-P. 1994, Hydrogenation of Toluene on Supported Nickel - from Catalyst Preparation to Reaction Kinetics. Doctoral dissertation. Åbo Akademi, Department of Chemical Engineering. Turku. 50 p.

Lu, J., Fu, B., Kung, M.C., Xiao, G., Elam, J.W., Kung, H.H. & Stair, P.C. 2012, Coking- and Sintering-Resistant Palladium Catalysts Achieved Through Atomic Layer Deposition, Science, vol. 335, no. 6073, pp. 1205. DOI: 10.1126/science.1212906.

Mackus, A.J.M., Weber, M.J., Thissen, N.F.W., Garcia-Alonso, D., Vervuurt, R.H.J., Assali, S., Bol, A.A., Verheijen, M.A. & Kessels, W.M.M. 2015, Atomic layer deposition of Pd and Pt nanoparticles for catalysis: on the mechanisms of nanoparticle formation, Nanotechnology, vol. 27, no. 3, pp. 034001. DOI: 10.1088/0957-4484/27/3/034001.

Mei, D., Glezakou, V., Lebarbier, V., Kovarik, L., Wan, H., Albrecht, K.O., Gerber, M., Rousseau, R. & Dagle, R.A. 2014, Highly Active and Stable MgAl2O4-Supported Rh and Ir Catalysts for Methane Steam Reforming: A Combined Experimental and Theoretical Study, Journal of Catalysis, vol. 316, pp. 11-23, DOI: 10.1016/j.jcat.2014.04.021.

Milne, T.A., Evans, R.J. & Abatzoglou, N. 1998, Biomass Gasifier “Tars”: Their Nature, Formation, and Conversion. Available online: https://www.nrel.gov/docs/fy99osti/25357.pdf.

Miyazawa, T., Kimura, T., Nishikawa, J., Kado, S., Kunimori, K. & Tomishige, K. 2006, Catalytic Performance of Supported Ni Catalysts in Partial Oxidation and Steam Reforming of Tar Derived from the Pyrolysis of Wood Biomass, Catalysis Today, vol. 115, pp. 254-262, DOI: 10.1016/j.cattod.2006.02.055.

Nacken, M., Baron, G.V., Heidenreich, S., Rapagnà, S., D'Orazio, A., Gallucci, K., Denayer, J.F.M. & Foscolo, P.U. 2015, New DeTar Catalytic Filter with Integrated Catalytic Ceramic Foam: Catalytic Activity Under Model and Real Bio Syngas Conditions, Fuel Processing Technology, vol. 134, pp. 98-106, DOI: 10.1016/j.fuproc.2015.01.020.

Nacken, M., Ma, L., Heidenreich, S. & Baron, G.V. 2010, Catalytic Activity in Naphthalene Reforming of Two Types of Catalytic Filters for Hot Gas Cleaning of Biomass-Derived Syngas, Industrial & Engineering Chemistry Research, vol. 49, no. 12, pp. 5536-5542. DOI: 10.1021/ie901428b.

O'Neill, B.J., Jackson, D.H.K., Lee, J., Canlas, C., Stair, P.C., Marshall, C.L., Elam, J.W., Kuech, T.F., Dumesic, J.A. & Huber, G.W. 2015, Catalyst Design with Atomic Layer Deposition, ACS Catalysis, vol. 5, no. 3, pp. 1804-1825. DOI: 10.1021/cs501862h.

Pakhare, D. & Spivey, J. 2014, A review of dry (CO2) reforming of methane over noble metal catalysts, Chemical Society Reviews, vol. 43, no. 22, pp. 7813-7837. DOI: 10.1039/C3CS60395D.

Park, H.J., Park, S.H., Sohn, J.M., Park, J., Jeon, J., Kim, S. & Park, Y. 2010, Steam Reforming of Biomass Gasification Tar using Benzene as a Model Compound Over various Ni Supported Metal Oxide Catalysts0960-8524, Bioresource Technology, vol. 101, pp. S103, DOI: 10.1016/j.biortech.2009.03.036.

Pellin, M.J., Stair, P.C., Xiong, G., Elam, J.W., Birrell, J., Curtiss, L., George, S.M., Han, C.Y., Iton, L., Kung, H., Kung, M. & Wang, H.-. 2005, Mesoporous catalytic membranes: Synthetic control of pore size and wall composition, Catalysis Letters, vol. 102, no. 3, pp. 127-130. DOI: 10.1007/s10562-005-5843-9.

Pina, M.P., Menéndez, M. & Santamaría, J. 1996, The Knudsen-Diffusion Catalytic Membrane Reactor: An Efficient Contactor for the Combustion of Volatile Organic Compounds, Applied Catalysis B: Environmental, vol. 11, pp. L27, DOI: 10.1016/S0926-3373(96)00081-1.

Polychronopoulou, K., Costa, C.N. & Efstathiou, A.M. 2004, The Steam Reforming of Phenol Reaction Over Supported-Rh Catalysts, Applied Catalysis A: General, vol. 272, pp. 37-52, DOI: 10.1016/j.apcata.2004.05.002.

Puurunen, R.L. 2005, Surface chemistry of atomic layer deposition: A case study for the trimethylaluminum/water process, Journal of Applied Physics, vol. 97, no. 12. DOI: 10.1063/1.1940727.

Resistant Alloy, FeCrAl 135. [Cited 2019, Mar 18th]. Available online: http://www.resistantalloy.com/fecral135.html.

Ross, J. 2012. Heterogeneous catalysis. Burlington: Elsevier Science. [Cited 1st July 2019]. ISBN 0-08-095684-X (electronic).

Rostrup-Nielsen, J.R. & Christiansen, L.J. 2011, Concepts in Syngas Manufacture, Imperial College Press, Singapore. 392 p. ISBN 9781908978004.

Russo, P., Ciambelli, P., Palma, V. & Vaccaro, S. 2003, Simultaneous Filtration and Catalytic Oxidation of Carbonaceous Particulates, Topics in Catalysis, vol. 22, no. 1, pp. 123-129. DOI: 10.1023/A:1021484216734.

Rönkkönen, H., Simell, P., Niemelä, M. & Krause, O. 2011, Precious Metal Catalysts in the Clean-Up of Biomass Gasification Gas Part 2: Performance and Sulfur Tolerance of Rhodium Based Catalysts, Fuel Processing Technology, vol. 92, pp. 1881-1889, DOI: 10.1016/j.fuproc.2011.05.004.

Rönkkönen, H., Simell, P., Reinikainen, M., Niemelä, M. & Krause, O. 2011, Precious Metal Catalysts in the Clean-Up of Biomass Gasification Gas Part 1: Monometallic Catalysts and their Impact on Gasification Gas Composition, Fuel Processing Technology, vol. 92, pp. 1457-1465, DOI: 10.1016/j.fuproc.2011.03.006.

Rönkkönen, H., Simell, P., Reinikainen, M., Krause, O. & Niemelä, M.V. 2010, Catalytic Clean-Up of Gasification Gas with Precious Metal Catalysts – A Novel Catalytic Reformer Development, Fuel, vol. 89, pp. 3272-3277, DOI: 10.1016/j.fuel.2010.04.007.

Schaub, G., Unruh, D., Wang, J. & Turek, T. 2003, Kinetic Analysis of Selective Catalytic NOx Reduction (SCR) in a Catalytic Filter, Chemical Engineering and Processing: Process Intensification, vol. 42, pp. 365-371, DOI: 10.1016/S0255-2701(02)00056-9.

Sehested, J. 2006, Four Challenges for Nickel Steam-Reforming Catalysts, Catalysis Today, vol. 111, pp. 103-110, DOI: 10.1016/j.cattod.2005.10.002.

Seim, H., Mölsä, H., Nieminen, M., Fjellvåg, H. & Niinistö, L. 1997, Deposition of LaNiO3 thin films in an atomic layer epitaxy reactor, Journal of Materials Chemistry, vol. 7, no. 3, pp. 449-454. DOI: 10.1039/A606316K.

Shang, Z., Li, S., Li, L., Liu, G. & Liang, X. 2017, Highly Active and Stable Alumina Supported Nickel Nanoparticle Catalysts for Dry Reforming of Methane, Applied Catalysis B: Environmental, vol. 201, pp. 302-309, DOI: 10.1016/j.apcatb.2016.08.019.

Shang, Z., Li, S., Wang, Q., Gu, X. & Liang, X. 2018, Nano-engineered nickel catalysts supported on 4-channel α-Al2O3 hollow fibers for dry reforming of methane, AIChE Journal, vol. 64, no. 7, pp. 2625-2631. DOI: 10.1002/aic.16160.

Sikarwar, V.S., Zhao, M., Fennell, P.S., Shah, N. & Anthony, E.J. 2017, Progress in Biofuel Production from Gasification, Progress in Energy and Combustion Science, vol. 61, pp. 189-248, DOI: 10.1016/j.pecs.2017.04.001.

Simell, P.A., Hepola, J.O. & Krause, A.O.I. 1997, Effects of Gasification Gas Components on Tar and Ammonia Decomposition Over Hot Gas Cleanup Catalysts, Fuel, vol. 76, pp. 1117-1127, DOI: 10.1016/S0016-2361(97)00109-9.

Simell, P., Hannula, I., Tuomi, S., Nieminen, M., Kurkela, E., Hiltunen, I., Kaisalo, N. & Kihlman, J. 2014, Clean syngas from biomass—process development and concept assessment,Biomass Conversion and Biorefinery, vol. 4, no. 4, pp. 357-370. DOI: 10.1007/s13399-014-0121-y.

Singh, J.A., Yang, N. & Bent, S.F. 2017, Nanoengineering Heterogeneous Catalysts by Atomic Layer Deposition, Annual Review of Chemical and Biomolecular Engineering, vol. 8, no. 1, pp. 41-62. DOI: 10.1146/annurev-chembioeng-060816-101547.

Spath, P. & Dayton, D. 2003, Preliminary Screening—Technical and Economic Assessment of Synthesis Gas to Fuels and Chemicals with Emphasis on the Potential for Biomass-Derived Syngas. Available online: https://www.nrel.gov/docs/fy04osti/34929.pdf.

Tijmensen, M.J.A., Faaij, A.P.C., Hamelinck, C.N. & van Hardeveld, Martijn R. M. 2002, Exploration of the Possibilities for Production of Fischer Tropsch Liquids and Power Via Biomass Gasification, Biomass and Bioenergy, vol. 23, pp. 129-152, DOI: 10.1016/S0961-9534(02)00037-5.

Tomishige, K., Li, D., Tamura, M. & Nakagawa, Y. 2017, Nickel–iron alloy catalysts for reforming of hydrocarbons: preparation, structure, and catalytic properties, Catalysis Science & Technology, vol. 7, no. 18, pp. 3952-3979. DOI: 10.1039/C7CY01300K.

Torres, W., Pansare, S.S. & Goodwin, J.G. 2007, Hot Gas Removal of Tars, Ammonia, and Hydrogen Sulfide from Biomass Gasification Gas, Catalysis Reviews, vol. 49, no. 4, pp. 407-456. DOI: 10.1080/01614940701375134.

Trimm, D.L. 1997, Coke Formation and Minimisation during Steam Reforming Reactions, Catalysis Today, vol. 37, pp. 233-238, DOI: 10.1016/S0920-5861(97)00014-X.

Tuomi, S., Kurkela, E., Simell, P. & Reinikainen, M. 2015, Behaviour of Tars on the Filter in High Temperature Filtration of Biomass-Based Gasification Gas, Fuel, vol. 139, pp. 220-231, DOI: 10.1016/j.fuel.2014.08.051.

Van de Velden, M., Baeyens, J., Brems, A., Janssens, B. & Dewil, R. 2010, Fundamentals, Kinetics and Endothermicity of the Biomass Pyrolysis Reaction, Renewable Energy, vol. 35, pp. 232-242, DOI: 10.1016/j.renene.2009.04.019.

Vassilev, S.V., Baxter, D., Andersen, L.K. & Vassileva, C.G. 2010, An Overview of the Chemical Composition of Biomass, Fuel, vol. 89, pp. 913-933, DOI: 10.1016/j.fuel.2009.10.022.

Viinikainen, T., Rönkkönen, H., Bradshaw, H., Stephenson, H., Airaksinen, S., Reinikainen, M., Simell, P. & Krause, O. 2009, Acidic and Basic Surface Sites of Zirconia-Based Biomass Gasification Gas Clean-Up Catalysts, Applied Catalysis A: General, vol. 362, pp. 169-177, DOI: 10.1016/j.apcata.2009.04.037.

Wang, H.Y. & Ruckenstein, E. 2000, Carbon Dioxide Reforming of Methane to Synthesis Gas Over Supported Rhodium Catalysts: The Effect of Support, Applied Catalysis A: General, vol. 204, pp. 143-152, DOI: 10.1016/S0926-860X(00)00547-0.

Wangen, E.S., Osatiashtiani, A. & Blekkan, E.A. 2011, Reforming of syngas from biomass gasification: Deactivation by tar and potassium species, Topics in Catalysis, vol. 54, no. 13-15, pp. 960-966. DOI: 10.1007/s11244-011-9718-6.

Wei, J. & Iglesia, E. 2004, Mechanism and Site Requirements for Activation and Chemical Conversion of Methane on Supported Pt Clusters and Turnover Rate Comparisons among Noble Metals, The Journal of Physical Chemistry B, vol. 108, no. 13, pp. 4094-4103. DOI: 10.1021/jp036985z.

Westermann, T. & Melin, T. 2009, Flow-through Catalytic Membrane reactors—Principles and Applications, Chemical Engineering and Processing: Process Intensification, vol. 48, pp. 17-28, DOI: 10.1016/j.cep.2008.07.001.

Woolcock, P.J. & Brown, R.C. 2013, A Review of Cleaning Technologies for Biomass-Derived Syngas, Biomass and Bioenergy, vol. 52, pp. 54-84, DOI: 10.1016/j.biombioe.2013.02.036.

Xie, C., Chen, Y., Engelhard, M.H. & Song, C. 2012, Comparative study on the sulfur tolerance and carbon resistance of supported noble metal catalysts in steam reforming of liquid hydrocarbon fuel, ACS Catalysis, vol. 2, no. 6, pp. 1127-1137. DOI: 10.1021/cs200695t.

Xie, C., Chen, Y., Li, Y., Wang, X. & Song, C. 2010, Sulfur Poisoning of CeO2–Al2O3-Supported Mono- and Bi-Metallic Ni and Rh Catalysts in Steam Reforming of Liquid Hydrocarbons at Low and High Temperatures, Applied Catalysis A: General, vol. 390, pp. 210-218, DOI: 10.1016/j.apcata.2010.10.012.

Yi, H., Du, H., Hu, Y., Yan, H., Jiang, H. & Lu, J. 2015, Precisely Controlled Porous Alumina Overcoating on Pd Catalyst by Atomic Layer Deposition: Enhanced

Selectivity and Durability in Hydrogenation of 1,3-Butadiene, ACS Catalysis, vol. 5, no. 5, pp. 2735-2739. DOI: 10.1021/acscatal.5b00129.

Yung, M.M., Jablonski, W.S. & Magrini-Bair, K. 2009, Review of Catalytic Conditioning of Biomass-Derived Syngas, Energy Fuels, vol. 23, no. 4, pp. 1874-1887. DOI: 10.1021/ef800830n.

Zalamea, S., Pina, M.P., Villellas, A., Menéndez, M. & Santamaría, J. 1999, Combustion of volatile organic compounds over mixed-regime catalytic membranes, Reaction Kinetics and Catalysis Letters, vol. 67, no. 1, pp. 13-19. DOI: 10.1007/BF02475821.

Zhang, Y.J., Draelants, D., Engelen, K. & V. Baron, G. 2002, Improvement of Sulphur Resistance of a Nickel-modified Catalytic Filter for Tar Removal from Biomass Gasification Gas. Available online: https://digital.library.unt.edu/ark:/67531/metadc776886/m2/1/high_res_d/836333.pdf

Zhang, Y., Draelants, D.J., Engelen, K. & Baron, G.V. 2003, Development of nickel-activated catalytic filters for tar removal in H2S-containing biomass gasification gas, Journal of Chemical Technology & Biotechnology, vol. 78, no. 2, pp. 265-268. DOI: 10.1002/jctb.767.

Zhao, H., Draelants, D.J. & Baron, G.V. 2000, Preparation and Characterisation of Nickel-Modified Ceramic Filters, Catalysis Today, vol. 56, pp. 229-237, DOI: 10.1016/S0920-5861(99)00280-1.

Appendix 1 (1/2). List of catalytic filters prepared.

Filter number	Filter model number by provider	Steel alloy	Pore diameter (µm)	Dimensions of uncoated filter		Application and characterization				
				d(mm)	h (mm)	Alumina-coating, 90 cycles	NiO coating	Rh coating	Reaction test	Analysis
2	M3000419	1.4767 mod.2	75-100	24,0	3,0					BET
4	M3000416	1.4767 mod.2	160-300	25,0	3,0	x	5 cycles, ALD-run 9			
5	M3000416	1.4767 mod.2	160-300	25,0	3,0	x	5 cycles, ALD-run 9			
6	M3000416	1.4767 mod.2	160-300	24,9	3,0	x	60 cycles, ALD-run 10		Run 5	
7	M3000416	1.4767 mod.2	160-300	24,9	3,0	x	60 cycles, ALD-run 10			SEM-EDS
10	M3000418	1.4767 mod.2	200-300	25,0	3,1	x	300 cycles, ALD run 12		Run 7	
11	M3000418	1.4767 mod.2	200-300	25,0	3,1	x	300 cycles, ALD run 12			
13	M3000416	1.4767 mod.2	160-300	25,0	3,1				Run 3	
14	M3000416	1.1467 mod.2	160-300	25,0	3,0	x				
15	M3000419	1.4767 mod.2	75-100	24,1	3,0	x	30 cycles, ALD run 11		Run 6	
16	M3000419	1.4767 mod.2	75-100	24,0	3,0	x	30 cycles, ALD run 11			SEM-EDS
17	M3000419	1.4767 mod.2	75-100	24,1	3,0	x		x		SEM-EDS
18	M3000419	1.4767 mod.2	75-100	24,1	3,0	x		x		SEM-EDS
19	M3000419	1.4767 mod.2	75-100	24,1	3,0				Run 9	

Appendix 1 (2/2). List of catalytic filters prepared.

Filter number	Filter model number by provider	Steel alloy	Pore diameter (µm)	Dimensions of uncoated		Application and characterization				
				d(mm)	h (mm)	Alumina-coating, 90 cycles	NiO coating	Rh coating	Reaction test	Analysis
20	Sika R 200AX	316L	NA	25,5	3,0	x	30 cycles, ALD run 7			SEM-EDS
21	Sika R 200AX	316L	NA	25,5	3,0	x	30 cycles, ALD run 7		Run 4	
22	Sika R 200AX	316L	NA	25,5	3,0	x	30 cycles, ALD run 7		Run 10	
23	Sika R 200AX	316L	NA	25,5	3,0	x	30 cycles, ALD run 7			
24	Sika R 200AX	316L	NA	25,5	3,0	x	1600 cycles, ALD run 13		Run 12	
25	Sika R 200AX	316L	NA	25,5	3,0	x	1600 cycles, ALD run 13			
26	Sika R 200AX	316L	NA	25,5	3,0	x		x		SEM-EDS
27	Sika R 200AX	316L	NA	25,5	3,0	x		x		SEM-EDS
29	Sika R 200AX	316L	NA	25,5	3,0					BET
32	Sika R 100AX	316L	NA	25,5	3,0	x	15Ni, ALD run 8			
33	Sika R 100AX	316L	NA	25,5	3,0	x	15Ni, ALD run 8			
35	Sika R 100AX	316L	NA	25,5	3,0	x			Run 11	
40	Sika R 100AX	316L	NA	25,5	3,0				Run 8	
43	Sika R 100AX	316L	NA	25,5	3,0					BET

Appendix 2. List of ALD runs.

Run	Preparations for filters	Deposition method	Precursor	Sublimation temperature (°C)	Reactant	Cycles	Substrate temperature (°C)	precursor pulse time, s	precursor purge time, s	precursor carrier gas flow, SCCM	reactant pulse time, s	reactant purge time, s	reactant carrier gas flow, SCCM	boost, stopflow
Alumina														
1	as received	diffusion	TMA	-	H_2O	90	225	0,5	25	200	0,5	25	200	stopflow
2	as received	diffusion	TMA	-	H_2O	90	225	0,5	25	200	0,5	25	200	stopflow
3	as received	diffusion	TMA	-	H_2O	90	225	0,5	25	200	0,5	25	200	stopflow
4	as received	diffusion	TMA	-	H_2O	90	225	0,5	25	200	0,5	25	200	stopflow
5	as received	diffusion	TMA	-	H_2O	90	225	0,5	25	200	0,5	25	200	stopflow
6	as received	diffusion	TMA	-	H_2O	90	225	0,5	25	200	0,5	25	200	stopflow
Nickel														
7	alumina-coating	flow-through	$Ni(thd)_2$	175	O_3	30	225	9	25	50	3	25	50	sublimation boost, 5 pulses/cycle
8	alumina-coating	flow-through	$Ni(thd)_2$	175	O_3	15	225	9	25	50	3	25	50	sublimation boost, 5 pulses/cycle
9	alumina-coating	flow-through	$Ni(thd)_2$	175	O_3	5	225	9	25	50	3	25	50	sublimation boost, 5 pulses/cycle
10	alumina-coating	flow-through	$Ni(thd)_2$	175	O_3	60	225	9	25	50	3	25	50	sublimation boost, 5 pulses/cycle
11	alumina-coating	flow-through	$Ni(thd)_2$	175	O_3	30	225	9	25	50	3	25	50	sublimation boost, 5 pulses/cycle
12	alumina-coating	flow-through	$Ni(thd)_2$	175	O_3	300	225	9	25	50	3	25	50	sublimation boost, 5 pulses/cycle
13	alumina-coating	diffusion	$Ni(thd)_2$	175	O_3	1600	225	9	25	50	3	25	50	sublimation boost, 5 pulses/cycle
Rhodium														
14	alumina-coating	diffusion	$Rh(acac)_3$	180	O_2	100	250	45	25	50	9	25	50	sublimation boost, stopflow
15	alumina-coating	diffusion	$Rh(acac)_3$	180	O_2	100	250	45	25	50	9	25	50	sublimation boost, stopflow
16	alumina-coating	flow-through	$Rh(acac)_3$	180	O_2	100	250	45	25	50	9	300	50	sublimation boost
17	alumina-coating	flow-through	$Rh(acac)_3$	180	O_2	100	250	45	25	50	9	180	50	sublimation boost

Appendix 3. Gases and chemicals for reaction test runs

Substance	Provider	Purity
CO	AGA	99.97%
CO_2	AGA	99.99%
CH_4	AGA	99.995%
H_2	AGA	99.999%
C_2H_4	AGA	99.95%
N_2	AGA	Liquid nitrogen
H_2S	AGA	0.5000 mol-% in nitrogen
benzene	Merck	99.7%
toluene	Merck	99.9%
naphthalene	Merck	99 %

Appendix 4 (1/3). Results of the reaction tests

List of reaction tests performed.

Run	Mass of coke formed on filter, g	Filter material	Filter coating
3	0,082	1.4767 mod. 2, 160-300 µm	blank
5	0,085	1.4767 mod.2, 160-300 µm	60 Ni
6	0,106	1.4767 mod. 2, 75-100 µm	30 Ni
7	NA	1.4767 mod.2, 200-300 µm	300 Ni
8	0,653	316L 100AX	blank
9	0,0926	1.4767 mod.2, 75-100 µm	blank
10	0,45	316L 200AX	30 Ni
11	0,355	316L 100AX	Blank-alumina
12	0,378	316L 200AX	Ni 1600
14	-	empty reactor	empty reactor
15	0,031	IWI -particles	13 % Ni

Appendix 4 (2/3). Results of the reaction tests

Yields and conversions (1/2)

Run	Measured temperature (°C)	Conversion				Gas yield				Pressure drop, mbar
		C_6H_6	C_7H_8	$C_{10}H_8$	C_2H_4	H_2	CO	CO_2	CH_4	
3	651	4 %	8 %	-1 %	0 %	-1 %	0 %	1 %	2 %	-16
	755	-53 %	61 %	-4 %	36 %	-6 %	-1 %	1 %	13 %	-24
	807	-85 %	94 %	-11 %	53 %	-8 %	-1 %	2 %	24 %	-22
	860	-89 %	99 %	-10 %	74 %	-7 %	-2 %	2 %	35 %	-9
5	654	-2 %	0 %	0 %	-3 %	1 %	1 %	1 %	3 %	-18
	757	-49 %	47 %	-1 %	36 %	-3 %	2 %	3 %	13 %	16
	809	-96 %	95 %	-9 %	46 %	-5 %	1 %	3 %	22 %	-7
	862	-97 %	99 %	-12 %	81 %	-6 %	-2 %	4 %	41 %	125
6	654	-1 %	3 %	3 %	1 %	0 %	0 %	1 %	1 %	-2
	757	-52 %	54 %	4 %	36 %	-6 %	0 %	1 %	11 %	-1
	809	-92 %	96 %	0 %	51 %	-7 %	-1 %	2 %	22 %	0
	862	-89 %	99 %	6 %	84 %	-7 %	-3 %	3 %	41 %	143
7	706	-13 %	5 %	-10 %	30 %	0 %	2 %	2 %	6 %	-14
	809	-99 %	95 %	-15 %	48 %	-7 %	-2 %	0 %	20 %	-15
	862	-100 %	99 %	-14 %	84 %	-8 %	-3 %	1 %	40 %	134
8	707	-14 %	5 %	-4 %	37 %	0 %	2 %	3 %	7 %	-34
	810	-95 %	95 %	-6 %	51 %	-6 %	-2 %	1 %	21 %	-41
	863	-94 %	99 %	-1 %	75 %	-5 %	-1 %	2 %	34 %	-43
	916	-77 %	99 %	17 %	96 %	-3 %	2 %	1 %	42 %	-43
9	708	-13 %	6 %	-3 %	35 %	0 %	2 %	3 %	6 %	-38
	811	-98 %	96 %	-10 %	49 %	-7 %	-2 %	0 %	20 %	-27
	865	-99 %	99 %	-13 %	80 %	-8 %	-2 %	1 %	39 %	-4
	917	-84 %	99 %	7 %	100 %	-6 %	0 %	1 %	47 %	-7

Appendix 4 (3/3): Results of the reaction tests

Yields and conversions (2/2)

Run	Measured temperature (°C)	Conversion				Gas yield				Pressure drop, mbar
		C_6H_6	C_7H_8	$C_{10}H_8$	C_2H_4	H_2	CO	CO_2	CH_4	
10	711	-6 %	13 %	8 %	41 %	2 %	-1 %	5 %	7 %	45
	812	-83 %	95 %	2 %	52 %	-6 %	0 %	1 %	21 %	49
	865	-82 %	99 %	-1 %	74 %	-6 %	0 %	2 %	33 %	43
	918	-75 %	99 %	5 %	93 %	-4 %	4 %	3 %	43 %	40
11	712	-12 %	8 %	-5 %	37 %	1 %	1 %	3 %	6 %	-23
	813	-94 %	95 %	-13 %	49 %	-7 %	-1 %	0 %	19 %	-25
	867	-96 %	99 %	-18 %	72 %	-7 %	-1 %	1 %	31 %	-31
	920	-87 %	99 %	-11 %	92 %	-4 %	4 %	1 %	42 %	-26
12	712	-11 %	10 %	1 %	41 %	1 %	3 %	4 %	7 %	-22
	815	-88 %	96 %	-3 %	53 %	-6 %	-1 %	1 %	20 %	-26
	868	-89 %	99 %	-7 %	78 %	-6 %	0 %	2 %	33 %	-24
	921	-82 %	99 %	0 %	93 %	-4 %	4 %	2 %	43 %	-14
14	715	-13 %	10 %	-1 %	43 %	1 %	3 %	4 %	7 %	68
	818	-92 %	96 %	-7 %	52 %	-6 %	-1 %	1 %	20 %	62
	865	-95 %	99 %	-15 %	75 %	3 %	8 %	9 %	39 %	-26
	918	-81 %	99 %	1 %	97 %	4 %	10 %	10 %	50 %	-26
15	710	-18 %	15 %	0 %	61 %	4 %	6 %	2 %	6 %	27
	808	-58 %	98 %	44 %	75 %	9 %	11 %	-2 %	13 %	12
	854	24 %	100 %	77 %	98 %	20 %	22 %	-1 %	13 %	16
	900	73 %	100 %	93 %	100 %	24 %	26 %	-8 %	-9 %	19

Appendix 5. Derivation of the equation of error in concentration of component *I* by partial differential equation method.

$$dX_i = \left| \frac{\partial \frac{\left(F_{dry,in} + F_{water,in}\right) \cdot y_{i,in} - F_{tot,out} \cdot y_{i,out}}{\left(F_{dry,in} + F_{water,in}\right) \cdot y_{i,in}}}{\partial F_{dry,in}} \right| \Delta F_{dry,in}$$

$$+ \left| \frac{\partial \frac{\left(F_{dry,in} + F_{water,in}\right) \cdot y_{i,in} - F_{tot,out} \cdot y_{i,out}}{\left(F_{dry,in} + F_{water,in}\right) \cdot y_{i,in}}}{\partial F_{water,in}} \right| \Delta F_{water,in}$$

$$+ \left| \frac{\partial \frac{\left(F_{dry,in} + F_{water,in}\right) \cdot y_{i,in} - F_{tot,out} \cdot y_{i,out}}{\left(F_{dry,in} + F_{water,in}\right) \cdot y_{i,in}}}{\partial y_{i,in}} \right| \Delta y_{i,in}$$

$$+ \left| \frac{\partial \frac{\left(F_{dry,in} + F_{water,in}\right) \cdot y_{i,in} - F_{tot,out} \cdot y_{i,out}}{\left(F_{dry,in} + F_{water,in}\right) \cdot y_{i,in}}}{\partial y_{i,out}} \right| \Delta y_{i,out}$$

$$= \left| \frac{F_{tot,out} \cdot y_{i,out}}{(F_{dry,in} + F_{water,in})^2 \cdot y_{i,in}} \right| \Delta F_{dry,in}$$

$$+ \left| \frac{F_{tot,out} \cdot y_{i,out}}{(F_{dry,in} + F_{water,in})^2 \cdot y_{i,in}} \right| \Delta F_{water,in} + \left| \frac{F_{tot,out} \cdot y_{i,out}}{F_{dry,in} + F_{water,in}} \right| \Delta y_{i,in}$$

$$+ \left| - \frac{F_{tot,out}}{\left(F_{dry,in} + F_{water,in}\right) \cdot y_{i,in}} \right| \Delta y_{i,out}$$

$$= \left| \frac{F_{tot,out} \cdot y_{i,out}}{(F_{dry,in} + F_{water,in})^2 \cdot y_{i,in}} \right| (\Delta F_{dry,in} + \Delta F_{water,in})$$

$$+ \left| \frac{F_{tot,out} \cdot y_{i,out}}{F_{dry,in} + F_{water,in}} \right| \Delta y_{i,in} + \left| - \frac{F_{tot,out}}{\left(F_{dry,in} + F_{water,in}\right) \cdot y_{i,in}} \right| \Delta y_{i,out}$$